A Radiative Model for the Study of the Feedback Mechanism between Photolytic Aerosols and Solar Radiation

María Santa María Iruzubieta

Thesis submitted to the Faculty of the Virginia Polytechnic Institute and State University in partial fulfillment of the requirements for the degree of

Master of Science
in
Mechanical Engineering

Dr. J.R. Mahan, Chairman
Dr. E.P. Scott
Dr. L.K. Peters

December 11, 2001
Blacksburg, Virginia

Keywords: Monte Carlo ray-trace, photolytic aerosols

A Radiative Model for the Study of the Feedback Mechanism between Photolytic Aerosols and Solar Radiation

María Santa María Iruzubieta

(ABSTRACT)

Since the early 70's chemistry and transport models (ChTMs) have been proposed and improved. Tropospheric ChTMs for trace species are detailed numerical formulations intended to represent the atmospheric system as a whole, accounting for all the individual processes and phenomena that influence climate changes.

The development of computer resources and the retrieval of emission inventories and observational data of the species of interest have enhanced the model evolution towards three-dimensional global models that account for more complicated chemical mechanisms, wet and dry deposition phenomena, and interactions and feedback mechanisms between meteorology and atmospheric chemistry.

The purpose of this study is to ascertain the sensitivity of the solar radiative field in the atmosphere to absorption and scattering by aerosols. This effort is preliminary to the study of feedback mechanisms between photolytic processes that create and destroy aerosols and the radiation field itself.

In this study, a cloud of water-soluble aerosols, randomly distributed in space within hypothetical 1-cm cubes of atmosphere, is generated. A random radius is assigned to each

aerosol according to a lognormal size distribution function. The radiative field characterization is analyzed using a Mie scattering code to determine the scattering phase function and the absorption and scattering coefficients of sulfate aerosols, and a Monte Carlo ray-trace code is used to evaluate the radiative exchange.

The ultimate goal of the effort is to create a tool to analyze the vertical distribution of absorption by aerosols in order to determine whether or not feedback between photolytic processes and the radiation field needs to be included in a Third Generation Chemistry and Transport model.

Acknowledgments

I would like to thank my advisor, Dr. J. R. Mahan for his trust and unconditional support during the past few years, for his visionary understanding of the research world and his endless enthusiasm. I am grateful to Mr. Robert B. Lee III, from NASA Langley Research Center for funding this research under NASA Grant NAG-1-2128-SUPL3.

I would like to express my gratitude to Dr. Elaine P. Scott for serving on my advisory committee.

I would like to thank Dr. Norberto Fueyo, from the University of Zaragoza, for blindly accepting to be my co-advisor and for his diligence and valuable help, and Dr. Antonio Valero for his wise advice and his faith in me and the possibilities of this venture.

I am indebted to Dr. Gérard Brogniez, from the Laboratoire d'Optique Atmosphérique of the Université des Science et Technologie de Lille, without whose help I could not have succeeded in this endeavor.

I would like to thank Dr. Leonard Peters, vice provost for research and graduate studies and dean of the graduate school at Virginia Tech, for his initial guidance and for referring me to Dr. Rahul Zaveri, from the Pacific Northwest National Laboratory, who provided me with inestimable help and reassurance on my research.

Also, I would like to express my gratitude to Dr. Brasseur's team at the University of Colorado, for their readiness to help and their cooperation.

In the Thermal Radiation Group I learned the meaning of partnership and comradeship. I made lifetime friends during my stay in Blacksburg. There are no words accurate enough to express the immense treasure I hold in my friends. My homoquímicas in Zaragoza to whom I owe the administrative success of this degree. Alfredo, Arancha, Berta, César, Cristina, Engracia, Javi, María, Margarita, Norma, Teresa y Verónica thank you for dealing with all that paperwork, for being so special and for keeping a place in your hearts for me in my absence. My friends in Logroño, my jewel Belén, our special bond kept me going, I owe you much.

To my family, for their unstoppable belief in me, their infinite love and their cheerfulness. To my parents, because I am you, and you are I, and together we succeeded. And to my dearest David, because without you I am nothing and this is your work as much as it is mine.

Agradecimientos

Quisiera agradecer a mi tutor Dr. J. R. Mahan su confianza y su apoyo incondicional a lo largo de estos años, por su visionario entendimiento del mundo de la investigación y por su inagotable entusiasmo. Quisiera agradecer igualmente al National Aeronautics and Space Administration su apoyo económico a esta investigación con la beca NASA NAG-1-2128-SUPL3.

Quisiera agradecer al Dr. Norberto Fueyo de la universidad de Zaragoza haber aceptado ciegamente ser mi co-tutor, su diligencia y su estimada ayuda. Así mismo, al Dr. Antonio Valero, por sus sabios consejos y su fe en mí y en las posibilidades de esta aventura del doble diploma.

Estoy en deuda con el Dr. Gérard Brogniez, del Laboratoire d'Optique Atmosphérique de la Université des Science et Technologie de Lille, sin cuya ayuda no hubiera podido llevar a cabo esta investigación.

Al Dr. Leonard Peters, vicerrector de investigación y estudios graduados y decano de la escuela de graduados de la universidad de Virginia Tech, por orientarme inicialmente y referirme al Dr. Rahul Zaveri del Pacific Northwest National Laboratory, el cual me brindó inestimable ayuda y confianza en mi investigación.

Por último, quisiera expresar mi gratitud al equipo del Dr. Brasseur en la universidad de Colorado por su disposición a ayudar y su cooperación.

En el grupo de Termo-radiación he aprendido el significado de camaradería y compañerismo. No puedo expresar con palabras el inmenso tesoro que son mis amigos. A mis homoquímicas en Zaragoza les debo el éxito administrativo de este proyecto. Alfredo, Arancha, Berta, César, Cristina, Engracia, Javi, María, Margarita, Norma, Teresa y Verónica, gracias por encargaos de todo el papeleo, por ser tan especiales y por guardarme un sitio en vuestro corazón durante mi larga ausencia. A mis amigos en Logroño, a mi joya Belén, nuestro lazo especial me hizo seguir, te debo mucho.

A mi familia, por su imparable confianza en mí, su infinito amor y sus ánimos. A mis padres, porque yo soy vosotros, y vosotros sois yo, y juntos lo hemos conseguido. Y a mi muy querido David, porque sin ti no soy nada, y este es tu trabajo tanto como es el mío.

TABLE OF CONTENTS

LIST OF FIGURES

LIST OF TABLES

Chapter 1 Introduction

"The climate is a beautiful system, exceedingly rich in interconnections and complexities"

(H.A.Dort, 1986)

The above citation highlights the main characteristic of the climate, its complexity. A single satisfactory definition of climate is probably unobtainable because the climate system encompasses so many variables and so many time and space scales. But for our purposes, *climate* may be defined as the average of the long-term weather associated with the temperature, wind, cloudiness, and precipitation in a particular location [Lenoble, 1993].

This thesis is a required first step towards the evaluation of the relevance of the feedback mechanisms between tropospheric photolytic aerosols and the solar radiative field to be included in a third-generation chemistry and transport model of trace chemical species in the atmosphere.

The purpose of the analytical part of this research is to create an efficient model to determine the vertical extinction rate of radiation due solely to absorption and scattering by aerosols.

1.1 Background

Available chemistry and transport models (ChTMs) represent an ongoing effort to reproduce and forecast the behavior of the atmosphere. They are intended to ascertain the concentration of trace species over the atmosphere in a wide range of temporal and spatial scales.

Chemical compounds are released into the atmosphere from natural or anthropogenic sources. Once in the atmosphere, these chemical compounds undergo physical and chemical reactions. They may be transported over large distances by winds or washed from the atmosphere by rain; they may drop to the Earth's surface or chemically react to generate new chemical species or aerosols; or they may act as cloud condensation nuclei (CCN) and influence cloud coverage, and hence climate and meteorology.

ChTMs intend to quantify these phenomena. Throughout the years, chemistry and transport models increased the complexity of their chemistry schemes and accounted for more physical processes. In addition, feedback effects between climate, meteorology and chemistry have been progressively included.

ChTMs are classified according to different criteria. For instance, they may be divided between Eulerian or Lagrangian models, depending on the way position within a field is defined. We distinguish between on-line and off-line models depending on the mode of operation. Finally, ChTMs may be chronologically classified. A review of the ChTMs' historical progress follows. An updated detailed summary of the evolution of chemistry and transport models, as well as the potential features of any third-generation model, is presented in Chapter 6. The worth of evaluating the relative relevance of each of the new feedback mechanisms to be included in a next-generation model will be appreciated after reading Chapter 6.

After the industrial revolution in the 19th century, the scientific community was mainly concerned with the effects of human activities on the environment. The first generation of models (FGM) addressed the study of alternative emission control strategies by studying the effects of pollutant concentration on the chemistry of the atmosphere. Computer restrictions prohibited the simulation of coupled dynamic meteorology and chemistry modules.

Most of the ChTMs currently in use date from the late 1970s and early 1980s. These second-generation models (SGM) employ extensive chemical mechanisms and improved treatments of physical and chemical processes within and below the clouds.

The complexity of modeling radiative transfer in planetary atmospheres issues from the numerous feedback processes involved as it can be observed from the interaction diagram on Figure 1.1. In most chemical modeling studies of planetary atmospheres, interactions between absorption, Rayleigh scattering, and absorption and scattering by aerosols are conveniently decoupled to ease the analysis. Current models carry out their studies by using an observed temperature profile and empirical transport coefficients. Nowadays, computer resources propitiate the development of a third generation of models (TGM). These new versions of the ChTMs would profit from parallel computing architectures, would utilize recent developments in numerical methods, would handle cloud physics and precipitation chemistry more effectively, and would address interactive processes.

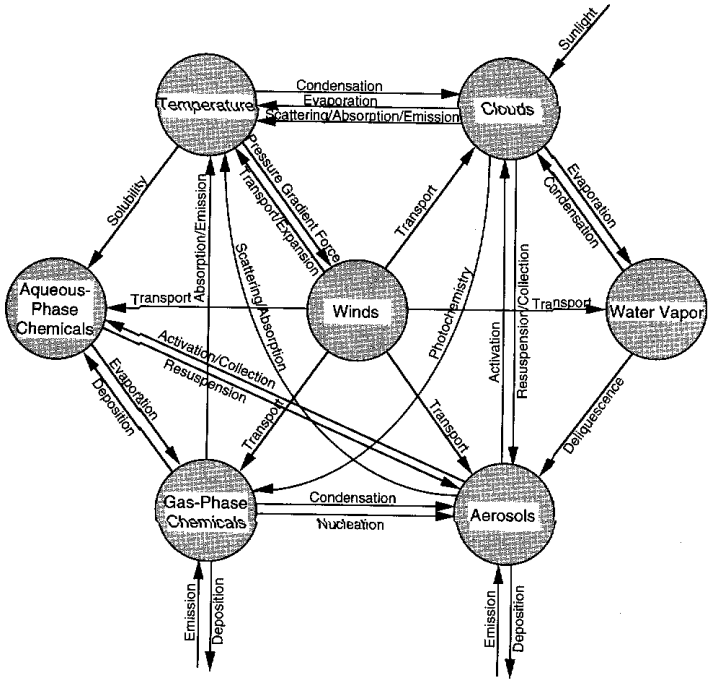

Figure 1.1. Third-Generation Model feedbacks and interaction processes

[Peters L. K., 1995]

ChTMs involve numerous research arenas and their coverage is expanding. A study focusing on aerosol chemistry reveals that no active feedback mechanism has yet been proposed between aerosols and sunlight. Our hypothesis is that aerosol size might be affected by photolytic reactions. By absorption or release of gaseous chemical species, aerosols might grow or shrink. Simultaneously, solar radiant flux is affected by the scattering and absorbing effects of aerosols.

Whereas much research has been conducted on the photolytic origin of clouds, scarce bibliography on this subject applied to aerosols is found. A relatively new research field at the forefront of scientific investigation, it is therefore an intriguing one.

The hypothesis is that the aerosols located on top of an atmospheric column will act as an umbrella for the aerosols at the bottom, will absorb more radiation, and therefore undergo photolytic chemical reactions more vigorously than those lower in the column. The vertical variation in the strength of these chemical reactions will provoke differential shrinkage or growth of those aerosols thereby affecting their optical properties.

Future work on this subject will address coupling the radiative module with a kinetic code that models the growth rate of atmospheric aerosols. The purpose of the analytical part of this research is to create an efficient model to determine the vertical extinction rate of radiation due solely to absorption and scattering by aerosols, while keeping track of the physical characteristics of the particles, namely their radius and relative position.

1.2 Goals of the effort

The present effort identifies three main goals:

- First, to develop an radiative analytical model to estimate the vertical distribution of the absorption rate of solar radiation by tropospheric aerosols. The radiative

field characterization is analyzed by applying the Mie scattering theory to determine the optical properties of the aerosols. A Monte Carlo ray-trace code is used to evaluate the radiative exchange

- Second, to create a broad bibliography about chemistry and transport models of trace species as a background for the Thermal Radiation Group at Virginia Tech in anticipation of eventual doctoral research in this area
- Third, to provide a second-generation model to the Thermal Radiation Group at Virginia Tech and a database to test its application

The analysis tool requirements are:

- to be able to localize and physically characterize every aerosol individually
- to be able to model solar radiation. That implies the simulation of polychromatic, non-collimated, naturally polarized light
- to be versatile, able to accommodate any kind of tropospheric aerosol population
- to be efficient
- to be user-friendly and accessible to future users and researchers that might continue this research

Chapter 2 Aerosols And Solar Radiation

"Artists can color the sky red because they know it is blue. Those of us who are not artists must color things the way they really are or people might think we are stupid."
[Henry David Thoreau, 1817-1862].

Those of us who have enjoyed a sunset know that the sky can appear to be on fire on certain days. The redness of the sky is due to the scattering effects of molecules. This chapter intends to be an introduction to aerosol science, as well as a summary of aerosol optical effects, focusing on the influence of aerosols on the solar radiation, hopefully by the end of the chapter we will be able to explain scientifically why the sky is blue (or red).

Aerosols are a fascinating and very rich subject. The study of atmospheric particles is very interdisciplinary. It encompasses atmospheric science, chemistry, fluid mechanics and optics, to name only a few arenas. Our knowledge about aerosols is also very relevant for ordinary life. It might be curious for some people, for example, to find out that smoke is not a gas, and that some respiratory illnesses are due to harmful dusts. Aerosol atmospheric influence can be hazardous, aerosols are responsible for greenhouse effect enhancement and they act as cloud condensation nuclei and influence visibility.

An aerosol is defined as a dispersed system composed of liquid or solid particles suspended in a gaseous medium. The term atmospheric aerosol refers therefore to the solid or liquid particles suspended in the atmosphere. The study of aerosols started paradoxically. In the nineteenth century, scientists like Tyndall, Maxwell and Aitken were investigating the smallest division of matter and aerosol particles were the only ones known at the moment [Reist P. C., 1984]. World War II impelled the research about aerosols for several reasons; the most important of them was probably the radioactive

aerosols associated with the development of fissionable materials for atomic bomb construction. Also, the possibility of chemical and biological warfare and developments in radar technology both require an understanding of the effect of clouds on the transmission of signals.

Aerosols are classified and described, in this chapter. Their role and influence on climatology are then explained.

This chapter is organized in three parts. The first part describes the Earth's radiation budget and classifies aerosols, underlining their role and their effect on climatology. The second part introduces the solar radiation distribution function and its optical characterization. The final part points out the relationship between photolytic aerosols and the solar radiation and its hypothetical consequences.

2.1 Aerosols

2.1.1 Aerosols and the Earth radiation budget

The energy balance among the Sun, the Earth-atmosphere system, and space is referred to as the Earth's Radiation Budget.

The incoming solar flux is partly reflected or backscattered to space by the atmosphere and by the Earth's surface. The part of the solar energy that enters the atmosphere is partly absorbed by the atmosphere itself or by the Earth's surface. This way, the air and the surface are radiatively heated. The remainder of the short-wave solar energy is reflected back by the surface of the Earth. Figure 2.1 identifies the fraction of incoming solar radiation that undergoes each of these phenomena.

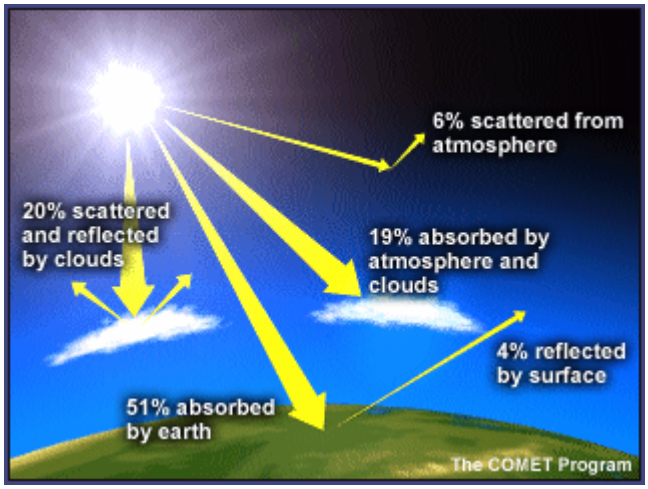

Figure 2.1. Solar radiation contribution to the Earth's radiation budget [http://www.ucar.edu/learn/1_3_1.htm]

On the other hand, the Earth's surface emits long-wave radiation in the infrared and far infrared portion of the electromagnetic spectrum . Part of the energy emitted by the surface is trapped in the atmosphere due to the so-called greenhouse effect. The energy trapped in the atmosphere is due primarily to water vapor, clouds and CO_2 and other naturally occuring gases such as O_3, N_2O and CH_4, and some anthropogenically generated gases such as the chlorofluorocarbons ($CFCl_3$ and CF_2Cl_2). The remaining long-wave energy is radiated into space.

Figure 2.2 illustrates the Earth's radiation budget. The role of aerosols on the Earth's radiation budget is the greatest unknown in climatology studies. It is known that aerosols act as condensation nuclei contributing to the formation of cloud particles. Aerosols also increase the planetary albedo; that is, the reflectivity of the atmosphere, this phenomenon provokes a net cooling of the Earth, which in turn leads to increased cloudiness. Then, in this sense, cloud formation is a negative feedback mechanism. On the other hand, clouds trap downwelling radiative energy from the Sun and upwelling reflected and emitted

radiation from the Earth's surface causing a net, warming of the Earth's surface. In this sense cloud formation can be a positive feedback mechanism.

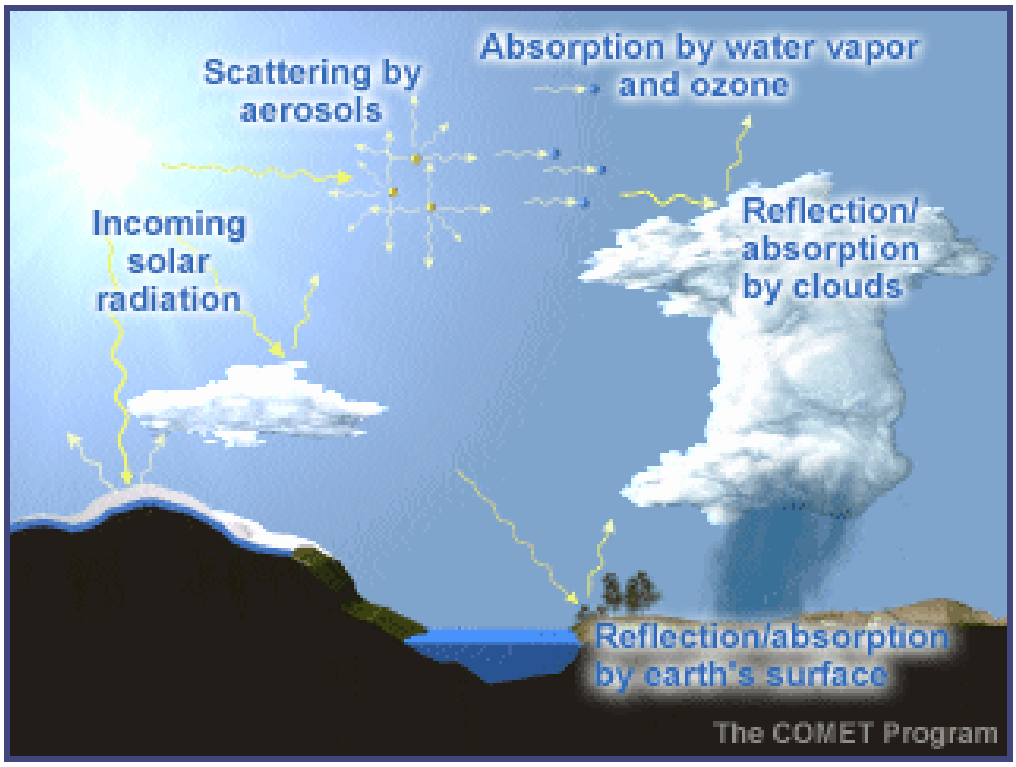

Figure 2.2. Earth's radiation budget feedback effects
[http://www.ucar.edu/learn/1_1_1.htm]

The Earth's radiation budget is globally in equilibrium; that is, considering the total surface of the planet over a sufficiently long period of time the energy losses and gains are in balance. Any imbalance would evolve into a global climate change, like the climate change that ended the last ice age 10,000 years ago. However, the surface of the Earth and its atmosphere are not in radiative equilibrium. Figure 2.3 illustrates the temperature gradient in the atmosphere. This energy imbalance between high and low altitudes in the atmosphere contributes to mass exchanges associated with winds.

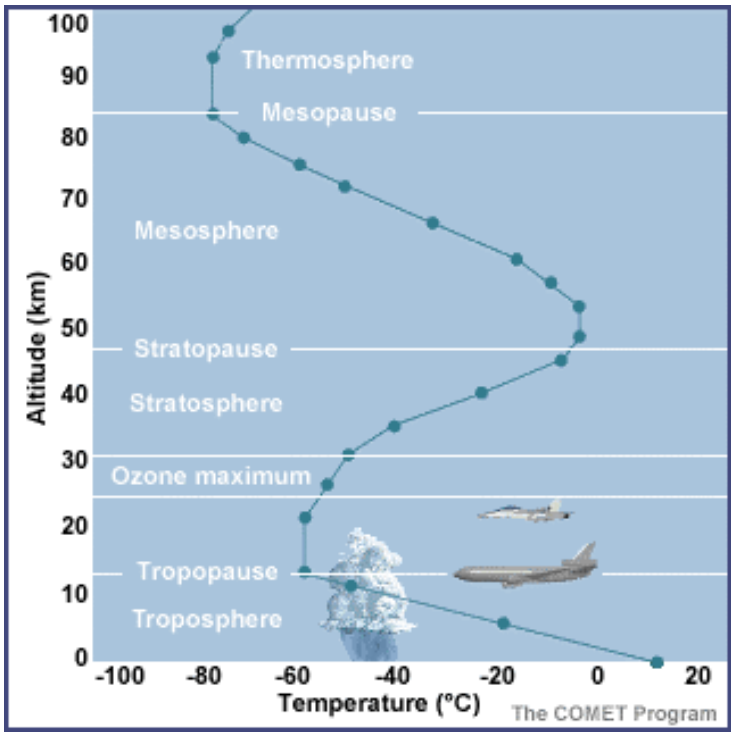

Figure 2.3. Atmospheric temperature profile

[http://www.ucar.edu/learn/1_1_1.htm]

2.1.2 Aerosol Classification

Aerosols may be classified according to their residence time, their source strength, or their chemical composition. The next section establishes the aerosol classification according to chemical composition and origin.

The residence time of an aerosol ranges from several seconds to some years. The residence time of a particle emphasizes the time scale over which an interaction with its environment takes place. Average residence time and source strength indicate whether a component should be included in the present aerosol climatology, however these are not critical measures in the classification of aerosols.

Vertically, aerosols can be divided between tropospheric and stratospheric. Tropospheric aerosols, placed 0 to 15 km above Earth's surface, include all the aerosols coming from ground-level sources. Their residence time is on the order of a few days and their concentration varies significantly with time and location. The height reached by different particles is a function of their size. Some tropospheric aerosols are transported over long distances, for example the carbonaceous particles from industrial activities that reach the poles.

Stratospheric aerosols, located 15 to 50 km above Earth's surface, come mostly from gas-to-particle conversion. The concentration of aerosols in the stratosphere is maximum at an altitude of between 18 and 20 km, in the so-called Junge layer. The concentration and distribution of aerosols in the stratosphere is more constant than in the troposphere. Nevertheless volcanic eruptions are capable of ejecting an enormous amount of gases and ashes into the stratosphere. This greatly perturbs these values as their residence time is on the order of months or even years.

Probably the best way to classify aerosols is according to their origin. According to this criterion, we may distinguish between primary aerosols and secondary aerosols.

Primary aerosols

Primary, or direct, aerosols are injected into the atmosphere directly in a liquid or a solid state. This category includes extraterrestrial sources, oceans, deserts, volcanoes and biological material. Aerosol concentration retrievals seem to confirm the fact that natural primary aerosol sources, with their considerable amount of large particles, greatly exceed anthropogenically produced counterparts, at least from the point of view of source strength [D'Almeida, 1991]. Thus, most of the aerosols cited in this summary are from natural sources.

Meteorites and interplanetary dust are extraterrestrial sources of aerosols. Comets and meteors disaggregate on collisions, yielding solid particles in the terrestrial stratosphere. It is also probable that through vertical scavenging some of these particles reach the troposphere. Their concentration is maximum above the poles, and their lifetime is on the order of months or even years. Extraterrestrial particles can reach several millimeters in diameter. They tend to have an elemental composition such as Fe, Si, Mg, S, Ar, Ca, Ni, Al, Na, Cr, Mn, Cl, K, Ti, and Co; and they are very influential in scattering of sunlight at high altitude [Cameron, 1981].

Considering that two-thirds of the Earth's surface is covered by water, oceans are, after desert dust, the most prolific source of direct aerosols. Waves and tides, raindrops, snowflakes, supersaturation of seawater by temperature changes, and whitecaps are the major mechanisms for bubble production over the oceans [Blanchard, 1980]. These bubbles burst and release spheroids of liquid water into the atmosphere. This effect is called "jet drop of the sea". Sizes of sea salt particles range between 0.1 to 100 μm radius. When these microscopic water droplets evaporate they leave behind sea salt aerosols composed basically of $(NH_4)_2SO_4$ and NaCl.

As mentioned before, volcano eruptions can greatly influence the aerosol concentration. Volcanoes emit nonsoluble dusts and ashes (SiO_2, Al_2O_3, Fe_2O_3, among others) into the stratosphere, as well as some reactive gases such as HCl or sulfur compounds (H_2S and SO_2). Volcanoes are the most important sporadic natural source of atmospheric sulfur.

Arid zones of the planet are subject to high temperature gradients that enhance the grinding process of stones, producing the so-called crustal aerosols. Crustal aerosols are minerals (quartz), soils (clay) and dusts blown by the wind from deserts into the

atmosphere. No secondary aerosol production mechanism in the dry soil is yet known. Mineral aerosols may be suspended in the air for hours or even weeks.

Small particles of carbon (soot components) produced by combustion activities are an example of industrial primary aerosols to avoid the false conclusion that all primary aerosols come from natural sources. Soot particles are hydrophobic and not subject to coagulation.

Finally, some primary aerosols are derived from biological material. However, natural sources of biological aerosols have such low source strength that they generally may be neglected. Some examples are: disintegration of bulk material, pollen, spores, fungi and algae produced over forests and savannahs, all of which are particles with radii larger than 1 μm. Some of these species are hygroscopic and act as cloud condensation nuclei [D'Almeida, 1991].

Secondary aerosols.

Atmospheric chemical processes generate the secondary, or indirect, aerosols by converting available man-made or natural trace gases into solid or liquid particles. This phase transition is known in the field as gas-to-particle conversion (GPC). The resulting size of the particles is generally below 0.1 μm. The main precursor gases are sulfur (S) and nitrogen (N) as well as organic vapors. Organic reactions have been speculated to attack the ozone layer in the atmosphere and to constitute an OH-radical sink [Hidy, 1984].

Sulfur is produced from both natural sources and anthropogenic sources. Some examples of sulfur sources are the marine flora, the terrestrial biota, volcanic eruptions, combustion

processes of coal and oil, petroleum refining industries and traffic. Some of the trace sulfur gases in the atmosphere that will undergo GPC are:

- Sulfur dioxide (SO_2) from fuel combustion
- Hydrogen sulfide (H_2S) from biogenic anaerobic production and volcanoes
- Carbon disulfide (CS_2) released by geothermal sources
- Carbonylsulfide (COS) stems or dimethylsulfide (CH_3SCH_3) –for now on DMS- produced by bacteria and fresh water green and blue algae

These sulfur gases will oxidize to form hydrogen sulfate (H_2SO_4), the thermodynamically stable form of sulfur in the presence of oxygen. Sulfate particles are highly soluble in water. By absorbing water, they contribute to the formation of clouds acting as cloud condensation nuclei.

On the other hand, nitrate is the end product of a wide variety of reactions in the atmosphere involving trace gases such as nitrogen oxides, volatile nitrogen and gaseous nitrates. Some of the most common gaseous nitrogen compounds in the air are:

- Nitrous oxide (N_2O) released from soils, from the decomposition of fertilizers and vegetation and from the decomposition of dinitrogen trioxide (N_2O_3)
- Nitrogen dioxide (NO_2) from the oxidation of either ammonia (NH_3) or Nitric oxide (NO), produced by combustion processes and released after electric processes in the atmosphere such as lightning
- Nitric oxide (NO), nitrogen trioxide (NO_3), dinitrogen trioxide (N_2O_3), dinitrogen tetraoxide (N_2O_4), dinitrogen pentoxide (N_2O_3), ammonia (NH_3), and peroxyacetylnitrate -PAN- ($CHCOONO_3$)

These trace gases will undergo GTP reactions to end up as ammonium nitrate (NH_4NO_3), the most common pure nitrate particle, or as ammonium sulfate ($(NH_4)_2SO_4$). Nitric acid (HNO_3) is formed by the interaction of nitrogen dioxide and water vapor

Forests provide more than 60 percent of the organic vapors of the atmosphere, namely terpene and isoprene [Zimmermann et al., 1978]. The remainder comes from anthropogenic production of olefins ($:=C_nH_{2n}$).

The pie chart in Figure 2.4 presents the average percentage of aerosol particles, produced either by natural sources or by man-made sources, in Terragrams per year, with a radius smaller than 100 μm.

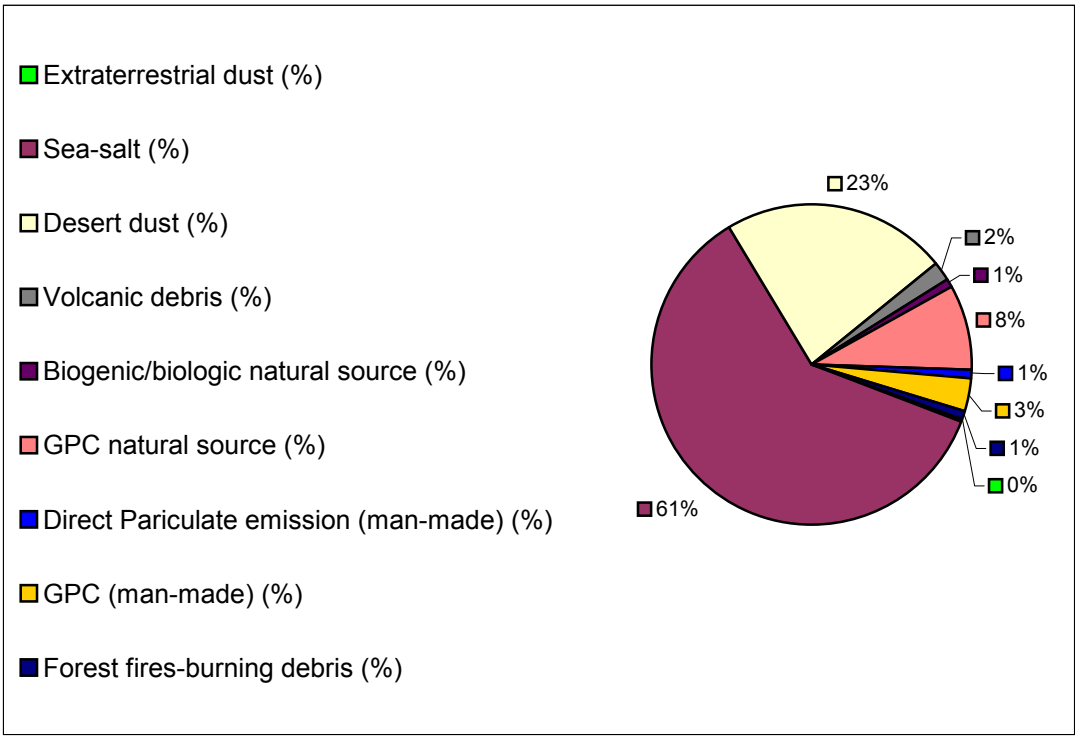

Figure 2.4. Source strength of atmospheric aerosols

As shown in Figure 2.4, aerosol production is balanced almost fifty-fifty between man-made and natural sources.

A summary of the main aerosol components is presented in Table 2.1. The Table also gives the microphysical properties for an assumed relative humidity of 0 percent, and the source of the data. It is convenient to introduce Table 2.1 at this point even if the microphysical properties of the components are not described until the next section. This is because discussion of aerosol classification in the current section makes reference to this table.

Table 2.1. Aerosol components, microphysical parameters for an assumed relative humidity of 0 percent, along with the source of the data [D'Almeida, 1991]

Comp. Reference	Aerosol component	r_i, μm	σ_i	Reference
(1)	Dust-like	0.471	2.512	Shettle and Fenn (1976)
(2)	Water-soluble	0.0285	2.239	Shettle and Fenn (1976)
(3)	Soot	0.0118	2.00	WCP-112 (1986)
(4.1)	Sea-salt (SRA-oceanic)	0.30	2.51	Shettle and Fenn (1976)
(4.2)	Sea-salt (nuc. Mode)	0.05	2.03	WCP-55 (1983)
(4.3)	Sea-salt (acc. mode)	0.40	2.03	WCP-55 (1983)
(4.4)	Sea-salt (coarse mode)	3.3	2.03	WCP-55 (1983)
(5.1)	Mineral (background, nuc. mode)	0.07	1.95	D'Almeida (1987)
(5.2)	Mineral (background acc. mode)	0.39	2.00	D'Almeida (1987)

Comp. Reference	Aerosol component	r_i, μm	σ_i	Reference
(5.3)	Mineral (background coa. mode)	1.90	2.15	D'Almeida (1987)
(5.4)	Mineral (wind carry dust, nuc. mode)	0.05	1.65	D'Almeida (1987)
(5.5)	Mineral (wind carry dust, acc. Mode)	0.27	2.67	D'Almeida (1987)
(5.6)	Mineral (wind carry dust, coa. Mode)	4.00	2.40	D'Almeida (1987)
(5.7)	Mineral (long-range transport to maritime env.)	0.5	2.2	Schütz (1980)
(5.8)	Mineral (polewards)	0.4	1.6	Shaw (1979), Parungo et al. (1981)
(6)	H2SO4 droplets	0.0695	1.86	WCP-55 (1983)
(7)	Volcanic	0.217	1.77	WCP-55 (1983), Harshvardhan et al. (1984)
(8)	Meteoric	----	----	Shaw (1979)
(9)	Sulfate	0.0695	2.03	Shaw (1979)
(10.1)	Biogenic (nuclei mode)	0.04	----	Meszaros (1977)
(10.2)	Biogenic (coarse mode)	2.50	----	Barrie et al. (1981), Desalmand (1985 a, b), Podzimek (1987).

In Table 2.1, r represents the mean radio of the aerosols, and σ the standard deviation of the population.

Table 2.2 outlines the main aerosol types, their aerosol components and their geographical location, based on the traditional World Climate Programme (WCP)

classification. The numbers in parenthesis are a reference to the aerosol components as given in Table 2.1.

Table 2.2. Aerosol types, components and geographical location [D'Almeida, 1991]

Aerosol type	Aerosol components	Location
Clean-continental or rural	Water soluble (2), Dust-like (1)	Rural environments
Clean-forest	Water-soluble (2), Biogenic (10.1, 10.2), Dust-like (1)	Amazon, Africa, and Asian thick forest.
Average continental	Water soluble (2), Dust-like (1) Soot (3)	Continental environment slightly influenced by man-made pollution.
Desert (background)	Mineral (5.1-5.3)	Arid and semiarid regions in wintertime.
Desert (wind carrying dust)	Mineral (5.6-5.8)	Arid and semiarid regions in summertime.
Urban or Industrial	Water soluble (2), Dust-like (1), Soot (3)	Highly polluted continental environments.
Clean-maritime	Sea-salt (4.2-4.4), Non Sea Salt sulfates (9)	Undisturbed maritime environment: southeast Atlantic, Indian Ocean.
Maritime-mineral	Sea-salt (4.2-4.4), Mineral (5.4) NSS-sulfate (9)	Maritime environment influenced by desert air masses.
Maritime-polluted	Water-soluble (2), Soot (3), Sea-salt (4.1)	Polluted maritime environment: Mediterranean, North Atlantic.
Polar-polluted.	Soot (3), Mineral (5.5), Sea-salt (4.2), Sulfate (9)	Artic in wintertime.

Aerosol type	Aerosol components	Location
Clean-polar (Artic)	Mineral (5.5), Sea-salt (4.3), Sulfate (6), (Biogenic)	Artic in summertime.
Clean-polar (Antarctic)	Sea-salt (4.3), Mineral (5.5), Sulfate (6), (Meteoric (8), volcanic (7))	Antarctic.

2.1.3 Microphysical properties of aerosols

This section describes the shape and the size of the aerosols as its microphysical properties.

Aerosols can have many shapes but these can be divided into three general classes:

- *Isometric* particles have their three dimensions roughly the same
- *Platelets* represent particles with a short dimension and two long ones, such as a fragment of a leaf
- *Fibers* represent particles with one dimension longer than the other two

The solid particles have various irregular and complex shapes. In aerosol modeling it is commonly assumed that the aerosol shape is spherical, despite the fact that only water droplets are perfectly spherical. It is probably not unreasonable to assume that, on the average, nonspherical randomly distributed particles behave as spherical particles in scattering and absorption processes [Lenoble J., 1993]. Moreover no theory is available for such irregular particles, and measurements are not sufficiently accurate to clearly establish a difference between real aerosol characteristics and those computed from Mie theory for spherical particles. Spherically shaped aerosols are assumed for the present study. Further justification for this hypothesis can be found in D'Almeida (1991).

In this study, the particle size is represented by the particle radius.

An aerosol population can be *monodisperse* or *polydisperse* depending on the size distribution of the particles. Monodisperse refers to a medium where the aerosols are basically of the same size; and polydisperse refers to a medium where the aerosol sizes range between two limiting values. Polydisperse aerosols will be assumed in the present study, as it is extremely rare to find a monodisperse condition in nature.

If the radius interval is sufficiently small, as in the case of a single type of aerosols, then it is possible to represent a distribution of radii within that range by a smooth curve. This curve is called the size distribution function for aerosols. Three theories are frequently used to represent the size distribution function of atmospheric aerosols:

- The Junge power-law function, suggested by the scientist C.E. Junge and valid for particle size between 0.1 and 100 μm [Junge, 1952].

$$n(r) = Cr^{-\nu-1}, r_2 \le r \le r_2$$

$$\text{and} \quad n(r) = 0, r < r_1 \text{ and } r > r_2 \tag{2.1}$$

  where ν and r_1 are adjustable parameters. The constant C is fixed by the total number of particles N.

- The modified Gamma distribution function. This function is a generalization of the distribution proposed for clouds. It is a very flexible function that easily adapts to the representation of any population of particles. The number of particles of a given radius is estimated according to

$$n(r) = \frac{dN}{dr} = Cr^{\alpha} \exp[-\beta r^{\gamma}] \tag{2.2}$$

  where N is the total number of particles and r represents the particle radius. The parameters C, α, β, and γ have been established for the main aerosol types.

- The log-normal distribution function. This distribution function introduced by C. N. Davies in 1974, is perhaps most commonly used [Davies, 1974]. His first intention was to adjust Junge's function to represent large particles. The log-normal distribution function is also very suitable when dealing with a population of several types of aerosols, or with particles coming from different sources. The number of particles of source i of a given radius is estimated according to

$$n_i(r) = \frac{dN_i(r)}{d(\log r)} = \frac{N_i}{(2\pi)^{0.5}\log(\sigma_i)} \exp[-\frac{1}{2}(\frac{\log(r) - \log(r_{M_i})}{\log(\sigma_i)})^2] \qquad (2.3)$$

where $n_i(r)$ is the total number of particles of radius r from source i. The standard deviation of the function is represented by σ, and r_{Mi} is the mode or median radius of the particle ensemble stemming from the source i.

For a mixture of particles Equation 2.3 is modified to take into account multiple, independent sources. The total number of particles of radius r coming from all the independent sources will be

$$n(r) = \frac{dN(r)}{d(\log r)} = \sum_i \frac{dN_i(r)}{d(\log r)} \qquad (2.4)$$

2.1.4 Optical properties of aerosols

This section introduces the aerosol optical properties and the theory employed to estimate their values. The effects of tropospheric aerosols on the Earth radiation budget are both scattering and absorption of long (5 to 50 μm) and short (0 to 5 μm) wavelength radiation. Their influence on long-wavelength emission is small because they are located in low atmospheric layers and their temperature is similar to that of the surface of the Earth. Their presence in the atmosphere increases planetary reflectance and produces a negative feedback on the planetary radiation budget, whereas the aerosol layer itself is heated by absorption of solar radiation.

Radiative transfer is usually modeled as being between two surfaces or through a participating media such as the atmosphere. Radiative transfer from surface to surface is actually an extreme case of radiative transfer through a participating medium, where the emission, absorption, and scattering are concentrated in the boundary layer over the surface of the material.

In 1908, Gustav Mie solved Maxwell's equations for a plane, monochromatic wave incident upon a homogeneous sphere in a non-absorbing medium [Mie, 1908]. Detailed mathematical treatment of the Mie theory can be found in the literature [Lenoble (1993); Siegel and Howell (1981); van de Hulst (1981)].

Mie theory is commonly used to estimate the fundamental radiative properties of particles of any given shape and size given the size parameter and the complex index of refraction of the particles [Lenoble, 1993; Brewster, 1992; Siegel and Howell, 1981]. These radiative properties include the extinction, scattering and absorption coefficients, as well as the phase scattering function, the asymmetry factor and the single scattering albedo.

The physico-chemical characteristics of spherical particles are related to the dimensionless size parameter, x, according to

$$x = \frac{2\pi r}{\lambda} \tag{2.5}$$

where r is the particle radius and λ is the radiation wavelength.

The optical properties of the particles are represented by the index of refraction. The index of refraction corresponds to the ratio between the speed of light (or wavelength) in

vacuum to that in another medium. When the propagating medium absorbs, the index of refraction is a complex number.

The complex index of refraction, $\bar{n}$ (dimensionless), is generally represented by

$$\bar{n} = n - i\kappa \qquad (2.6)$$

where n is the real component of the complex index of refraction and κ the imaginary component. By definition, κ is always positive.

Figure 2.5 presents the complex index of refraction for clean continental or rural aerosols. The index of refraction values come from Table 4.3 D'Almeida (1991). They have been checked and completed for the shortest wavelength values (0.2 and 0.25 µm) with a second source [Shettle E.P., 1979].

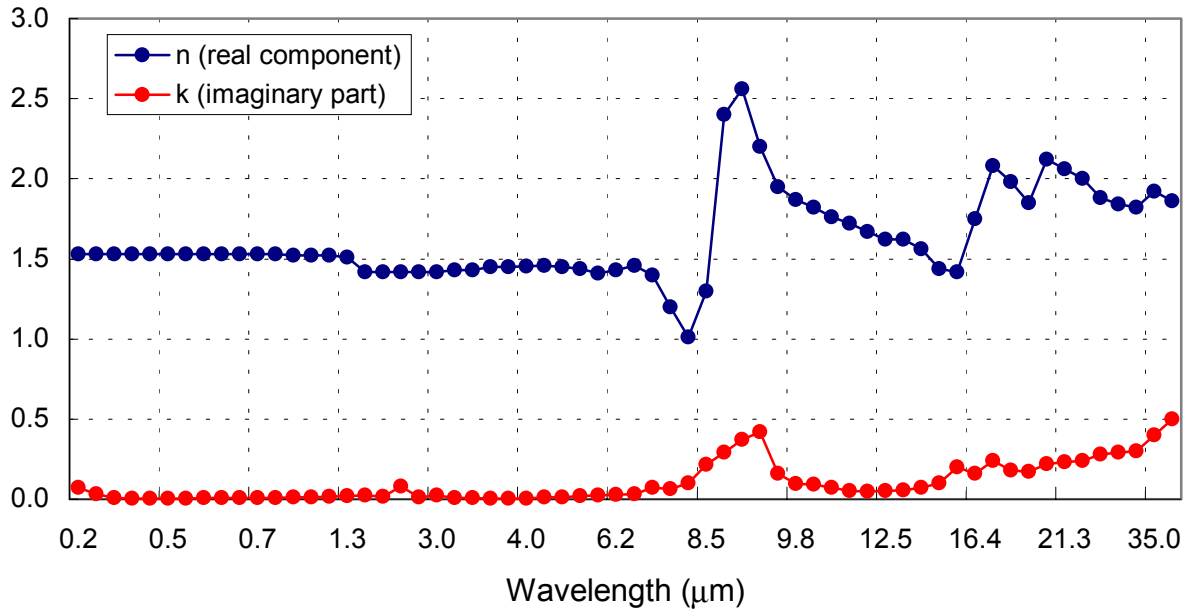

Figure 2.5. Complex index of refraction values as a function of wavelength for rural aerosols

Figure 2.6 represents a beam of light traversing a differential volume element of a participating media along a path length, ds, scattered from a solid angle Ω into a solid angle Ω'.

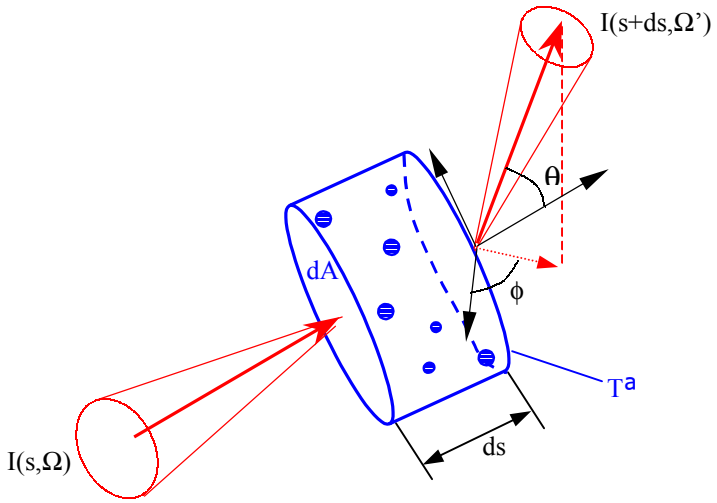

Figure 2.6. Radiative energy balance on a differential, scattering volume

The radiative energy balance along the path length s, which treats absorption and the scattering of radiation as energy extinction mechanisms and treats emission as an energy source, can be expressed as

$$\frac{dL_\lambda}{ds} = \sum L_{emitted,\lambda} - \sum L_{extinction,\lambda} \qquad (2.7)$$

where L_λ is the radiance of the radiation beam (W m^{-2} sr^{-1}) at wavelength λ (μm).

Consider the case of a non-scattering, non-emitting media, where the radiation beam experiences only energy losses due to absorption. The energy absorbed will be stored in the volume element and converted into other forms of energy by, for example, photochemical processes.

In this case, the energy balance is

$$\frac{dL_\lambda}{ds} = -\sigma_{abs,\lambda} L_\lambda \tag{2.8}$$

The absorption coefficient, σ_{abs} (m^{-1}), can be defined from Equation 2.8 as the property of a medium that describes the amount of absorption of thermal radiation per unit path length within the medium.

For the case of a nonabsorbing, nonemitting media, the scattering of photons by inhomogeneities in the medium reduces the radiant energy. The scattered radiant energy continues to propagate in the form of radiation, but it is considered lost as to the direction of propagation of the incident radiation.

In the case of a scattering differential volume element, Equation 2.7 becomes

$$\frac{dL_\lambda}{ds} = -\sigma_{scat,\lambda} L_\lambda \tag{2.9}$$

Equation 2.9 defines the scattering coefficient, σ_{scat} (m^{-1}), as the property of a medium that describes the amount of scattering of thermal radiation per unit path length for propagation in the medium.

The sum of the scattering coefficient and the absorption coefficient is called the extinction coefficient.

$$\sigma_{ext,\lambda} = \sigma_{abs,\lambda} + \sigma_{scat,\lambda} \tag{2.10}$$

The single scattering albedo, ω, is the ratio between the scattering coefficient and the extinction coefficient.

$$\varpi_\lambda = \frac{\sigma_{scat,\lambda}}{\sigma_{ext,\lambda}} \tag{2.11}$$

A perfectly absorbing atmosphere will have a single-scattering albedo equal to zero, and a perfectly scattering atmosphere will have a single-scattering albedo of unity. However, both limiting cases are extremely rare.

The radiative properties of a cloud of aerosol interacting with solar radiation are governed by three dimensionless parameters: the size parameter (Equation 2.5), the complex index of refraction (Equation 2.6) and the clearance-to-wavelength ratio.

Independent scattering assumes that the particles are separated by very large distances, and therefore act as independent nuclei of scattering. Dependent scattering occurs when the particle spacing becomes so small that the interaction of individual particles with radiation begins to be influenced by the close proximity of neighboring particles.

In 1982, Brewster and Tien published an article establishing that the criteria for estimating whether or not the scattering is independent are

$$\frac{c}{\lambda} > 0.3 \tag{2.12}$$

where c is the particle spacing and λ is the wavelength, and

$$f_v << 1 \tag{2.13}$$

where f_v is the particle volume fraction, [Brewster et al., 1982].

The dimensionless parameter c/λ is the clearance-to-wavelength ratio. The particle volume fraction is the ratio between the volume occupied by the particles and the control volume. For the current study it is assumed that the particle density and the mean radius

of the particles are such that both criteria are satisfied. Thus, independent scattering is assumed.

The scattering phase function gives the directional distribution of scattered energy. Assuming that the incident radiation is unpolarized or circularly polarized and that the particles are spherical, the scattering phase function is independent of ϕ, the azimuthal angle [Brewster 1992]. The phase function is defined as the ratio between the energy scattered from the incident direction, s, into the outgoing direction, s', and the energy that would have been scattered into that outgoing direction, s', if the scattering were isotropic; that is

$$p(s \rightarrow s') \equiv \underset{\Delta s \rightarrow 0}{Lim} \frac{I_{scatt}(s \rightarrow s')}{I_{scatt}(s \rightarrow s')_{isotropic}} \tag{2.14}$$

The phase function is normalized according to

$$\int p(\theta) d\Omega = 4\pi \tag{2.15}$$

where Ω is the solid angle, and θ is the zenith angle to the direction of incidence, s.

Finally, the asymmetry coefficient, g, is the average of the cosine of the scattering angle for scattered radiation.

$$g(\lambda) = \frac{\int \cos(\theta) p(\lambda,\theta) d\cos(\theta)}{\int p(\lambda,\theta) d\cos(\theta)} \tag{2.16}$$

The asymmetry factor therefore varies between [-1, 1]. The more particles that scatter in the forward direction, the closer the asymmetry factor is to unity.

For the case where the particles are very small compared to the wavelength of the incident radiation, ($r << \lambda$), Rayleigh scattering, so named after John William Strutt, the third Baron Rayleigh (1842-1919), applies. Rayleigh scattering, also called molecular scattering, hypothesizes that the electric field around the particles remains constant. Its solution states that the scattered energy in any direction is proportional to the inverse

fourth power of the wavelength of the incident radiation. Therefore the shorter-wavelength radiation will be Rayleigh scattered with a strong preference. Rayleigh scattering simplifies the molecule scattering phase function to

$$p(\theta) = \frac{3}{4}(1 + \cos^2 \theta) \qquad (2.17)$$

The daytime sky then appears blue because blue light corresponds to the short-wavelength portion of the solar visible spectrum (0.45 to0.51 μm); therefore, it undergoes strong Rayleigh molecular scattering into all directions, giving the sky its overall blue background. Without molecules in the atmosphere, the sky would appear black except for the direct view of the sun. This is the case of outer space beyond the terrestrial atmosphere. As the sun is setting, the path that the light must travel through the atmosphere becomes longer than at noon when the solar rays are almost perpendicular to Earth's surface. In traversing this longer path, more of the short-wavelength portion of the spectrum is scattered out of the direct path defining a sunbeam. As a result, at sunset the sun takes on a red color as the longer-wavelength red rays, whose wavelength ranges between 0.65 and 0.7 μm, are able to penetrate the atmosphere with less attenuation than the rest of the visible spectrum [Siegel R. et al., 1981].

2.2 Solar radiation

The sun is the only significant source of radiant energy for the planet Earth. Figure 2.7 is an amazing picture taken by SOHO's Extreme-Ultraviolet Imaging Telescope (EIT). It was taken on February 28, 2000 at wavelength Fe IX/X (171 Å).

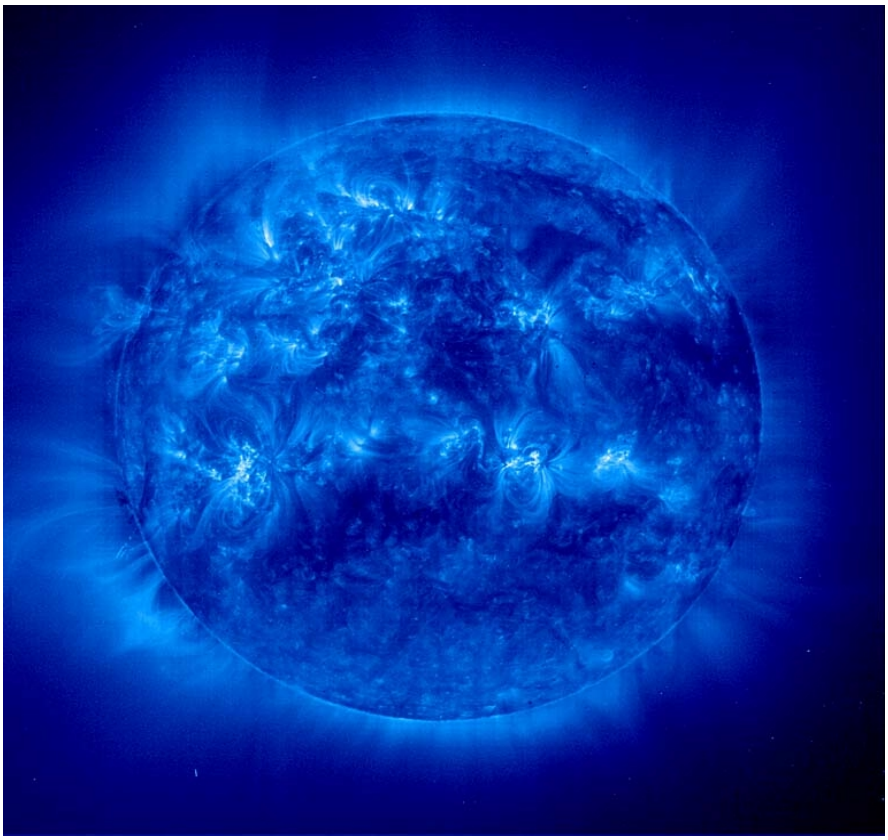

Figure 2.7. The sun

[http://nssdc.gsfc.nasa.gov/image/solar/eit_sl_171.jpg]

Its radiative power can be approximated by the Planck's blackbody radiation distribution function for a blackbody at a temperature of 5777 K [Lenoble, 1993]. It is true that solar irradiance varies with solar activity, but these variations are only important in the far-ultraviolet and X-ray spectrum, which affect the middle and the high atmosphere. Only a negligible part of the solar energy is contained in this wavelength.

In 1901, Max Planck (1858-1947), a German physicist, established the correct blackbody distribution function [Planck, 1901].

The Planck's spectral distribution of emissive power and radiant intensity in a vacuum as a function of the absolute temperature, T (K), and the wavelength, λ (μm) are given by

$$e_{\lambda b}(\lambda) = \pi i'_{\lambda b}(\lambda) = \frac{2\pi C_1}{\lambda^5 (e^{\frac{C_2}{\lambda T}} - 1)} \tag{2.18}$$

where $e_{\lambda b}$ is the emissive power (W $m^{-2}\mu m^{-1}$), $i_{\lambda b}$ is the radiant intensity ($Wm^{-2}\,\mu m^{-1}\,sr^{-1}$) and C_1 and C_2 are constants.

The constant C_1 corresponds to

$$C_1 = hc_0^{\,2} \tag{2.19}$$

and C_2 corresponds to

$$C_2 = \frac{hc_0}{k} \tag{2.20}$$

where h is Planck's constant ($h = 6.6262\times10^{-34}$) in (J s), k is Boltzmann's constant ($k=1.3806\times10^{-23}$) in ($J\,K^{-1}$) and c_0 is the speed of light in a vacuum ($c_0=2.99\times10^{8}$) in ($m\,s^{-1}$).

For radiation traveling through a medium in which the speed of light is not close to c_0, Planck's spectral distribution becomes

$$e_{\lambda b}(\lambda) = \pi i'_{\lambda b}(\lambda) = \frac{2\pi C_1}{n^{\,2}\lambda^5 (e^{\frac{C_2}{n\lambda T}} - 1)} \tag{2.21}$$

where n is the index of refraction of the medium ($n = c_0/c$).

Air has an index of refraction so close to unity that Equation 2.18 is applicable [Siegel, 1981]. The solar emissive power is approximated by the curve presented in Figure 2.7, corresponding to Planck's spectral emissive power distribution function for a blackbody at a temperature of 5777 K.

The narrow band of the visible spectrum contains 43 percent of the total radiant energy of the Sun [http://www.ucar.edu/learn/1_3_1.htm].

Figure 2.8 shows that the peak of the solar emissive power occupies the visible region of the wavelength spectrum. It can be hypothesized that the human eye evolved, or was created, to be sensitive to the region where the solar energy received is maximum. Curiously, this does not apply to all creatures: turtles' eyes are sensitive to the infrared part of the spectrum, that is to say to longer wavelengths, and bees have eyes sensitive to the shorter wavelengths, that is to say, the ultraviolet part of the spectrum.

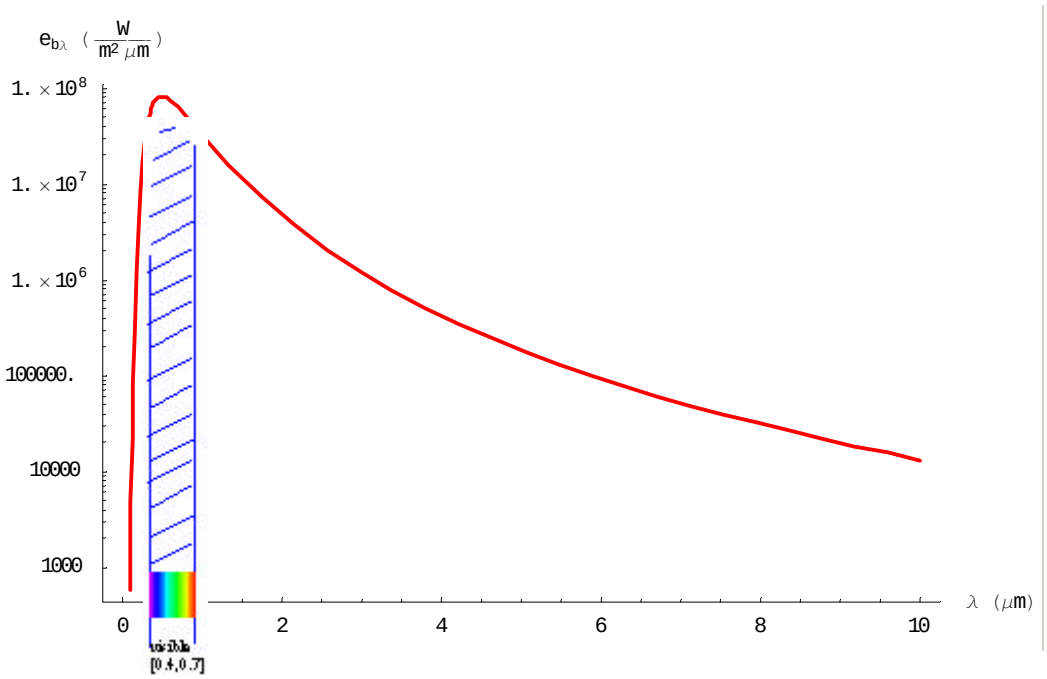

Figure 2.8. Spectral emissive power of a blackbody at 5777 K

According to Wien's displacement law, the wavelength of maximum emissive power λ_{max} (μm), of a body at a given temperature T (K) corresponds to

$$\lambda_{max}\, T = 2898 \qquad (2.22)$$

In the case of the sun, this maximum wavelength corresponds to 0.5 μm, matching the color turquoise.

2.1 Photochemical aerosols

Sunlight is the most important source of chemical activity in the middle and upper atmosphere and the ultimate cause of life in the biosphere. The absorption of UV radiation by atmospheric gases leads to the formation of extremely reactive radical species.

The energy absorbed by atoms results in one of three possibilities:

- resonance scattering
- absorption followed by fluorescence
- ionization

The interaction between molecules and radiation can initiate, in addition to the three effects listed above, the following processes:

- dissociation
- intramolecular conversion
- vibrational and rotational excitation

Vibrational and rotational excitations are very important processes for the Earth radiation budget, while ionization and dissociation determine the chemical composition of the atmosphere. We define photochemical aerosols as aerosols generated or affected by chemical reactions initiated by absorption of solar energy.

Photochemical gas reactions are the most important first-order (unimolecular) chemical reactions in the atmosphere. Their general reaction mechanism can be represented as

$$\begin{aligned} A + h\nu &\rightarrow A^* \\ A^* &\rightarrow B + C \end{aligned} \tag{2.23}$$

where the rate-limiting reaction is the ionization of species A.

The mass balance for the photolytic reactions of the mechanism above proposed would be

$$\frac{d[A]}{dt} = J_i[A] \tag{2.24}$$

where J_i is the photolysis rate constant, or photodissociation coefficient, and [A] represents the concentration of species A.

In 1998, Landgraf and Crutzen hypothesized that the photolysis rate constant for a gas (i) could be dependent on the wavelength, the height, the particle density, and the solar flux [Landgraf, 1998].

Lung Y. L. provides an exhaustive review of the absorption cross-sections and photolysis mechanisms of the main atmospheric gases for the solar planetary system atmospheres [Yung Y. L., 1999].

Chapter 3 Monte Carlo Ray-Trace (MCRT) Method

"I used to be a heavy gambler. But now I just make mental bets. That's how I lost my mind".

Steve Allen (1921 - __)

The quotation that starts this chapter refers to gambling because in a certain way, the Monte Carlo method is a game of chance. Actually, its own name is a reference to the gambling tables of Monaco. An accurate definition of the Monte Carlo method would be, a probabilistic approach to a non-probabilistic problem in an attempt to aid its analysis. That is to say, by means of the Monte Carlo method, some of the most complicated problems, such as the solution of differential equations or thermal radiation problems with complicated geometries implied, can be solved relatively easily.

The origin of the Monte Carlo method goes back to the 1940's, when scientists at Los Alamos were working on the development of nuclear weapons, modeling the diffusion of neutrons in fission material [Hammersley J.M., 1964]. For the solution of a radiative problem, the use of the Monte Carlo method supposes the trace of a meaningful random sample of energy bundles from their points of emission, throughout the volume elements, until their points of extinction are reached. This technique is referred to as the Monte Carlo ray-trace (MCRT) method. Since the energy travels in discrete parcels, the treatment of thermal energy as energy bundles is acceptable. The first time MCRT method was applied to thermal radiation was in the early 1960's [Fleck, 1961;Howell, 1964].

For a detailed description of the Monte Carlo ray-trace method the reader is referred to Mahan's book on radiation heat transfer [Mahan J.R., 2002].

It is essential for the applicability of the MCRT method to have a reliable random number generator. The following section deals with the efficient generation of random numbers in a Monte Carlo environment.

3.1 Random number generator

Nowadays, MCRT simulations are carried out in a computerized environment. During the course of a Monte Carlo simulation, up to 10^7 random numbers might be needed. The storage space required for a sufficiently large table to hold this many random numbers for each of these simulations would make the simulations impractical. That is why the random numbers are generally supplied by external code within the simulation. These codes are called pseudo-random number (PRN) generators.

A PRN generator uses a deterministic formula to produce a sequence of numbers whose properties approach those of true random numbers. However there is always a correlation and a periodicity among them. A pseudo-random number generator must meet the following requirements to be suitable for a MCRT simulation [James, 1990]:

- the numbers must be uniformly distributed
- the correlation between each number and the numbers that preceded it must be as low as possible
- the period of the sequence must be long enough to complete a simulation without repeating any part of the sequence
- a pseudo-random number sequence should be repeatable, given the same starting values (seeds)
- a pseudo-random number generator code should provide long, disjoint sequences

Also, it is desirable that the code is portable and executable among different processors, as well as efficient as millions of numbers would be required.

In this study, the pseudo-random number generator subroutine is called 'rmarin'. This is the random number generator proposed by George Marsaglia in Florida State University Report: FSU-SCRI-87-50. It provides sequences of pseudo-random numbers of sufficient length to complete an entire calculation width. The pseudo-random number generator subroutine demands two seeds whose values must be an integer number within the range [0, 31328] for seed 1 and within [0, 30081] for seed 2. This means that if several different groups are working on different parts of the same calculation, each group could be assigned its own first seed. This would leave each group with over 30,000 choices for the second seed. That is to say, this random number generator can create 900 million different subsequences with each subsequence having a length of approximately 10^{30}.

The uniformity of the numbers generated by the pseudo-random number generator can be appreciated in the histogram presented in Figure 3.1. In Figure 3.1, the random numbers generated by four different simulations are classified into 0.1 width bins. The results of each of the simulations are plotted in a different colour; the values of seed 1 and seed 2 are given below the histogram. Each simulation uses different seeds. Out of a total of 10^7 random numbers drawn, each of the bins contains approximately $10^6 \pm (1.9 \times 10^{-}4 \cdot \mathrm{Ntotal})$ random numbers. The probability of drawing a certain random number is $1/N_{total}$, where N_{total} is the total number of random numbers generated.

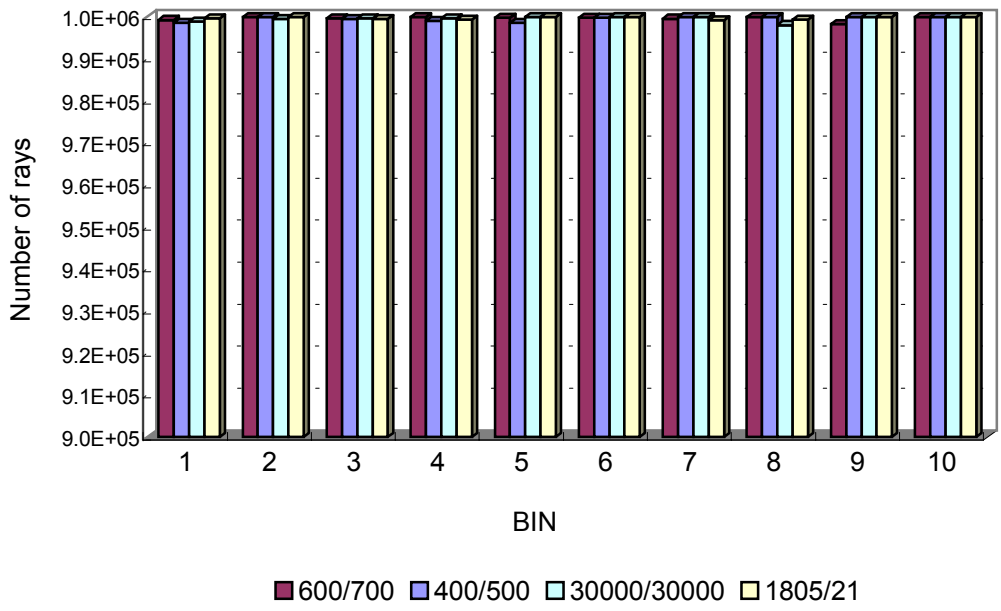

Figure 3.1. Pseudo-random number generator uniformity

Despite the fact that each random number is a potential source of uncertainty in the final result, these uncertainties are assumed to cancel out when the sampling size is sufficiently large.

3.2 MCRT method in a participating media

Current ChTMs three-dimensional grids divide the atmosphere into columns as shown in Figure 3.2. The Navier Stokes transport equations are applied and solved for each of the columns, the solution being the boundary condition determinant for the surrounding ones. Each column is subdivided into levels. Each column of the atmosphere is studied in a similar way. Vertical and horizontal species concentration and energy exchange between the levels of the columns are calculated. The meteorology data set is an input module for each atmospheric column. It includes the wind vectors (magnitude and direction), the humidity, the cloud coverage, the temperature and the height data. At surface level ground temperature, and the water and energy fluxes are inputs as well.

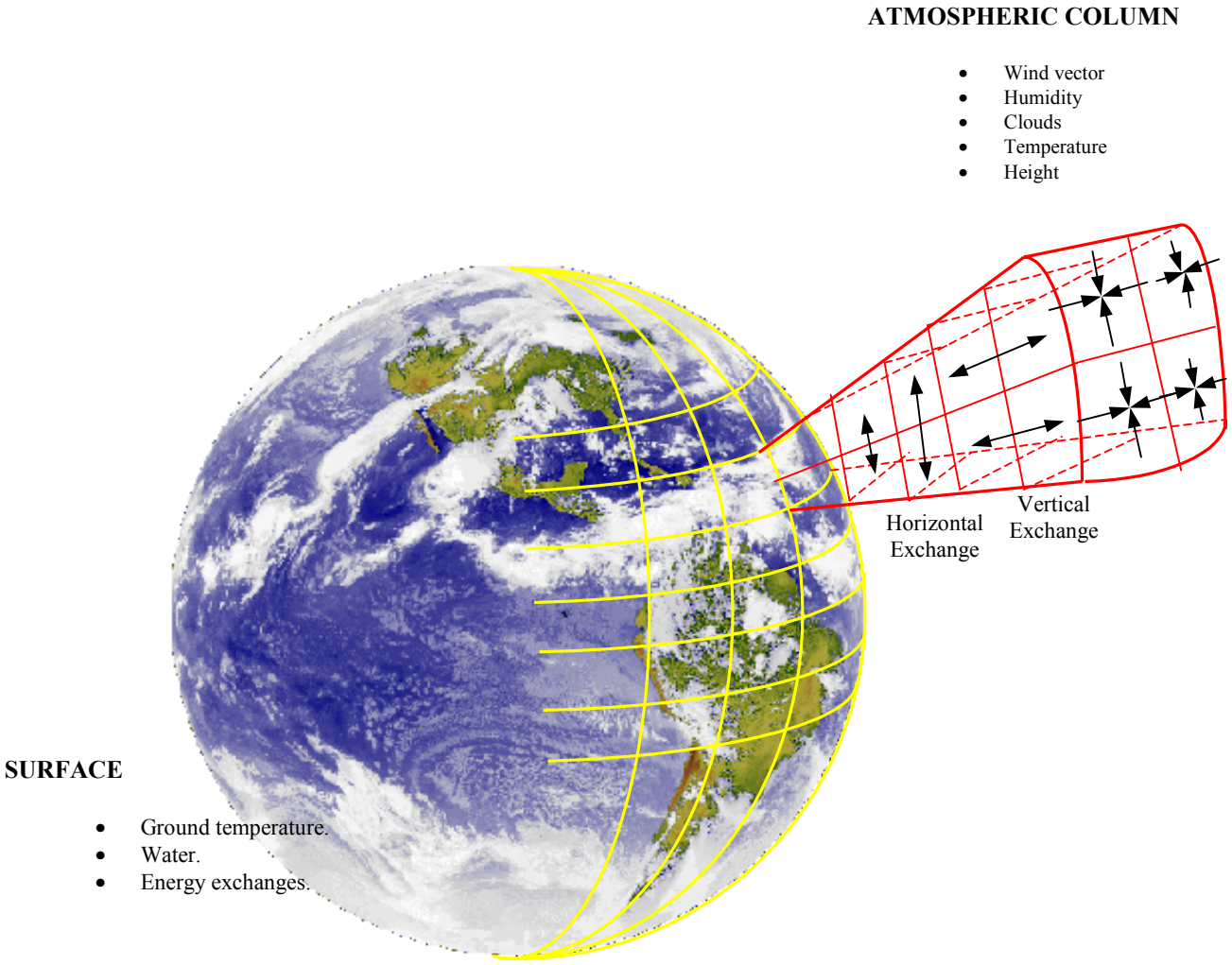

Figure 3.2. Chemistry and transport models 3D grid

One-centimeter atmospheric cubes, piled on top of each other, can form an atmospheric column. The size of the cube used in this study has been chosen because it is sufficiently large to ensure that it contains a statistically meaningful number of aerosol scattering centers, yet sufficiently small to permit a finely resolved vertical structure in the

atmosphere. In this section, the MCRT method used for the analysis of each of the 1-cm cubes is described.

Winds transport aerosols from their source points and mix them in such a way that anywhere over the planet, the characterization of the aerosol population will be a combination of the components introduced in Table 2.1. Therefore, any realistic model dealing with aerosols needs to consider mixing ratios and density of particles in the air. This is one of the most complicated features required for aerosol modeling, to specify each component or subcomponent in such way that its physical-chemical properties and its radiative behavior are described in the best possible way. It would be pointless for the results sought by this research to complicate the work presented here by dealing with an aerosol module representing different aerosol types. However, an unrealistic assumption about the atmospheric cube aerosol composition will invalidate any conclusion made from the results of this work. Seeking a reasonable solution for this dilemma, the author has decided to work with a cube of atmosphere placed above a non-forested savannah somewhere around the Equator whose aerosol composition can be reasonably hypothesized to be 100 percent clean continental aerosols.

Glancing through Table 2.2, the clean continental and the Antarctic aerosol types stand as the least mixed aerosol categories. Furthermore, both of them present almost constant composition throughout the year. The decision of working with clean continental aerosols was made based only on its highest (or lowest) percentage of mixing ratio between aerosol components, and also because such particles can be found along the Equator, which will validate the assumption of perpendicular incoming solar rays stated later on.

Clean continental aerosols are also referred to as rural aerosols; they intend to represent the aerosols under conditions not directly influenced by urban or industrial aerosol sources. Rural aerosols are 99.99 percent composed of water-soluble particles (nitrates,

sulfates, DMS and water-soluble organic substances). Water-soluble particles originate mainly from GPC. For our purposes, the 0.01 percent dust particles present in clean-continental aerosols are neglected.

The cube under consideration would have a particle density of 5000 rural aerosols cm^{-3}. This is a realistic density of particles according to the observational data reported in January 1990, over an area located at 5º latitude and -5º longitude, for a relative humidity of 15 percent [D'Almeida, 1991]. Humidity would be assumed to be zero in our simulations so that no coagulation of the sulfate aerosols or growing rates by water vapor absorption can be hypothesized.

Scattering is independent as proved on Section 2.1.4.

The composition of the air mixture inside the cube is assumed to be non-absorbing for the entire solar spectrum, so that the only effects to consider from the point of view of the radiative analysis are the scattering and the absorption by aerosols themselves.

The general approach to the modeling of radiation through a scattering atmosphere is as follows; the next section describes the generation of the preprocessed module that stores the aerosol population data.

3.2.1 Aerosol preprocessed data

The aerosols are considered to be spherical. Both the position and the size of the aerosols are preprocessed and stored in a table called 'AerRadLoc' which stands for AERosol, RADius and LOCation. The format of 'AerRadLoc' is four columns: the first contains

the radius of the aerosols in μm, the second, third and fourth columns correspond, respectively, to the x, y and z position in centimeters of the aerosols within the cube.

The aerosol size distribution is treated statistically. Size distribution functions, Equations 2.1, 2.2 and 2.3, are the so-called probability density functions; they represent the probability of having n aerosols of radius r. The probability of having one aerosol of radius r in a population of particles whose sizes range between r_{min} and r_{max} corresponds to

$$N(r) \equiv \frac{\int_{r_{min}}^{r} n(r^*)dr^*}{\int_{r_{min}}^{r_{max}} n(r^*)dr^*} \tag{3.1}$$

where n(r) is any size distribution function. Equation 3.1 is the *normalized cumulative distribution function*. The normalized cumulative distribution function can be shown to have the following useful property. If, in the present case, the radius r is chosen randomly, but with the weighting implied by the probability distribution function n(r) in the range from r_{min} to r_{max}, then the corresponding values of the normalized cumulative distribution function, N(r) form a set of uniformly distributed random numbers ranging from zero to unity [Gibbons, 1992]. In the present work this property is repeatedly exploited to obtain correctly distributed parameters; for instance, the aerosol radius in the present discussion or the solar wavelength in the next section.

The present study uses the log-normal size distribution function, Equation 2.3, to assign a radius to the aerosols. Figure 3.3 represents the lognormal size distribution function for rural aerosol radius ranging from 10^{-4} to 20 μm. Figure 3.4 represents its normalized cumulative size distribution function for aerosol radius ranging from 0 to 0.46 μm.

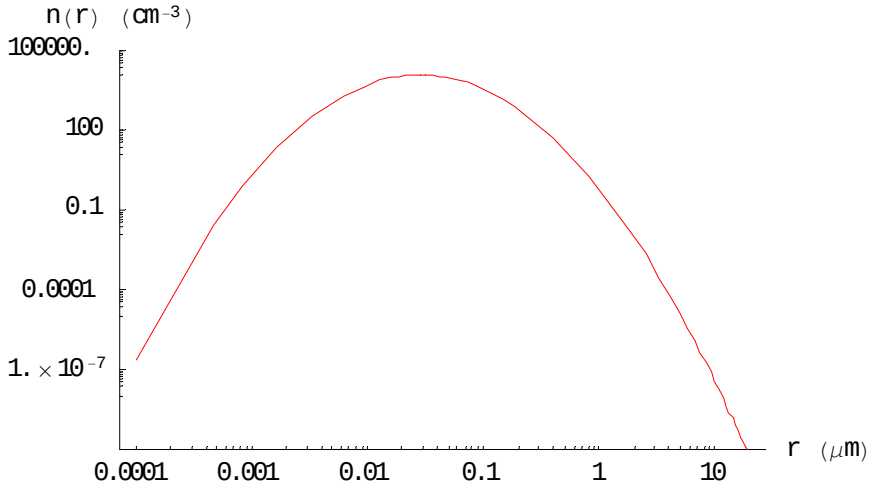

Figure 3.3. Log-normal size distribution function for rural aerosols

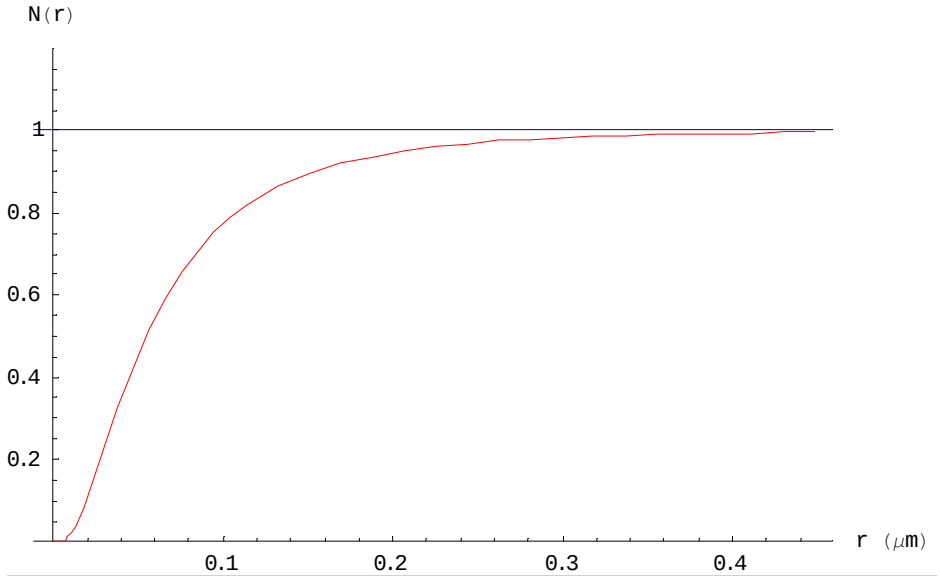

Figure 3.4. Normalized cumulative size distribution function for rural aerosols

The values of the parameters that characterize this population are:

- mode radius (r_M) and the standard deviation (σ); the values come from [WCP-112, 1986]
- minimum radius (r_{min}), maximum radius (r_{max}) and total particle density (N) for the month of January, 15 percent relative humidity and grid point at 5º latitude and -5º longitude

Table 3.1. Parameter values for the size distribution function of water-soluble particles

WATER SOLUBLE PARTICLES	
Mode radius, r_M (μm)	0.0285
Standard deviation, σ (μm)	2.239
Minimum radius, r_{min} (μm)	10^{-4}
Maximum radius, r_{max} (μm)	20
Total number density, N (cm^{-3})	5000

The probabilistic interpretation of the aerosol properties is the essence of the MCRT method. In order to decide the radius of each aerosol, a random number uniformly distributed between zero and unity, is drawn and compared to the probability of having an aerosol of radius r^* according to the normalized cumulative size distribution function

$$R_r \equiv \frac{\int_{10^{-4}}^{r^*} n(r)dr}{\int_{10^{-4}}^{20} n(r)dr} \tag{3.2}$$

A total of 10,000 aerosols were assigned a radius applying this technique. In order to verify the accuracy of this system, Figure 3.5 presents a histogram of the frequency with which an aerosol was assigned a certain radius.

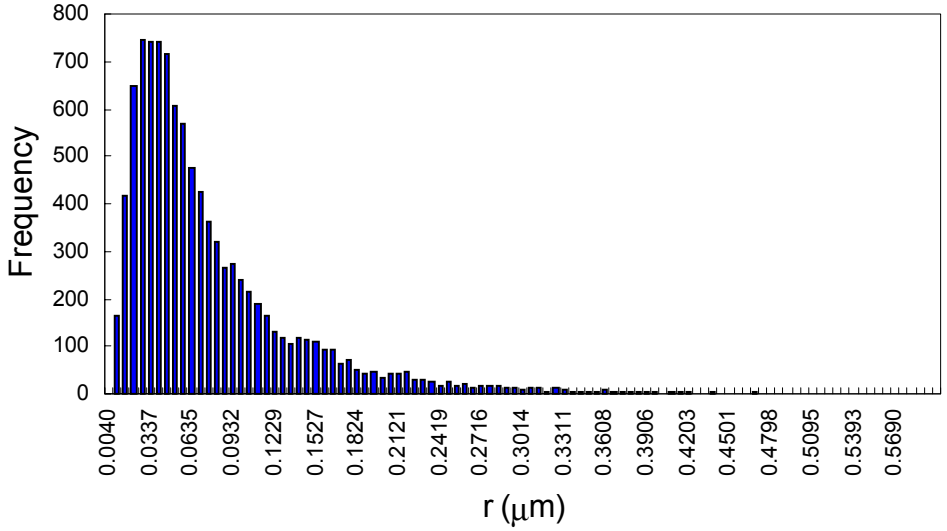

Figure 3.5. Random radius frequency

The frequency distribution attains a peak at a radius of approximately 0.03 μm, precisely the value expected by the log-normal distribution proposed.

The accuracy of the performance of the preprocessing code is better appreciated in Figure 3.6. In Figure 3.6, the blue curve is the normalized cumulative log-normal size distribution function, the same curve presented earlier in Figure 3.4, and the red circles

are the values of normalized cumulative number of aerosols of a given radius, assigned by the preprocessing code.

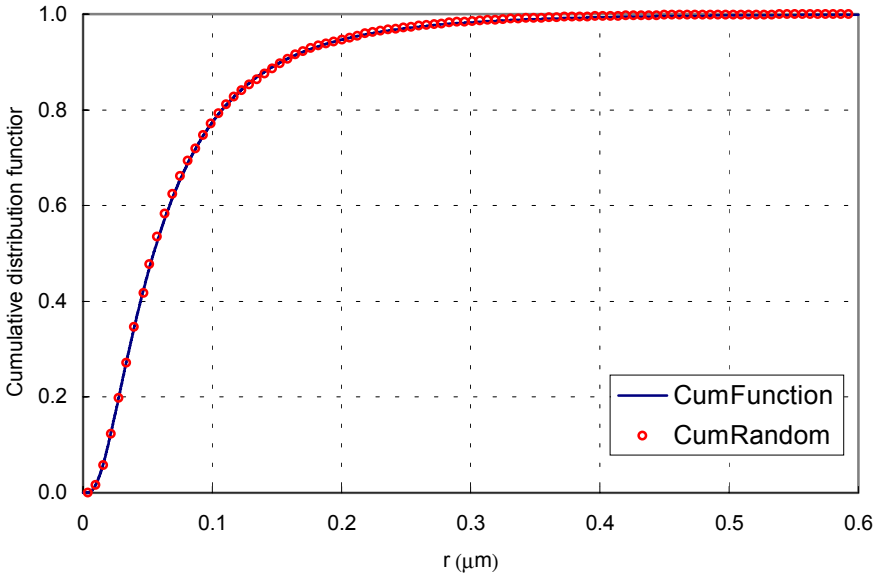

Figure 3.6. Normalized cumulative lognormal distribution function and the randomly assigned radius

The results obtained by this procedure are considered correct; hereby this property will be used to probabilistically interpret any required aerosol property.

The aerosols are uniformly distributed within the control volume. The dimensions of the cube are sufficiently small that the vertical and horizontal positioning of the aerosols have no significance, thus no vertical or horizontal weighting is assigned. Instead, the next two random numbers are drawn so that

$$x = x_0 + R_x \Delta x \tag{3.3}$$

$$y = y_0 + R_y \Delta y \tag{3.4}$$

$$z = z_0 \tag{3.5}$$

where Δx and Δy are the dimensions of the cube in centimetres and x_0, y_0 and z_0 are the coordinates of the source plane also in centimetres.

Complete vertical distribution retrievals exits for most aerosol types in the literature. A vertical-specific distribution can easily be accounted for in this preprocessing data generation step.

3.2.2 Methodology: MCRT method description

The simulations performed in this study launch the energy bundles vertically downwards from a square plane source lying directly above the cube with its edges aligned with the x- and y-axes as illustrated in Figure 3.7. Each of the rays is followed from its source point until it leaves the cube. The energy bundle might encounter an aerosol, in which case it will either be scattered, in Figure 3.7 ray A, or absorbed, ray B, or the ray might pass through the cube without striking any particle, ray C.

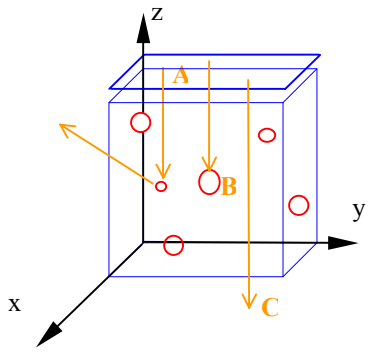

Figure 3.7. Ray tracing through an atmospheric cube in Cartesian coordinates

In our effort to create the most efficient model, two editions of the MCRT method were created, a spectral version and a band-averaged version.

3.2.3 Spectral MCRT in a participating media

This section describes the spectral edition of the MCRT applied to a scattering, absorbing, nonemitting one-centimeter atmospheric cube.

Special relevance was given to the user accessibility to the code; this way, a user-friendly interface was created to ease the initialization of all the variables. The initialization module assigns values to the seeds for the pseudo-random number generator, and determines the total number of energy bundle to be launched, and the initial direction of the rays.

The flowchart for the spectral MCRT simulation is presented in Figure 3.8.

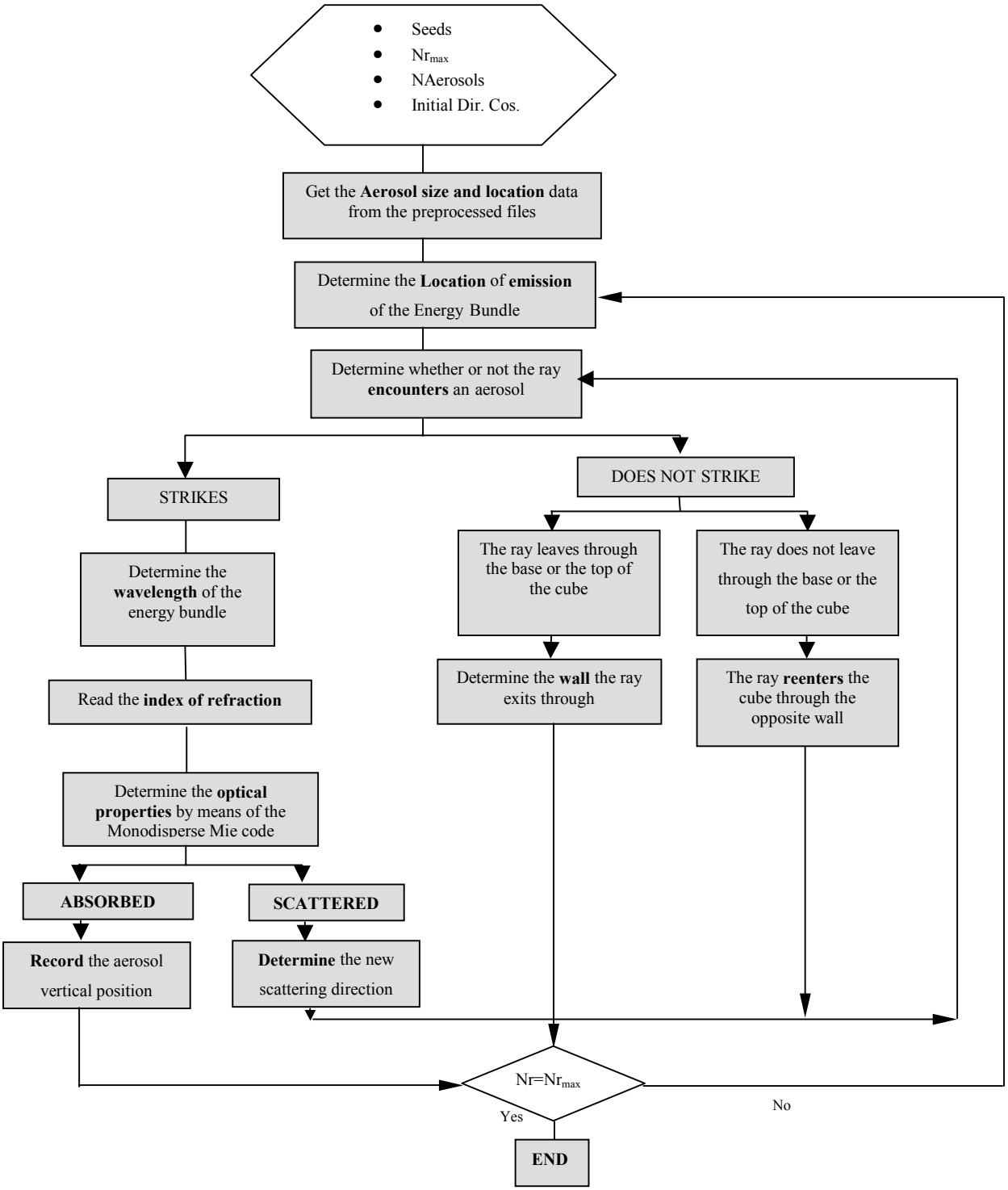

Figure 3.8. Flowchart of the spectral MCRT in a participating media

A line, whose direction is determined by the direction cosines, represents the path followed by the energy bundle. As shown in Figure 3.9, the direction cosines are the cosine of the angles that the ray forms with the Cartesian axes.

$$l = \cos(\alpha) \tag{3.6}$$

$$m = \cos(\beta) \tag{3.7}$$

$$n = \cos(\gamma) \tag{3.8}$$

The equation of the path followed by an energy bundle emitted at point a in the direction of point b would be

$$\frac{x_b - x_a}{l} = \frac{y_b - y_a}{m} = \frac{z_b - z_a}{n} \tag{3.9}$$

A ray launched from the origin of the Cartesian coordinate system is shown in Figure 3.9 to illustrate the geometrical meaning of the direction cosines.

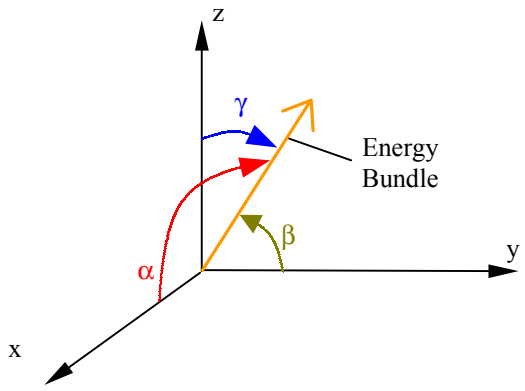

Figure 3.9. The angles formed by an energy bundle with the Cartesian coordinate axis

From Equation 3.9 it is easy to appreciate that the sum of the squares of the direction cosines must always add up to unity, and the cosines themselves, by definition, must have a value within the range [-1, 1]. We use these properties to verify that the code is calculating the right values.

The simulations described in this research launch collimated solar rays vertically downwards. This means that the initial direction cosines of each of the rays are always [0, 0, -1]. It is trivial to make the source not collimated and assign random initial cosine directors to the energy bundles. Despite the fact that the sun does not emit collimated light, the distance between the source, in this case the sun, and the receptor, in this case the terrestrial atmosphere is so great that the hypothesis is acceptable.

In the next step, the program acquires the physical characterization of the aerosols, position and radius, from the preprocessed 'AerRadLoc' data table.

To determine whether or not the ray encounters an aerosol as it traverses the atmospheric cube, the equation of a sphere centered on the position of each of the aerosols and with a radius equal to that of the aerosol, and the equation of the ray, are solved simultaneously for each of the aerosols. If the system of equations has a real solution, the distance between the source point and the aerosol is temporary stored and the next aerosol-sphere is checked. If more than one real solution is found, the aerosol nearest to the source point is selected.

Since the mean radius of the aerosols is 0.0285 μm; the probability that a line of differential diameter will intersect such a small sphere is remote. Representation of the energy bundles as lines is a simplifying hypothesis; the energy bundles are in reality electromagnetic waves of certain amplitude. The problem that arises from this hypothesis

is that only a few rays actually strike aerosols, the sampling obtained is insufficient. The application of the MCRT method is inefficient and impractical. In order to address the problem a new parameter is introduced, *pcsr* that stands for probable cross-section radius. The optimization of pcsr is explained in detail in Chapter 4. The pcsr is a unitless parameter that, added to the actual radius of the aerosols, produces a virtual collision cross-section of the spheres bigger than the real one. This greatly increases the probability of a strike. Other possible solutions to increase the efficiency of the method would be either to launch a significantly higher number of rays or to simulate the energy bundles as cylinders. The first possibility boosts the simulation CPU time drastically. The second possibility complicates the calculi appreciably.

The relationship between the radius of the aerosol r, and the probable cross section radius r′, is

$$r' = r \cdot (1 + pcsr) \tag{3.10}$$

Let us imagine that the numbers we are playing with are lucky and that the ray does encounter an aerosol as it passes through the cube. Now, it is necessary to optically characterize this ray, that is to say, to assign a wavelength to the ray.

We only assign a wavelength to the "lucky" rays, in order to save CPU time. The procedure to assign a wavelength to the energy bundles is analogous to that of assigning a radius to the aerosols. The next available random number is drawn, and matched to the probability of having an energy bundle of wavelength λ^* according to the normalized solar emissive power cumulative function

$$R_\lambda = \frac{\int_{\lambda_{\min}}^{\lambda^*} e_{\lambda b}(\lambda)d\lambda}{\int_{\lambda_{\min}}^{\lambda_{\max}} e_{\lambda b}(\lambda)d\lambda} \tag{3.11}$$

where $e_{b\lambda}(\lambda)$ is the Planck blackbody spectral emissive power distribution function and R_λ is a random number uniformly distributed between 0 and 1.

The index of refraction of the aerosols is wavelength dependent; therefore, the next logical step is to find the index of refraction corresponding to the wavelength just generated. However, the index of refraction is not available as a wavelength dependent function. Instead, only index values for certain wavelengths are known. These values were presented earlier in Figure 2.5.

In order to estimate the corresponding value of the index of refraction, we could either use a regressive technique to estimate the function for the whole spectrum and assume the approximation error, or sacrifice some CPU time and apply a look-up table method. The second alternative was adopted in this study. First, given a certain wavelength, the values of the indices of the immediately lower and immediately upper wavelengths are found. Then, the final index value is determined by linear interpolation between these two points. The name of the index of refraction look-up table file is "IndexRefractionData". It can be found in Appendix A.

Next, the optical properties of the aerosols are determined. As the scattering is independent, the scattering effects of each particle can be determined independently of the surrounding aerosols. The monodisperse Mie scattering theory calculates the scattering and absorption coefficients and the scattering phase function given the radius and the index of refraction of the aerosol and the wavelength of the energy bundle.

The "lucky" ray can either be absorbed or scattered by the aerosol. Once the absorption and the scattering coefficients are known, the next random number is drawn. If the random number is less than or equal to the ratio between the absorption coefficient and the extinction coefficient then the ray is absorbed, otherwise the ray is scattered

$$R_{abs} \leq \frac{\sigma_{abs,\lambda}}{\sigma_{ext,\lambda}} \tag{3.12}$$

where R_{abs} is the next random number.

If the ray is absorbed, the vertical position of the absorbing aerosol is recorded and the number of rays absorbed at that height is incremented.

Suppose that the ray is scattered. The next step is to determine the direction of scattering.

It was stated in Chapter 2 that the scattering of unpolarized light is independent of the azimuthal angle. Therefore, the azimuthal, or clock, angle ϕ, is uniformly distributed between 0 and 2π according to

$$\phi = 2\pi R_{\phi} \tag{3.13}$$

where R_{ϕ} is a random number uniformly distributed between zero and unity.

The zenith, or cone, angle θ however, is not uniformly distributed between zero and π. The scattering phase function indicates the directional distribution of scattered light. To determine the new scattering zenith angle, the next random number is equated to the probability of having the ray scattered with a zenith angle θ^*, according to the normalized cumulative scattering phase function

$$R_\theta = \frac{\int_0^{\theta^*} p(\theta)\sin(\theta)d\theta}{\int_0^{\pi} p(\theta)\sin(\theta)d\theta} \tag{3.14}$$

Equation 3.14 can be obtained from Equation 2.13 substituting the differential of the solid angle according to

$$d\Omega = \sin(\theta)d\phi d\theta \tag{3.15}$$

Both sinθ and p(θ) are independent functions of the azimuthal angle. Integrating Equation 3.15 for ϕ from zero to 2π, we obtain

$$\int_{\phi=0}^{2\pi}\int_{\theta=0}^{\pi} \sin(\theta)d\phi d\theta = 2\pi \int_{\theta=0}^{\pi} \sin(\theta)d\theta \tag{3.16}$$

Equation 3.16 can be introduced into Equation 2.13 to obtain Equation 3.14.

Once the scattering angles have been estimated, the direction of the scattered ray is calculated. Considering the center of the aerosol as the origin of the local coordinate system, the direction cosines of the scattered ray represented by a unit vector are

$$n_{local} = \cos\theta \tag{3.17}$$

$$l_{local} = \sin\theta\cos\phi \tag{3.18}$$

$$m_{local} = \sin\theta\sin\phi \tag{3.19}$$

The relationships shown in Equations 3.17, 3.18 and 3.19 are illustrated in Figure 3.10.

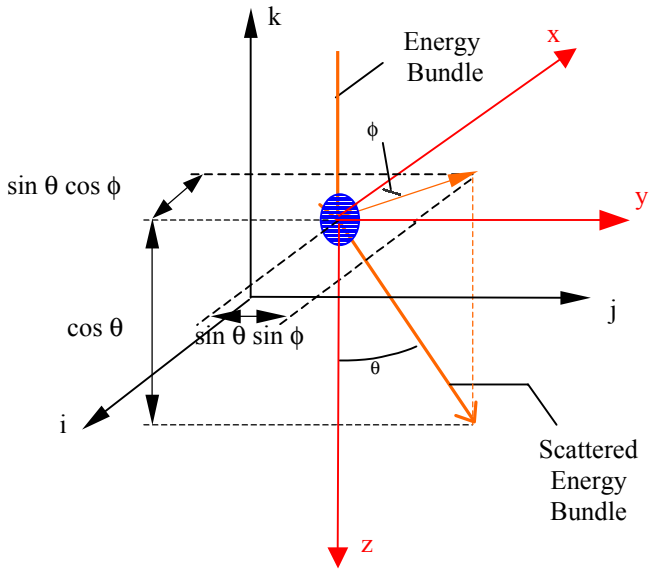

Figure 3.10. Illustration of the relationships between the direction cosines and the scattering angles

It is very important to realize that both angles ϕ and θ are referred to a local coordinate system. It is therefore necessary to transform the destination point from local to global coordinates. This transformation is done by the subroutine called "Local" and it is a two-step process. First, the local axes, x, y and z are calculated. The origin of the local coordinate system is placed at the centre of the aerosol struck by the energy bundle.

When building a coordinate system, the position of the first axis is irrelevant; that is why we arbitrary allow our local z-axis to be parallel to the incoming ray. The unit vector that represents the local z-axis is calculated according to

$$\vec{z} = \frac{DesPG - OriPG}{|DesPG - OriPG|} \tag{3.20}$$

where DesPG stands for DEStination Point in Global coordinates; that is to say, the center of the struck aerosol; and OriPG stands for the ORIgin Point in Global

coordinates, that is to say, the source point in case of a new ray, or the centre of the former scattering aerosol in case of a multiple scattered energy bundle.

The local y-axis is perpendicular to the plane formed by the local z-axis and the unit vector in the direction of the global x-axis, $\vec{i}$, according to

$$\vec{y} = \frac{\vec{z} \times \vec{i}}{\left| \vec{z} \times \vec{i} \right|} \tag{3.21}$$

If the magnitude of the cross product between $\vec{z}$ and $\vec{i}$ were zero, the local y-axis would be calculated perpendicular to the plane formed by the local z-axis, $\vec{z}$, and the unit vector in the direction of the global y-axis, $\vec{j}$. If $\left| \vec{z} \times \vec{i} \right|$ were still zero, the unit vector in the direction of the global z-axis, $\vec{k}$, would be used.

Finally, the local x-axis needs to be perpendicular to the plane determined by the local z- and y-axes

$$\vec{x} = \frac{\vec{z} \times \vec{y}}{\left| \vec{z} \times \vec{y} \right|} \tag{3.22}$$

Again, the denominator of Equation 3.22 is pre-evaluated to make sure that no division by zero is required from the program.

Once the local coordinate system axes are calculated, the new direction cosines are transformed from local to global coordinates by multiplying them by the rotational matrix.

$$\begin{pmatrix} x_x & y_x & z_x \\ x_y & y_y & z_y \\ x_z & y_z & z_z \end{pmatrix} \begin{pmatrix} l_{local} \\ m_{local} \\ n_{local} \end{pmatrix} = \begin{pmatrix} l_{global} \\ m_{global} \\ n_{global} \end{pmatrix} \tag{3.23}$$

At this point, the line that represents the direction of the new scattered ray is completely defined, the direction cosines in global coordinates are known, and the center of the scattering aerosol becomes the origin point of this scattered ray. The code re-evaluates to see if this redirectionated ray strikes an aerosol or if it leaves the cube.

This time two precautions are required when evaluating extinction. On the one hand, the last scattering aerosol, which is always going to be a candidate, needs to be skipped. This can be accomplished by comparing the candidate coordinates with the origin point coordinates. If they were the same to within some specified tolerance, the candidate point would be rejected. On the other hand, any back candidate needs to be eliminated as well. A back candidate would be any aerosol placed behind the origin point, yet along the line of the scattered energy bundle. A back candidate can easily be detected and eliminated because the distance between a back candidate and the origin point would always be negative.

Suppose now that the energy bundle does not encounter any more aerosols before reaching one of the walls. In this case, the energy bundle abandons the cube, and the next step is to determine the wall it would leave through.

If the ray exits the cube through one of the sidewalls, the program has the ray reenter the same cube through its symmetric point on the opposite wall, with the same direction cosines. The goal is to eliminate the divergence engendered by scattering. That is, we

assume that the cube in a segment of an infinite plane layer. Gauss divergence theorem states that

$$\int_v \nabla \vec{v} dV = \int_s \vec{v} \cdot \vec{n}\, dS \tag{3.24}$$

where $\vec{v}$ is a vector and $\vec{n}$ is the normal to the surface. If $\vec{v}$ represents the energy bundle and $\vec{n}$ and $\vec{n}'$ are the normal to the walls, then the normal vectors are related according to

$$\vec{n} = -\vec{n}' \tag{3.25}$$

Thus, the sum of the cross product between the exit ray and the normal to the exit sidewall and the cross product of the same vector and the normal to the opposite sidewall add up to zero. Figure 3.11 illustrates this idea.

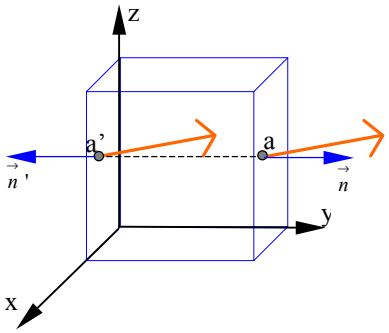

Figure 3.11. Elimination of the scattering divergence

Otherwise, if the ray leaves through the top or the bottom walls, the counter for the number of energy bundles launched is incremented and a new ray is traced.

When a sufficient number of rays has been traced, the simulation is terminated.

This is basically the MCRT method applied to an atmospheric cube with a given aerosol population. A goal of this study was not only to create this tool, but also to make it as efficient as possible. The Mie scattering module is undoubtedly the most time consuming subroutine in the whole code. In the spectral MCRT version of the code, the Mie scattering module is executed every time a ray is extinct. In order to reduce the total CPU time required by this model, a band-averaged MCRT version of the code was created. In a Band-averaged MCRT version the optical properties are preprocessed. The differences between the spectral and the band-averaged simulations are explained in the next section. The optimization of the band-averaged code is discussed in detail in the next chapter.

3.2.4 Band-averaged MCRT method in a participating media

The schema of a band-averaged MCRT is basically the same as in the spectral MCRT simulation. However, in the band-averaged simulation, the optical properties of the aerosols are pre-processed and stored in look-up tables. When an energy bundle encounters an aerosol, the code classifies the radius and the wavelength into bins of a prefixed width. Then the corresponding look-up table is determined and the optical property values are read and brought back to the main code to continue with the simulation.

In this study, the radius range from 10^{-4} to 20 μm is divided into 0.01 μm wide bins, and the wavelength range from 0.2 to 40 μm, is divided into 0.1 μm wide bins. The accuracy

of this approach is directly proportional to the width of the bins. The finer the bins, the closer the simulation will be to the spectral simulation.

Figure 3.12 shows the flowchart of a band-averaged MCRT simulation applied to a absorbing, scattering, non-emitting atmospheric cube. The differences with the spectral flowchart in Figure 3.8 are highlighted in red to clearly differentiate it from the flowchart in Figure 3.12.

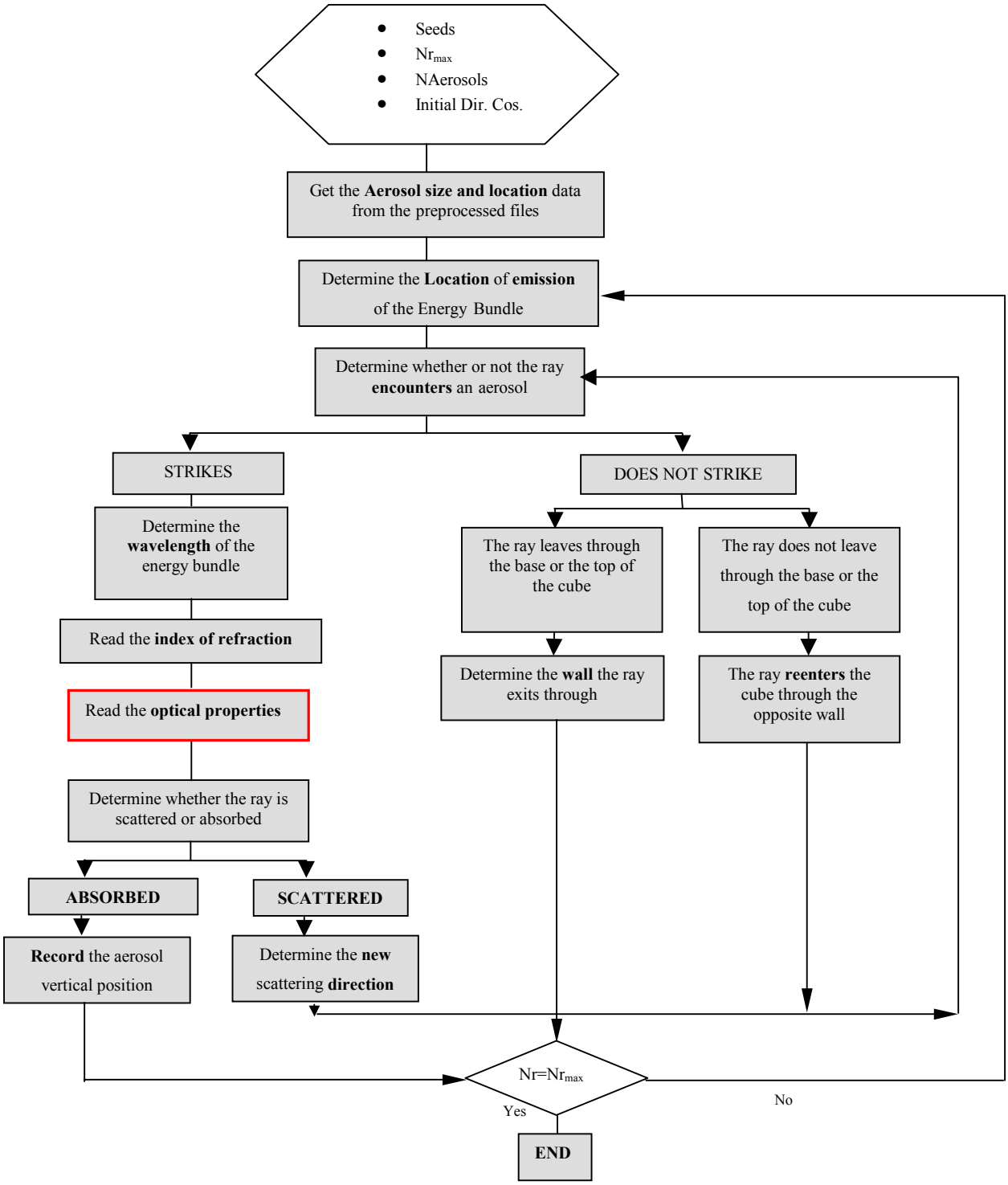

Figure 3.12. Flowchart of the band-averaged MCRT in a participating media

3.2.5 Spectral and band-averaged MCRT models efficiency comparison

The main objective behind using a band-averaged MCRT version instead of a spectral simulation is time economy. Despite the fact that, nowadays, computer speed increases constantly, and most studies are willing to trade speed for accuracy, when the number of rays becomes of the order of millions, the time saved is remarkable. The difference in CPU time is plotted versus the number of rays in Figure 3.13.

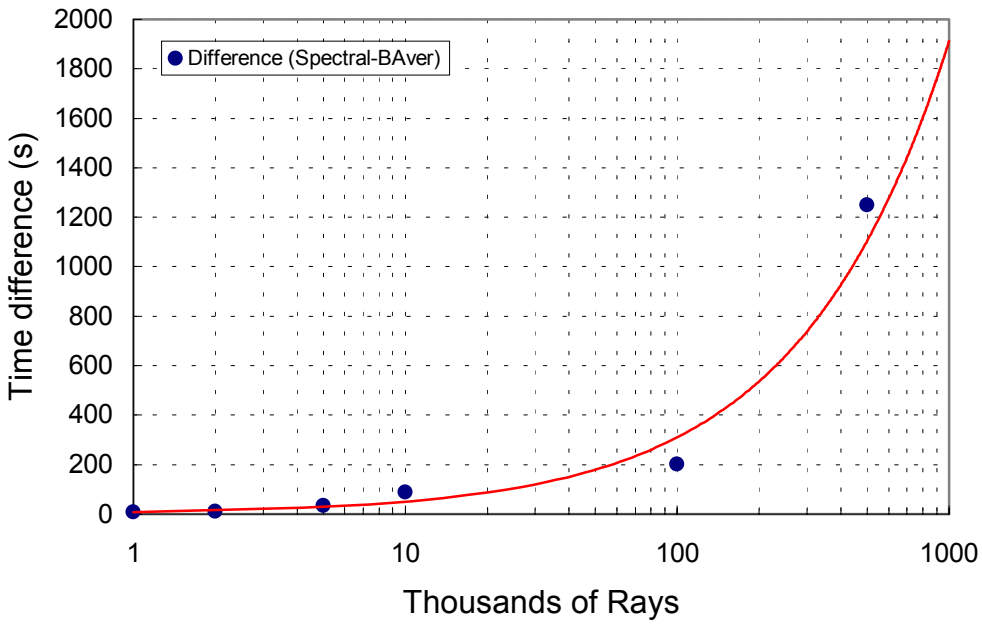

Figure 3.13. CPU time difference between the spectral and the band-averaged simulations

The red curve is the trend line, forecasting the difference in CPU time for a 1 million-ray performance that will be more than half an hour every million of rays.

These simulations were carried out using an Intel Pentium® II 450 MHz processor with 160 Megabytes of RAM operating under Windows® 98.

This chapter is a general description of the MCRT method applied to a participating media. The validation of the band-averaged MCRT version of the code and the optimisation of the pcsr parameter are widely discussed in the next chapter.

Chapter 4 Model Optimization

"I have had my results for a long time: but I do not yet know how I am to arrive at them".

Karl Friedrich Gauss (1777-1855). In A. Arber,

The Mind and the Eye, 1954.

In Chapter 3 the convenience of using a band-averaged version of the MCRT model was discussed in terms of time economy. In the present chapter the results obtained from the spectral and the band-averaged version simulations are contrasted. The goal is to determine the accuracy of the band-averaged MCRT method adaptation, as well as the minimum number of rays necessary for convergence.

The performance of the codes is validated by comparison with results from the literature in the first section of this chapter. The second section of the chapter is dedicated to outlining the process of optimization of the pcsr parameter. The third section discusses the results from a spectral and a band-averaged set of experiments. In the final section, we reflect on the conclusions drawn from this chapter.

4.1 Mie Theory code validation

The key for a correct performance of the MCRT code is to optimize the following:

- the Mie scattering theory subroutine, which defines the directional distribution of the scattered rays, as well as the ratio of rays absorbed to rays extinct
- the value of the pcsr parameter, which controls the ratio of rays that undergo extinction to the number of rays launched

Two interpretations of the Mie scattering theory were available for this study:

- a monodisperse version, whose FORTRAN90© code called 'uno' is included in Appendix A
- A polydisperse version whose FORTRAN90© code called 'pri' is also included in Appendix A

The Mie codes were developed at the Laboratoire d'Optique Atmosphérique of the Université des Science et Technologie de Lille (France).

The polydisperse version considers that the population of aerosols adjusts to a log-normal size distribution and that scattering is multiple; that is, more than one scattering event per ray absorbed or scattered occurs. The user specifies the parameters that characterize the aerosol log-normal size distribution, namely the minimum, maximum and mode radius and the standard deviation. The polydisperse code can only be applied to monochromatic radiation as it requires the index of refraction of the particles as an input and the index of refraction is a function of wavelength.

The polydisperse Mie code provides the values of the scattering, absorption and extinction coefficients, the single scattering albedo, the asymmetry factor, the scattering phase function and the degree of linear polarization. The cross section values are normalized to a one-particle density. The scattering phase function is not calculated for zenith angles of a constant step (for example 0, 2, 4..). Instead, it is calculated for specific angles, named Gauss angles, their cosine provided to the Mie code from file 'nmu192'. The reason behind calculating the phase scattering function at the Gauss angles is that the integration of the scattering phase function over scattering angles is more precise using the Gauss method. The polydisperse Mie code also creates a file, 'redl02550', for the development of the scattering phase function in terms of Legendre polynomials necessary to solve radiative transfer problems.

The intention of this study is to prepare a tool to analyze the feedback mechanism between solar radiation and photolytic aerosols and its sensitivity. As declared in the introduction is extremely important to account for the radius of each of the aerosols in particular, as well as the relative position of the aerosol within the column. The size distribution might vary with time, and eventually it will not adjust to a log-normal size distribution.

If the scattering is independent, as it is in this case, the monodisperse Mie theory code can be executed for every strike accounting for the physical properties of each specific aerosol. Furthermore, with this method, the index of refraction of the aerosol at the wavelength of the striking energy bundle can easily be retrieved from a look-up table, so that polychromatic radiation can be simulated. These conditions enable a microscopic analysis of the radiative effects of aerosols on the solar radiation field.

As indicated in the flowchart of Figure 3.8, the spectral MCRT code calls the monodisperse Mie subroutine for every strike. Similar to the polydisperse code, the outputs of the Mie subroutine are the absorption, scattering and extinction cross sections and the scattering phase function for specified angles, provided to 'uno' from file 'donmie'.

The validity of the polydisperse Mie theory code is verified by comparing its result with results from the literature. The results provided by the monodisperse Mie theory code are adjusted to those obtained from the polydisperse version by optimizing the value of pcsr.

The values of single-scattering albedo obtained from the polydisperse Mie theory code were compared against values found in the bibliography [D'Almeida, 1991].

Call from Chapter 2 that the single scattering albedo is the ratio between the scattering coefficient and the extinction coefficient. The scattering coefficient σ_{scatt} (m^{-1}), is related to the scattering cross section σ_{scatt}^{part} (m^2), according to

$$\sigma_{scatt}^{part} = \frac{\sigma_{scatt}}{N} \tag{4.1}$$

where N is the number density of the particles.

Similarly, the absorption coefficient is related to the absorption cross section according to

$$\sigma_{abs}^{part} = \frac{\sigma_{abs}}{N} \tag{4.2}$$

Figure 4.1 presents the single-scattering albedo values obtained from both sources for a wavelength range from 0 to 40 μm. The blue line is the single-scattering albedo from the polydisperse Mie scattering model. The red circles are the discrete data points found in the literature. The red circles lay perfectly on the curve generated by the polydisperse code. The correctness of the polydisperse code is therefore demonstrated.

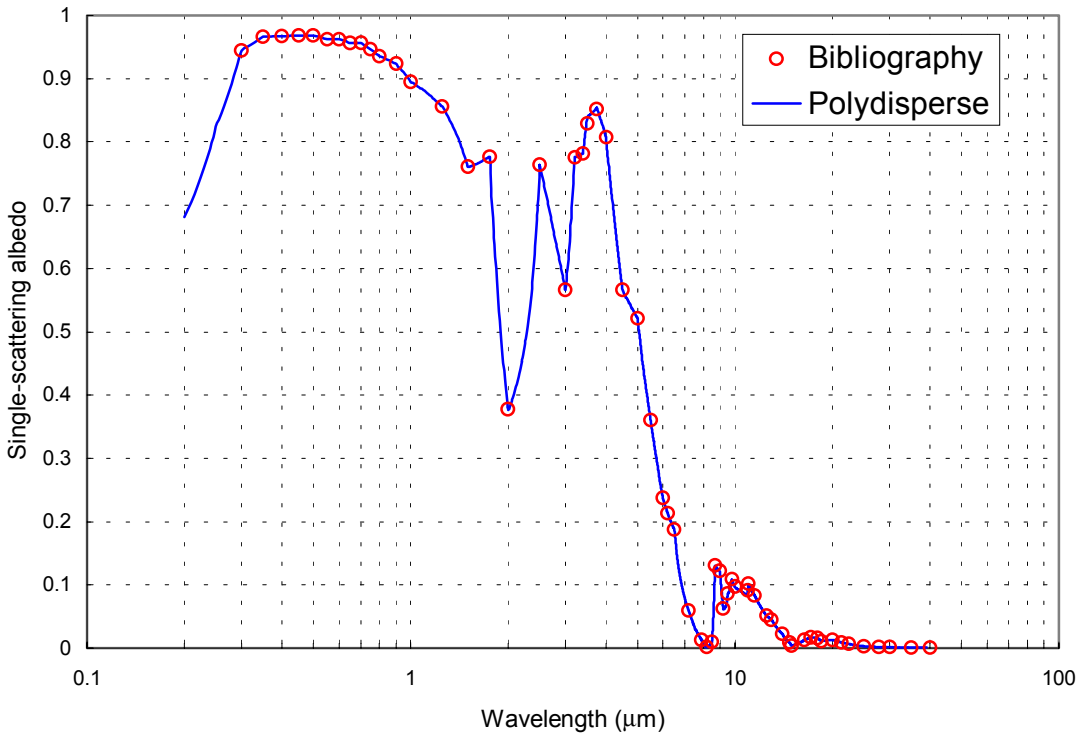

Figure 4.1. Single-scattering albedo as a function of wavelength for rural aerosols

4.2 Optimization of pcsr

The goal is to reproduce the phase scattering function of the polydisperse Mie code by means of the band-averaged microscopic MCRT method. Once this is accomplished, the band-averaged version, which is more flexible, will be available for the intended study.

Figure 4.2 shows the scattering phase function for the population of clean continental aerosols described in Chapter 3 according to the polydisperse Mie scattering theory, from a macroscopic analysis, at wavelength 0.5 µm. It shows a predominant forward scattering and only a slight back scattering.

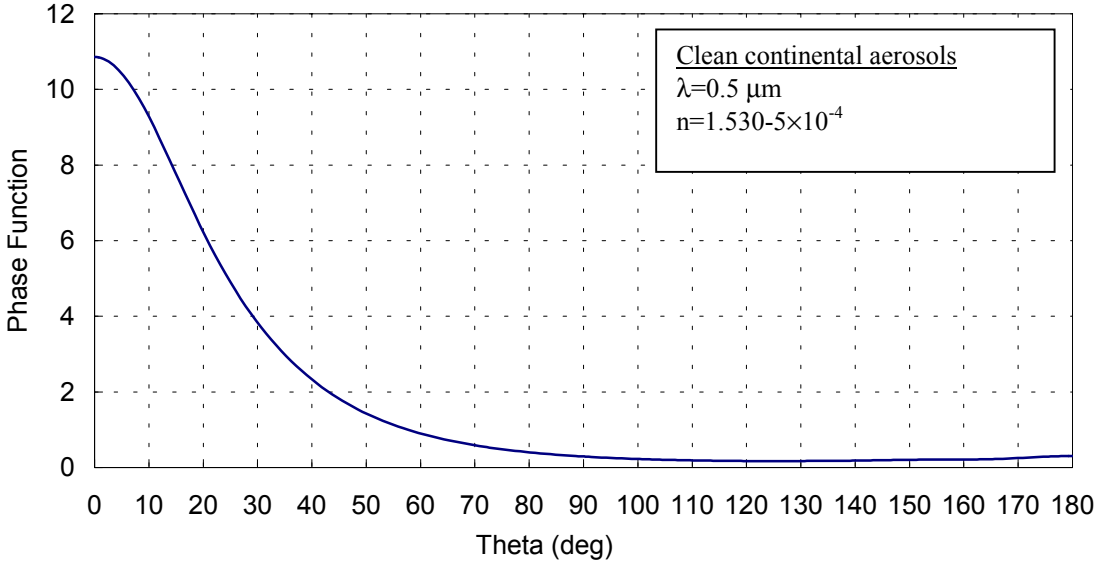

Figure 4.2. Scattering phase function from the polydisperse Mie scattering code [pri] for clean-continental aerosols

The diagram in Figure 4.3 shows the process of optimization of pcsr. First, the parameter pcsr is assigned an initial value. Then the microscopic MCRT code is run, scattering divergence is allowed since we are seeking to reproduce the directional distribution of the scattered light. The empirical monodisperse (microscopic) scattering MCRT phase function is compared with the theoretical macroscopic polydisperse scattering phase function. The value of pcsr is modified according to the results. A new simulation is run until the polydisperse and the monodisperse scattering phase functions converge within a certain tolerance.

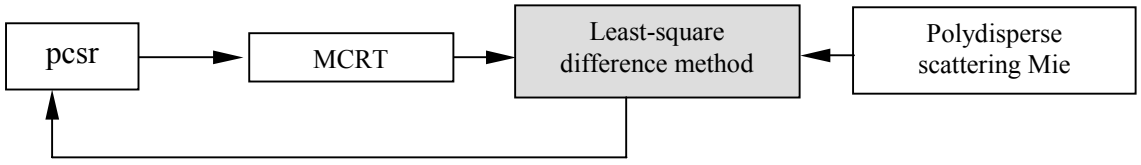

Figure 4.3. Flowchart of the pcsr optimisation process

In Chapter 3, the scattering phase function was defined as the ratio of the energy scattered from the incident direction s, into the outgoing direction s', to the energy that would have been scattered into that outgoing direction s', if the scattering had been isotropic.

In the MCRT method, the scattering phase function is interpreted as the ratio of the number of rays scattered into a certain direction to the number of rays scattered into that same direction when the scattering is isotropic. For isotropic scattering, the scattering phase function is constant and equal to unity; that is, light is scattered equally into all directions. Manipulating Equation 3.14, it can be shown that the isotropic scattering zenith angle can be probabilistically interpreted as

$$\theta = \cos^{-1}(1 - 2R_\theta) \tag{4.3}$$

where R_θ is a random number uniformly distributed between zero and unity.

4.2.1 Experimental scattering phase function

We thought about two possible ways to calculate the scattering phase function from the microscopic MCRT results. The first one is known as the method of equal areas. The second one is called the isotropic method.

The method of equal areas supposes the scattering particle imbibed in an imaginary sphere whose radio is big enough as to regard the scattering particle as a point. After an isotropic MCRT method simulation, this imaginary surface will be covered by a uniform distribution of points, symbolizing the exit points of the energy bundles.

This means that if we divide the imaginary spherical surface into rings of equal area, each of these imaginary rings will contain the same number of scattered rays after an isotropic MCRT simulation.

In the method of equal areas the scattering phase function is calculated as the ratio between the number of rays that go out through each of the equal area rings after a non-isotropic MCRT simulation, to the number of rays that would have gone out through the same ring were the scattering isotropic; that is to say, divided by the ratio between the total exiting number of rays over the total number of imaginary rings.

The area of a circular cap is

$$A = 2\pi rh \tag{4.4}$$

where r is the radius of the sphere and h is the height of the circular cap.

To divide the area of the sphere into a certain number of equal area rings it can be proved that h is constant and equal to the diameter of the sphere divided by the total number of rings.

We called the other possibility to estimate the scattering phase function from the microscopic MCRT simulation, the isotropic method. The isotropic method consists on running the same MCRT case considering isotropic and non-isotropic scattering. Then estimating the number of rays that go out through every ring in each case. It is important to realize that this time the rings do not need to have equal areas. The scattering phase function is the ratio between the number of rays that goes out through a ring after the non-isotropic simulation to the number of rays that goes out through the same ring after the isotropic simulation.

The second possibility, the isotropic method, is preferred for this study and therefore applied for the results presented in this document.

4.2.2 Results

The pseudo-random number generator is initialized at the beginning of each simulation, maintaining the seeds constant. For the results presented in this work, the seeds were equal to 600 for seed number 1 and 700 for seed number 2.

A set of experiments was done for pcsr ranging from 0 to 5000. The results for pcsr equal to 700, 800, 900, 1000, 1100 and 1200 are shown in Figures 4.4, 4.5, 4.6, 4.7, 4.8 and 4.9, respectively. The difference between these simulations and results from the polydisperse scattering code is calculated in the least-square method sense. This is

$$E = \sum_{\theta=0}^{180} [f(\theta) - p(\theta)]^2 \qquad (4.5)$$

where p(θ) is the polydisperse scattering phase function and f(θ) is the MCRT approximation. The values of the differences are collected in Table 4.1.

Because the MCRT method over-samples the straightforward scattering, the sum of the square errors is calculated for two ranges, for θ between [0, 180] and, neglecting the first data point, for θ between [1, 181]. Observing the differences collected in Table 4.1, a value of pcsr equal to 900 appears to be near the optimum value. The number of rays that exit with a scattered zenith angle equal to zero is too high. However, due to the excellent convergence for the rest of the zenith angle range, we tolerate this discrepancy and conclude that the MCRT method proposed in this work can accurately represent the optical effects on the radiative field of an absorbing, scattering, non-emitting media.

Table 4.1. Least-square difference between the polydisperse scattering phase function and the MCRT results

Least-Square Difference						
Theta	700	800	**900**	1000	1100	1200
[0-180]	508.84	326.66	427.31	560.85	236.53	498.33
[1-180]	142.39	133.64	124.80	144.97	148.30	181.15

In Figures 4.4, 4.5, 4.6, 4.7, 4.8 and 4.9 the results from the polydisperse Mie scattering code are shown as well as the microscopic MCRT method simulation results for specific values of pcsr, applying the monodisperse Mie scattering code. The polydisperse Mie scattering code results are shown in each figure as a solid blue line.

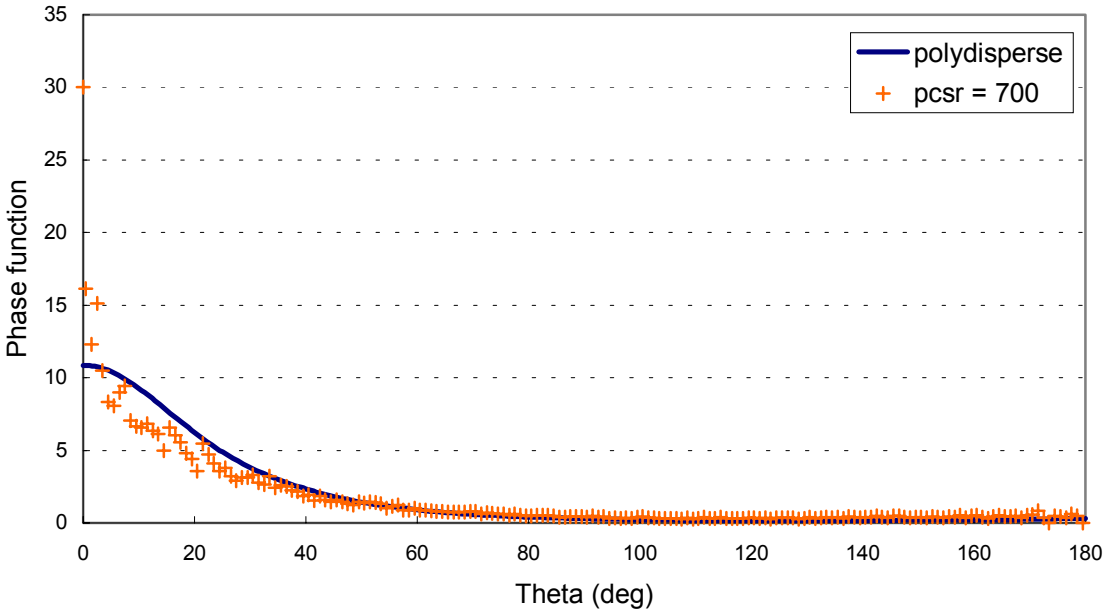

Figure 4.4. Comparison between the polydisperse scattering phase function and the MCRT simulation for pcsr 700

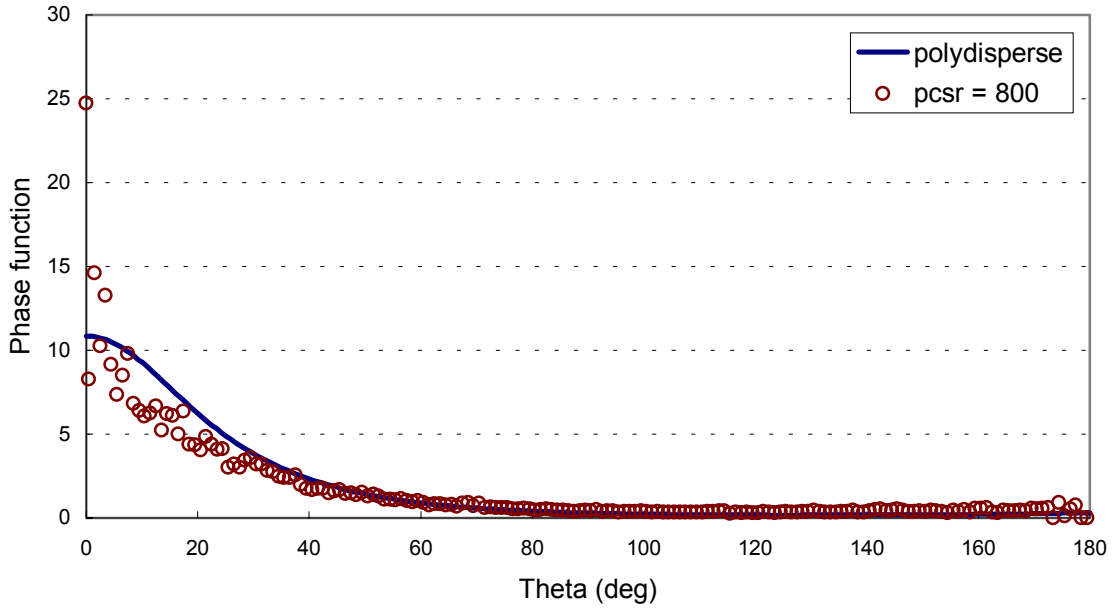

Figure 4.5. Comparison between the polydisperse scattering phase function and the MCRT simulation for pcsr 800

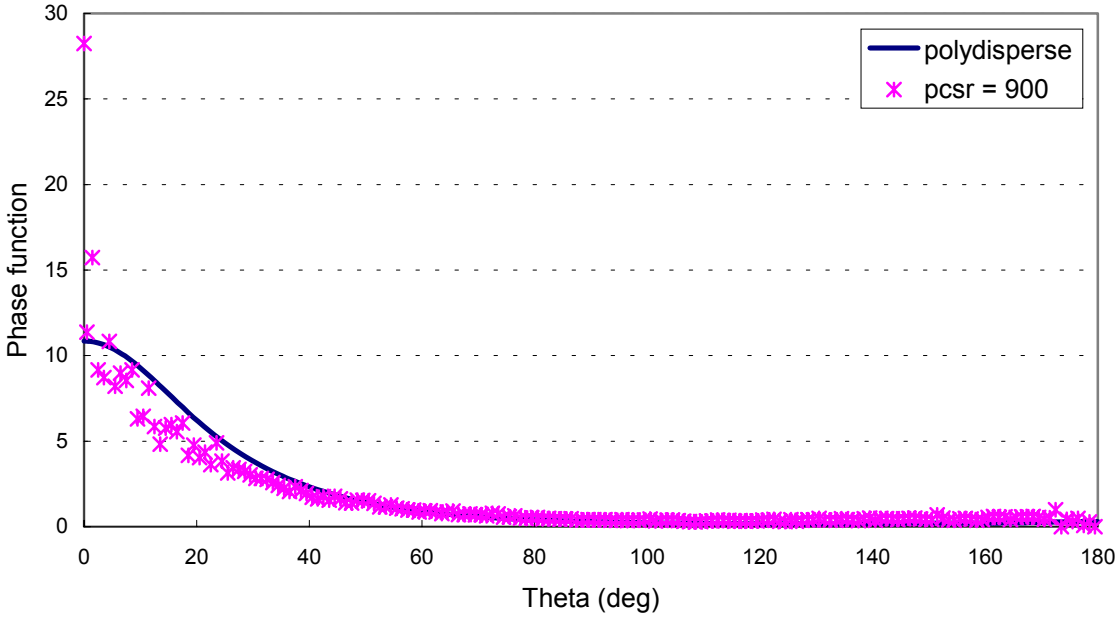

Figure 4.6. Comparison between the polydisperse scattering phase function and the MCRT simulation for pcsr 900

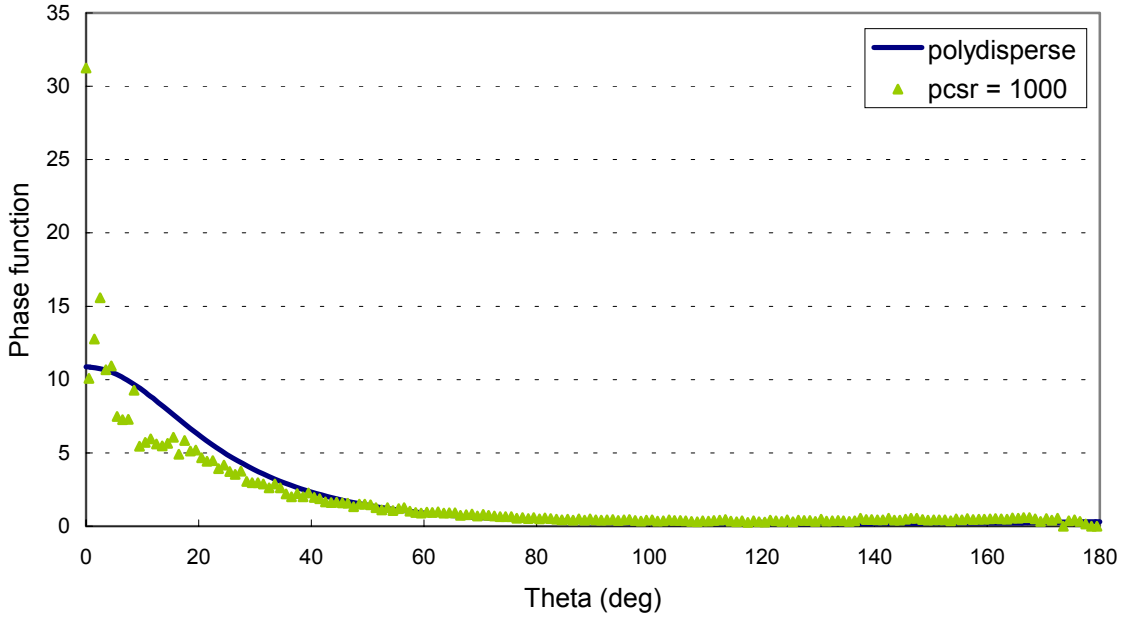

Figure 4.7. Comparison between the polydisperse scattering phase function and the MCRT simulation for pcsr 1000

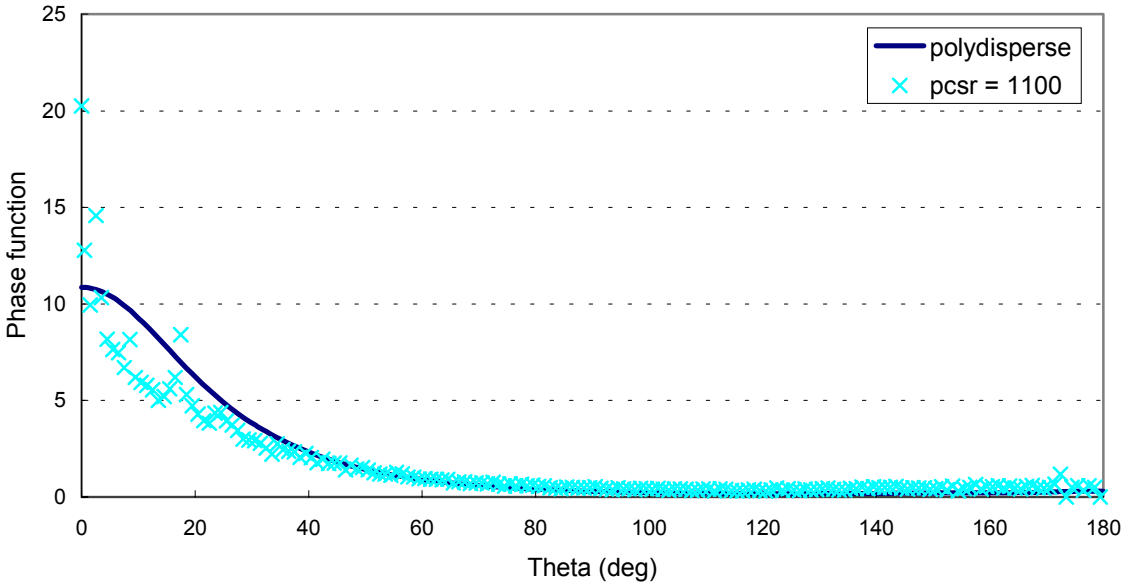

Figure 4.8. Comparison between the polydisperse scattering phase function and the MCRT simulation for pcsr 1100

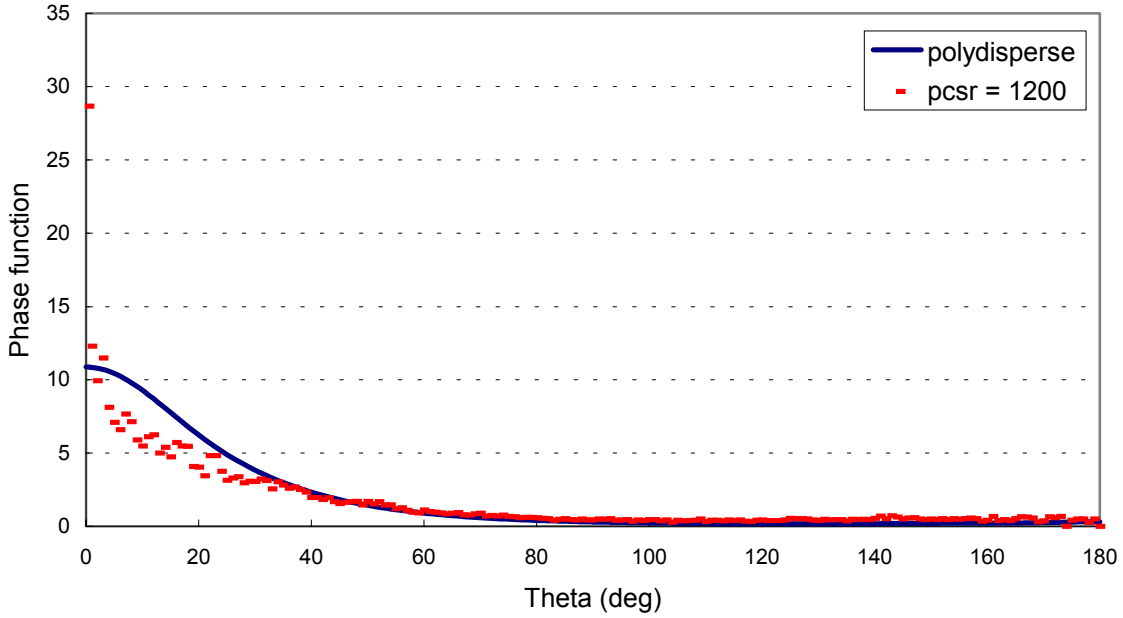

Figure 4.9. Comparison between the polydisperse scattering phase function and the MCRT simulation for pcsr 1200

Figure 4.10 is included to ease the visual comparison of the influence of the pcsr parameter. Figure 4.10 collects the results of the simulations for values of pcsr equal to 800, 900, 1000 and 1100. The violet squares that represent the results for pcsr equal to 900 are the closest to the theoretical value from the polydisperse Mie theory.

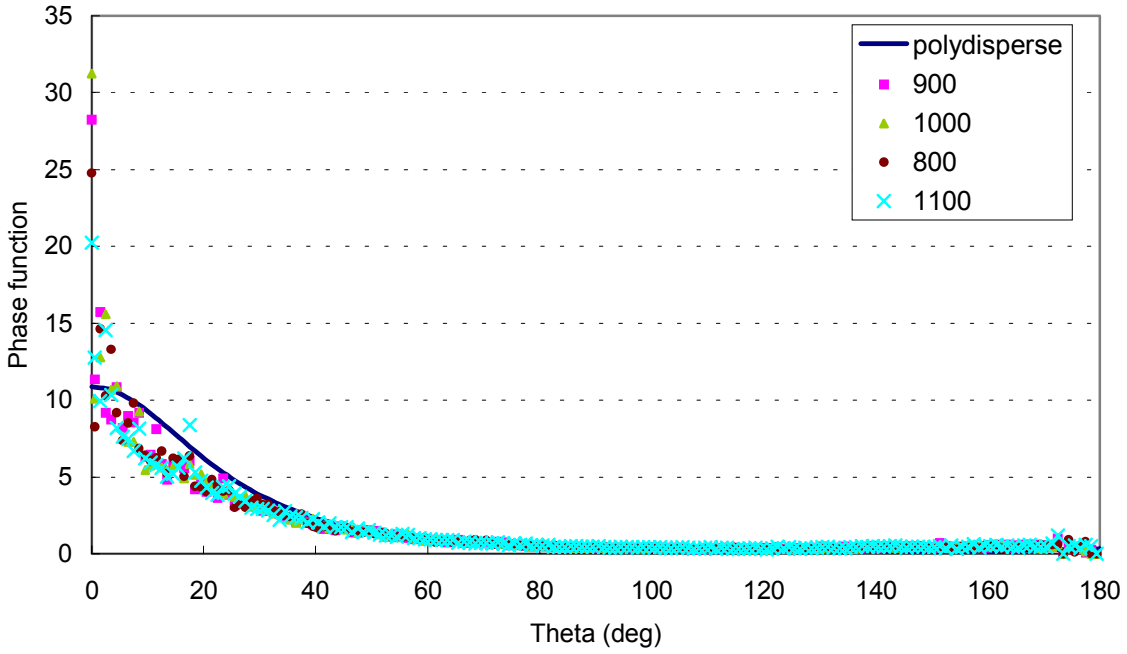

Figure 4.10. Comparison of the experimental results for the scattering phase function for different pcsr values

4.3 Band-averaged versus spectral MCRT

From the comparison between the band-averaged and the spectral simulation results, we may draw three conclusions:

- first, and most important, the results from both simulations are in adequate agreement
- second, convergence is verified
- third, the convenience of using the band-averaged model version over the spectral version is demonstrated

The conditions of the simulations are relaxed because the goal is only to contrast both versions of the MCRT code. On the one hand, scattering divergence is allowed in order to be able to visually compare the results from either version. On the other hand, pcsr is given a low value so that only single scattering is present. Also the simulations are

monochromatic with the value of the wavelength equal to the wavelength of maximum solar emissive power $\lambda_{max.}$ That is, λ equal to 0.5 μm.

The pseudo-random number generator is initialized with the same starting values in both the spectral and the band-averaged versions of the code. The results presented here were done for a value of seed 1 equal to 700 and a value of seed 2 equal to 800. Another set of similar experiments was done for seed 1 equal to 300 and seed 2 equal to 400. The conclusions were equivalent. Only the set of experiment results for seeds 700 and 800 is presented in this thesis.

The value of pcsr is set to 200. This pcsr assures an efficiency of 6 percent maintaining a single-scattering atmosphere. That is to say, only 6 percent of the launched rays undergo extinction, and there is only one scattering event per striking ray.

The faces of the cube are numbered as shown in Figure 4.11. In order to be able to visually compare the results from both versions, the cube walls are gridded into 1 mm squares. Once a scattered ray leaves the cube through a wall, the exit point is identified and the corresponding grid point ray counter is incremented.

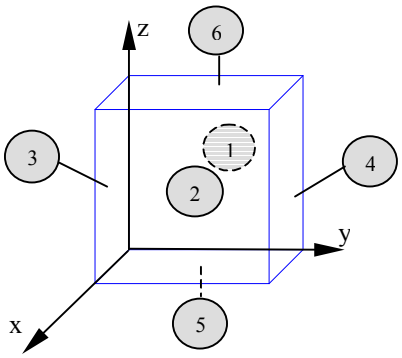

Figure 4.11. Numeration of the faces of each of the 1 cm atmospheric cubes

The cube is unfolded, keeping the origin of coordinates at the bottom back left corner of the cube. Figure 4.12 illustrates the unfolded layout of the atmospheric cube and the grid applied to each of its faces.

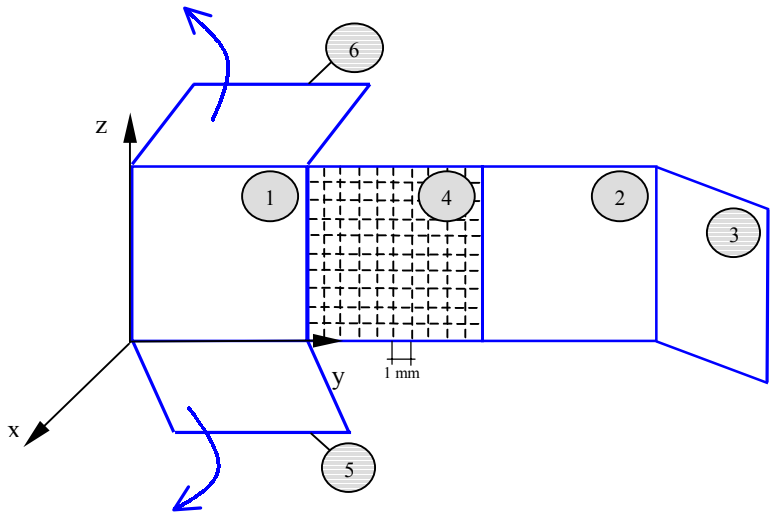

Figure 4.12. Unfolded layout of the atmospheric cube

After the simulations, the final image is a surface plot, where each of the grid-squares is assigned a color according to the percentage of rays that left the cube through it. The gridding method applied is the method of minimum curvature. For the 1,000-ray simulation, and the 10,000-ray simulation a different color scale was used, otherwise insufficient contrast would occur to visualize the results. The rest of the simulation results are analyzed applying the same color scale to visualize the trends. Observe that backscattering is negligible. That is, an insignificant number of rays leaves through the top of the cube. Consequently, wall number 6 is not represented in the figures.

Figure 4.13 presents the results from the 1,000-ray simulation.

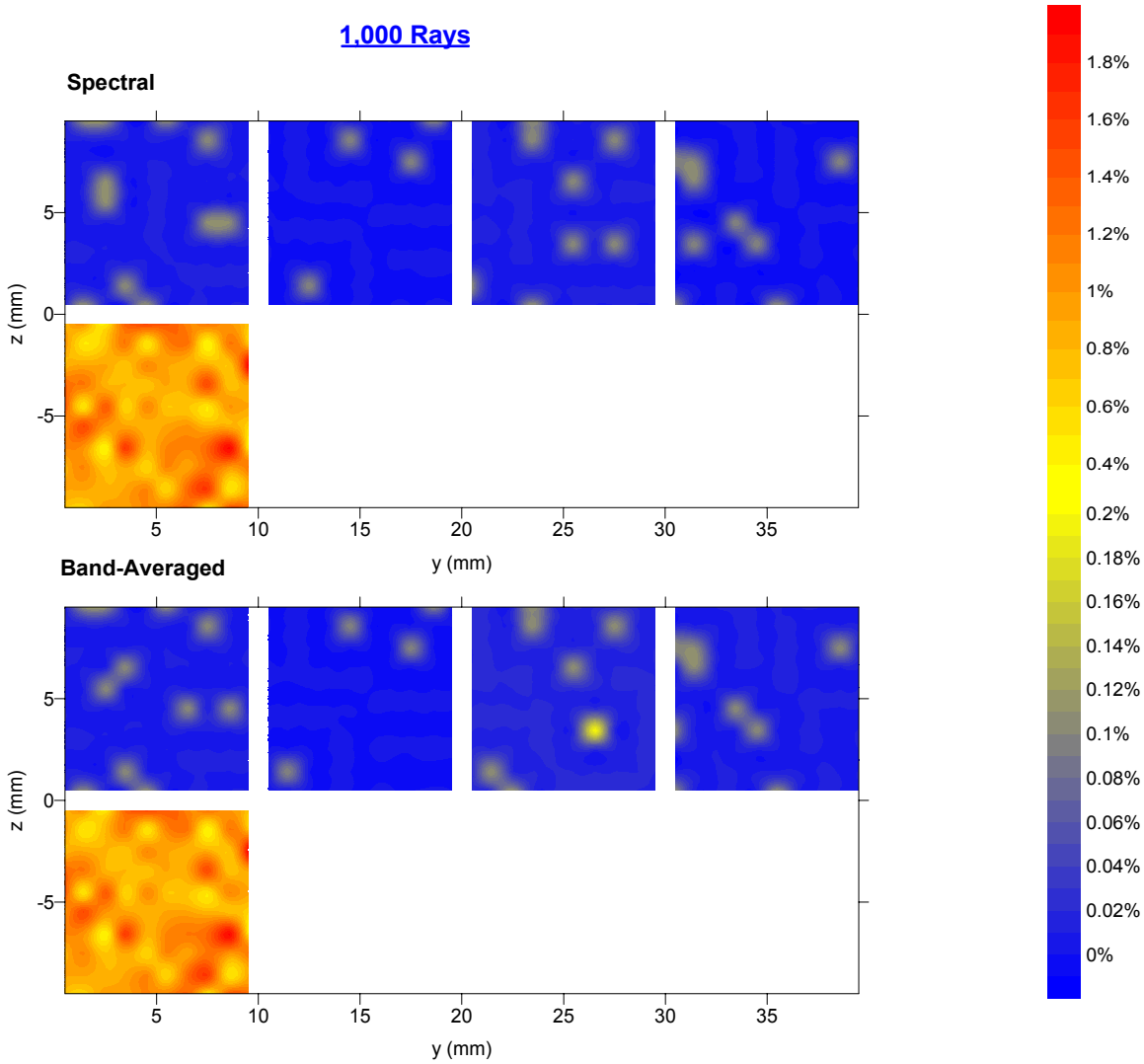

Figure 4.13. MCRT results for 1,000 rays launched

A thousand rays is obviously an insufficient number of rays. However, some interesting features can be remarked from Figure 4.13.

First, the similarity among the spectral and the band-averaged layouts is obvious, but due to the low number of energy bundles launched, we will not conclude that both versions are giving the same results, yet.

Second, we see that the inaccuracy of the band-averaged simulation consists on a tendency to group rays that would leave through different grid points if a more sensitive code were used. This can be appreciated when observing wall number 2 on Figure 4 .13. The final layout of the band-averaged simulation presents a very shining yellow point, its coordinates [26, 3], on wall number 2. However, the spectral layout shows two greenish points around that location.

A possible explanation for this effect is that the band-averaged version grouped those two points into a single one. In the spectral version of the MCRT code, the scattered rays are assigned the scattering angles according to their specific phase function. Yet, in the band-averaged version, the ray wavelength as well as the radius of the scattering aerosol are discretized, reducing the accuracy of the simulation. This can be improved by using a finer discretization. Again, we deal with a compromise among precision and time economy. The discrete bins proposed in Chapter 3 are considered perfectly accurate for this research.

This effect is repeated throughout the simulations. Figure 4.14 is a three-dimensional plot of the aspect of wall number 2 after the 1,000-ray simulation. It intends to illustrate the inconsistency discussed above. Around coordinates [22,2], we can appreciate the same observable fact. The picture after the spectral simulation shows a couple of well-defined peaks at [20.5,1.5] and at [24,0.5]. However, the band-averaged plot shows these two peaks wider and merging. That probably means that a higher number of rays would evolve into a single taller peak.

This lack of accuracy is mild and, eventually, it will not be a constraint to apply the band-averaged model for scattering non-divergent simulations, where the point rays leave the sidewalls is not relevant.

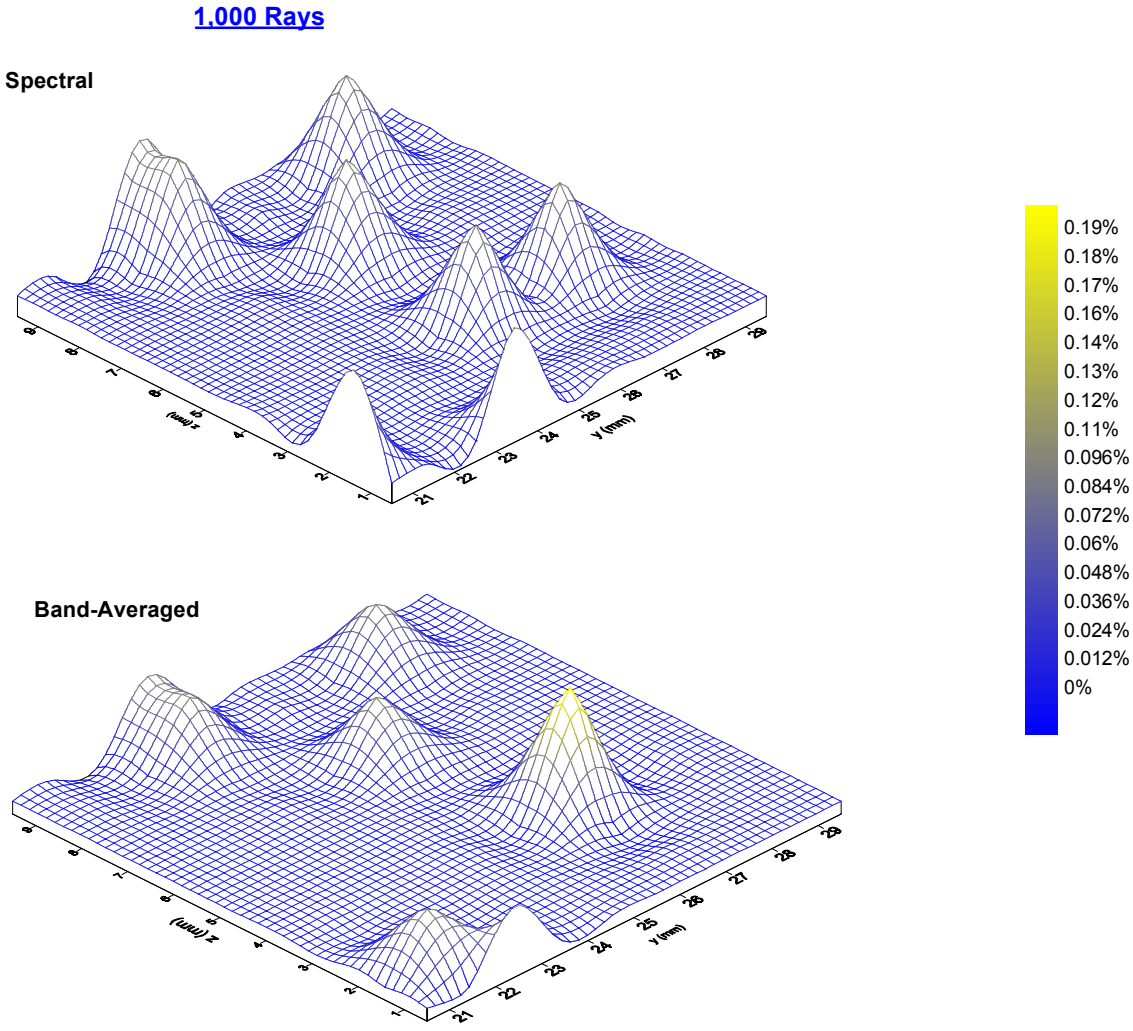

Figure 4.14. Three-dimensional view of wall number 2 from 1,000-ray simulation

The same experiment was repeated for an increasing number of energy bundles. The more rays are traced the more uniform the final layout of the cube becomes. Nevertheless, there is some preferential scattering towards some directions. Next, the final plots of the simulation results are presented.

Figure 4.15 presents the results from the 10,000-ray simulation. The similitude between both versions of the MCRT is observable.

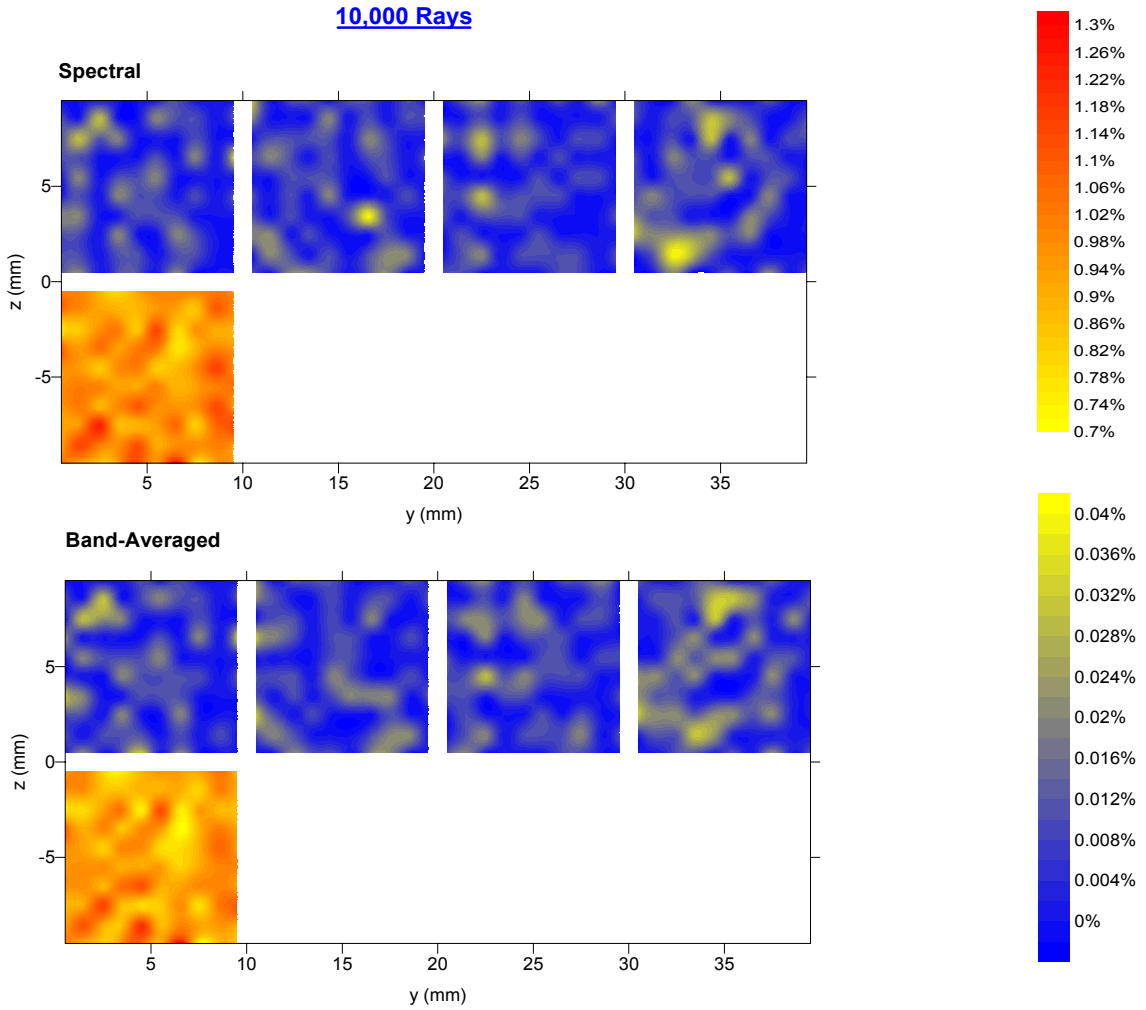

Figure 4.15. MCRT results for 10,000 rays launched

The reddish tones of wall number 5 in every simulation are a consequence of the preferential forward scattering as well as the rays that traverse the cube without undergoing either absorption or scattering.

Figure 4.16 is the final layout of the 100,000-ray simulation.

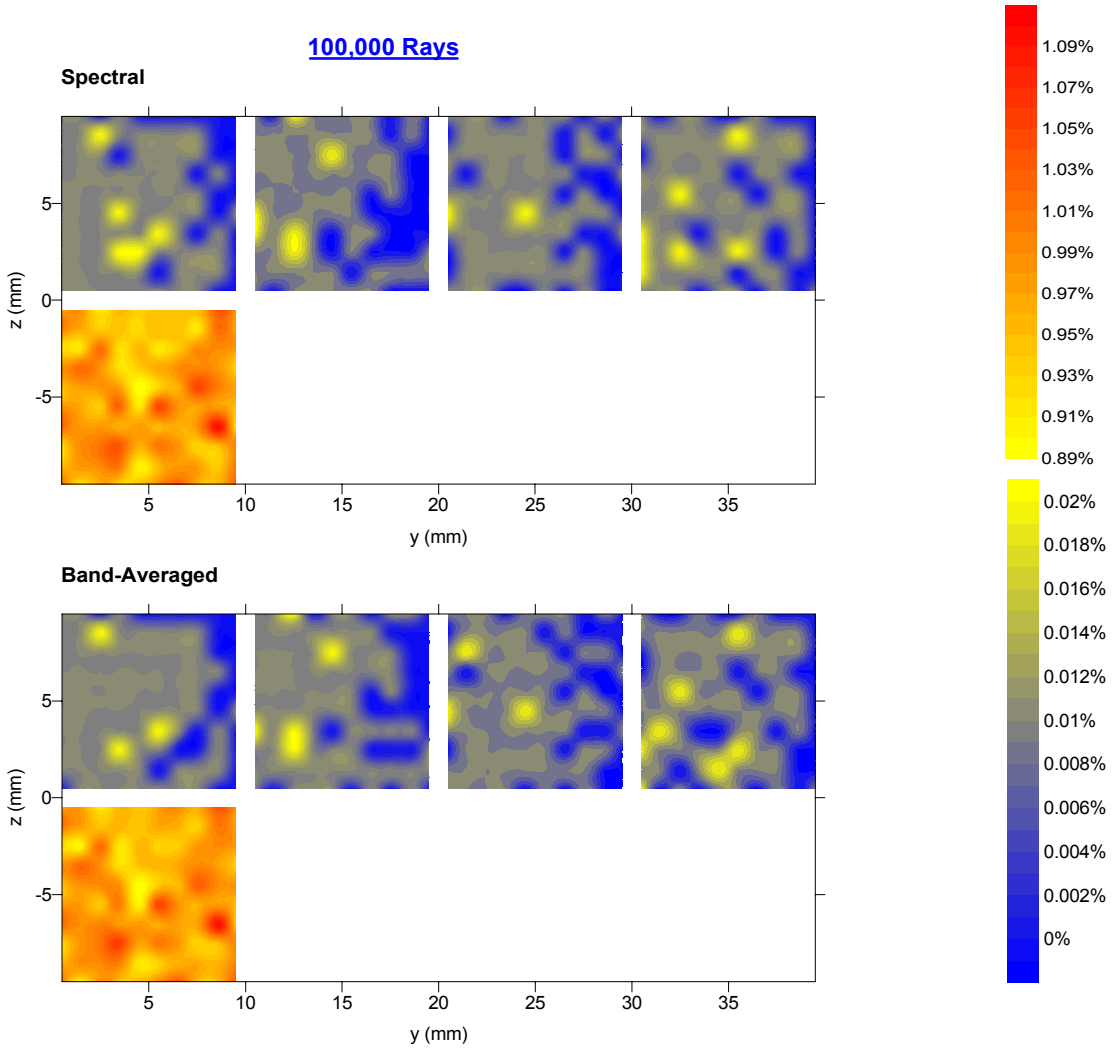

Figure 4.16. MCRT results for 100,000 rays launched

Once again, both versions of the MCRT code give almost identical final layouts. The directionability of the scattering, represented by shining points, is roughly the same after both simulations.

There is not remarkable difference on walls number 4 and 3 of either version. Wall number 1 however, bypasses the peak located at [3, 4] distributing the rays that go out through that point in the spectral MCRT simulation between the two other preferential scattering nubs located around [6, 3].

Wall number 5 similarities are noteworthy. The four preferential scattering nucleuses, represented by the red spots to be found at [3, 2], [6, 5], [4, 9] and [8,6], of the spectral simulation have been perfectly captured by the band-averaged model not only on location but also on shape and amplitude.

This amazing resemblance suggests that a higher number of rays will approach both version results. Let us analyze the rest of the simulation layouts to verify this theory.

Figure 4.17 presents the results of the 250,000-ray simulation. The curious thing about this figure is the decoupling effect observed on the band-averaged plot. So far, the typical discrepancy encountered when comparing both version layouts was that the band-averaged simulation would group the rays of two scattering nubs otherwise differentiated by the spectral simulation. In this figure, there are two clear examples of the opposite effect. The band-averaged simulation decouples what appears to be a single scattered nub in the spectral MCRT simulation layout. The first one is on wall number 1, around the point of coordinates [4, 2]. The second example is on wall number 2, at [24, 7].

The explanation of this irregularity resides, once again, on the discretization of the physical and optical properties of the aerosols.

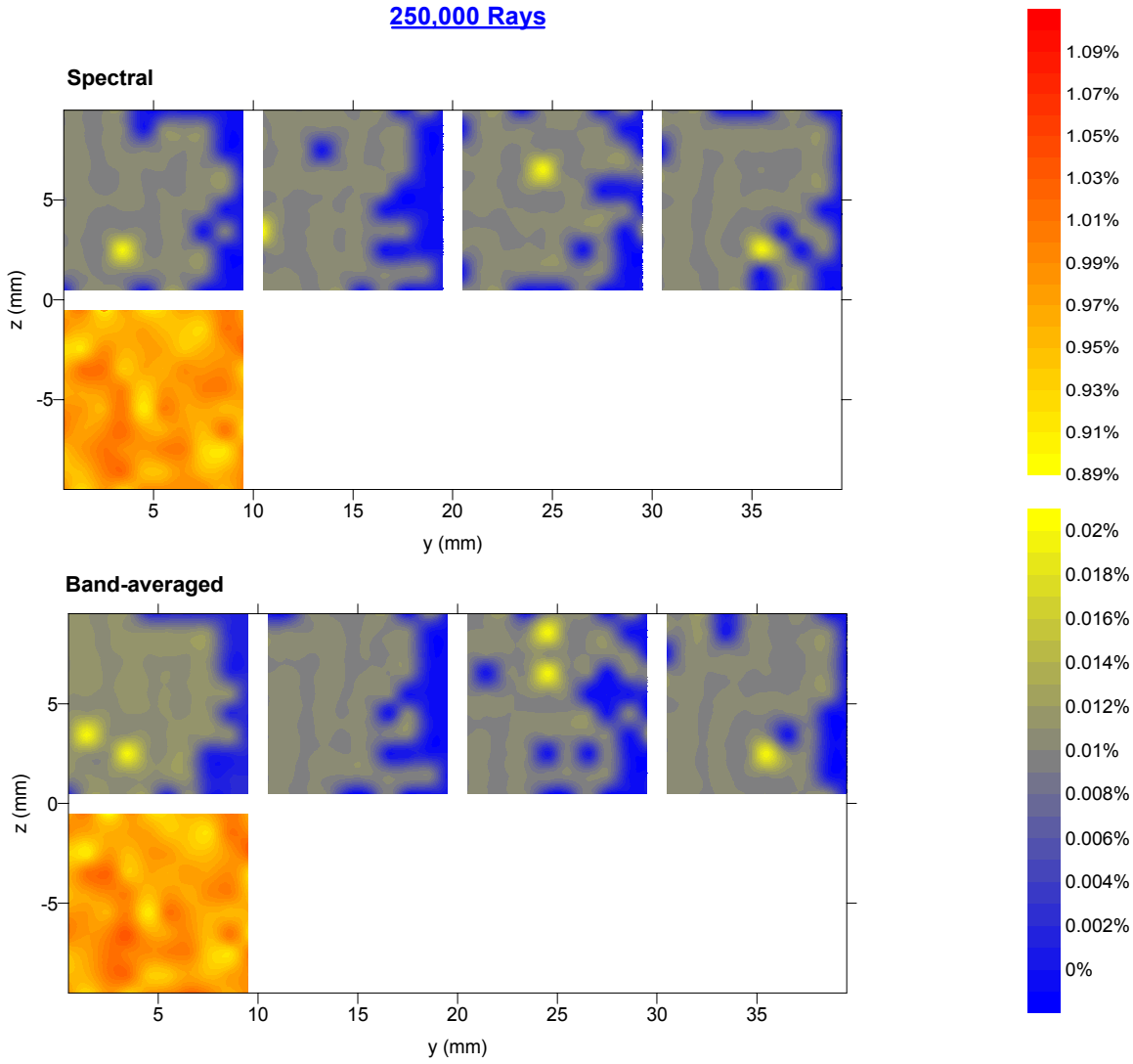

Figure 4.17. MCRT results for 250,000 rays launched

Figure 4.18 represents the final layouts of the 500,000-ray simulation of the spectral and the band-averaged MCRT method. For half a million rays the outputs of both versions are astoundingly agreeing.

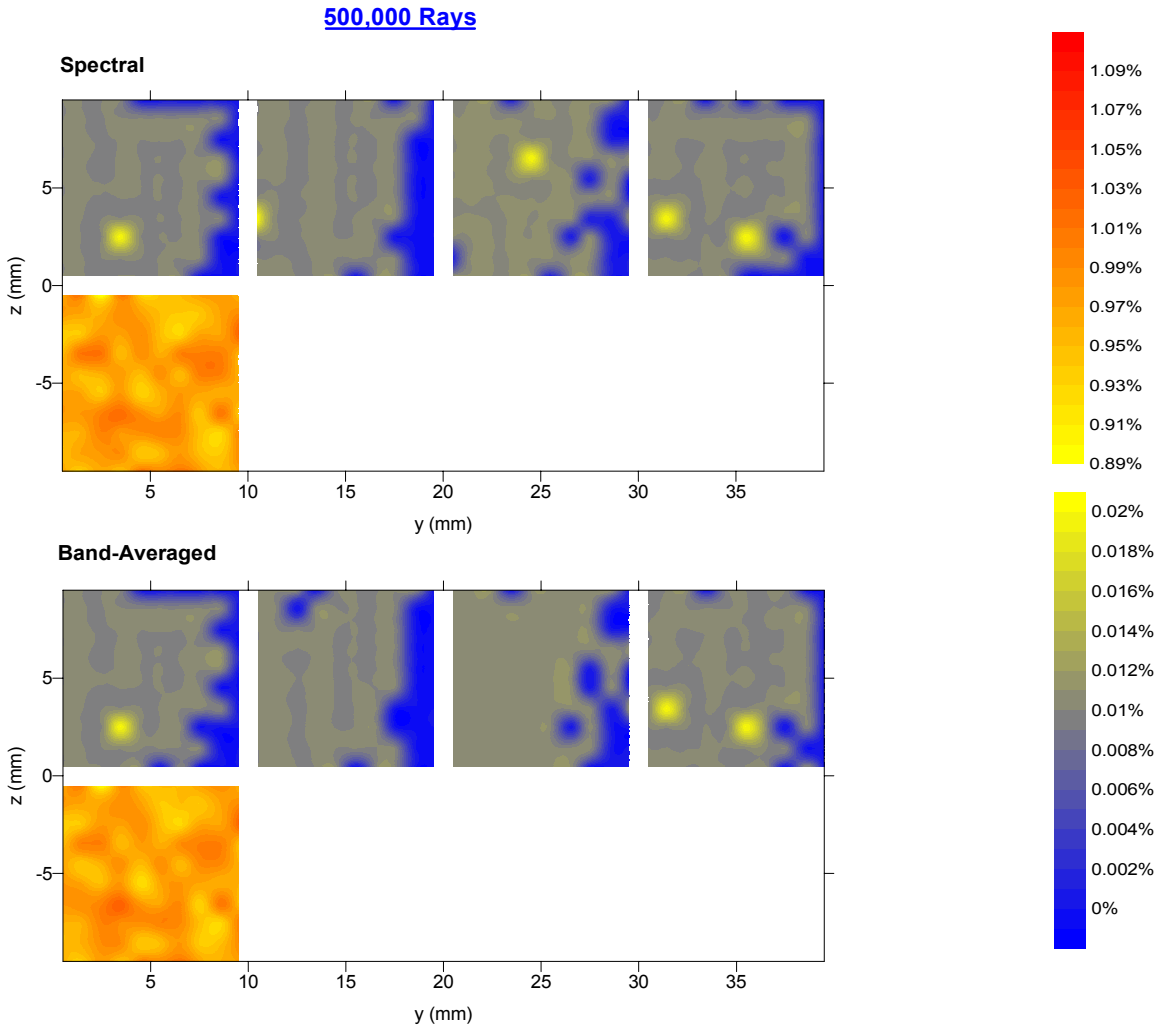

Figure 4.18. MCRT results for 500,000 rays launched

Up to what detail both results are alike is realized when looking to the greenish part of the grid. Figure 4.19 is an oversized detail of wall number 3 from the 500,000-ray simulation.

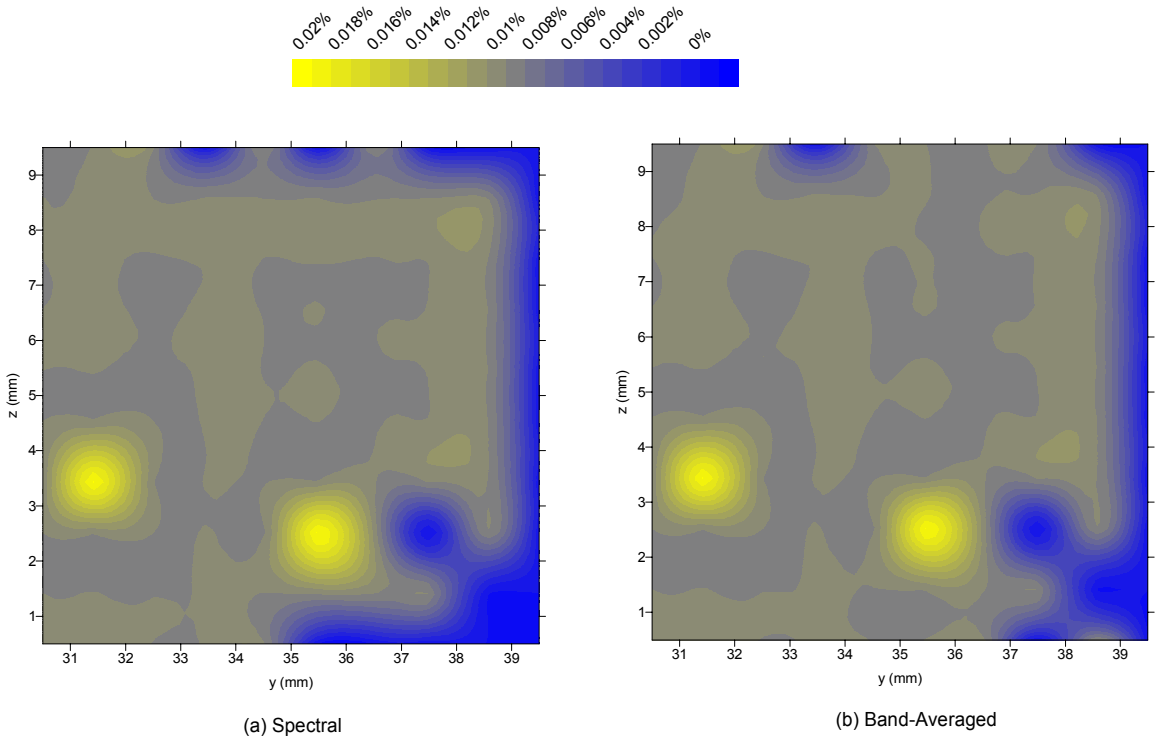

Figure 4.19. Wall number 3 from the (a) spectral MCRT simulation and (b) band-averaged MCRT simulation

Except for some over sampling in the top border of Figure 4.19 (b), both pictures are identical.

Despite the similarity between both images shown on Figure 4.18, there are two preferential scattering nubs that are still not reflected by the band-averaged simulation. The first one is the yellow peak on the side of wall number 4, coordinates [10, 3], on the spectral layout. This peak emerged after the 100,000-ray simulation, but half a million rays launched are still not enough to reflect it in the band-averaged simulation results.

The other peak bypassed by the band-averaged simulation is located on wall number 2, coordinates [24, 7]. This peak had been outlined on the spectral layout after the 250,000-ray simulation.

After one million rays launched, Figure 4.20, similitude among both version final layout is again perceptible. Now, the band-averaged simulation agrees on the two inconsistent points discussed above. Wall number 5 results are indistinguishable.

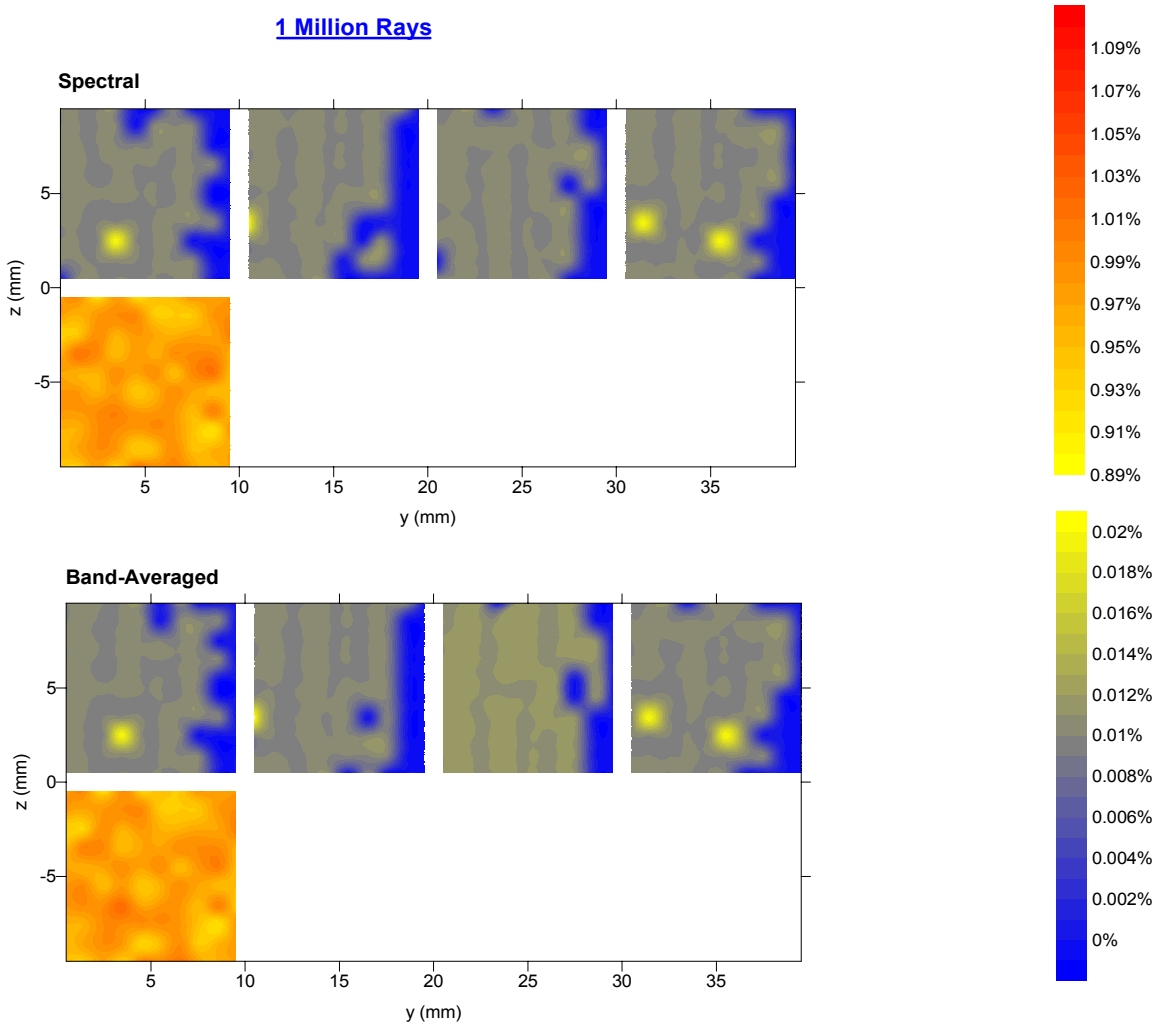

Figure 4.20. MCRT results for one million rays launched

Figures 4.21 and 4.22 are a three-dimensional view of the results of the 500,000-ray and the 1 million-ray simulation included here to ease the visualization of the predictable match of both pictures.

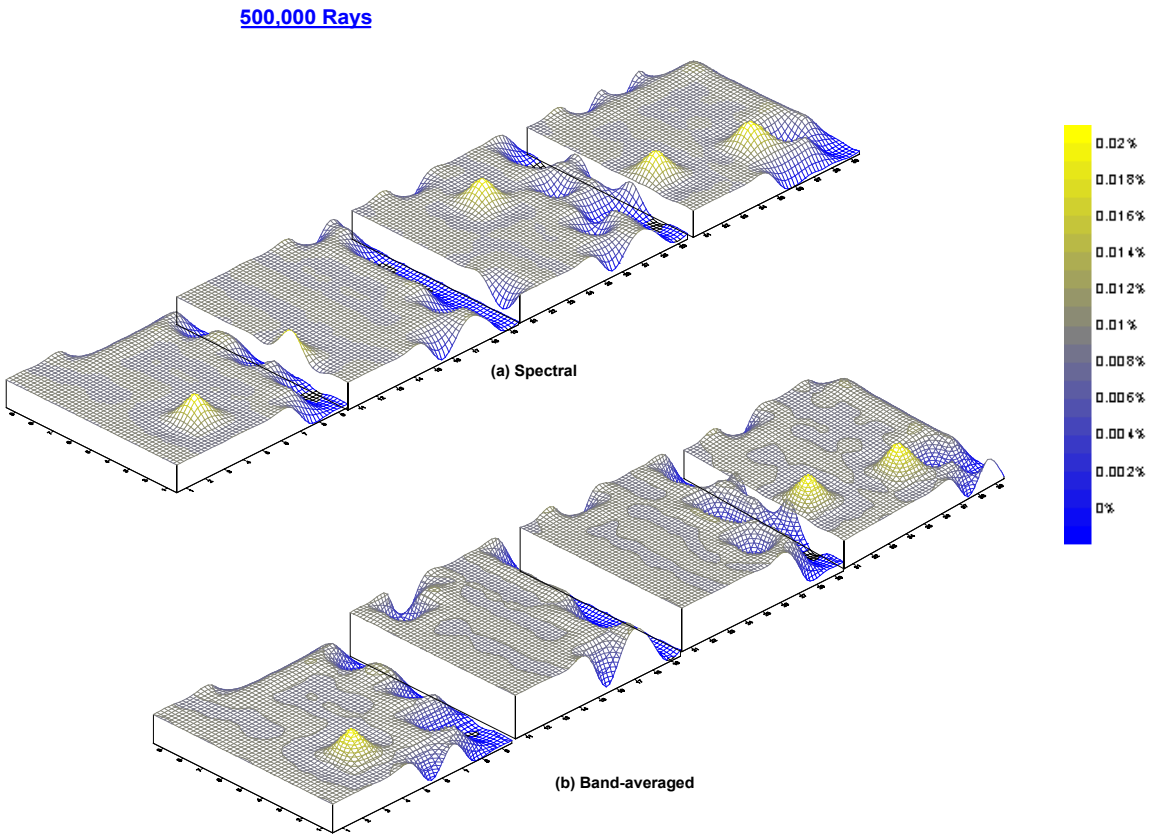

Figure 4.21. Three-dimensional view of the results of the 500,000-ray simulation

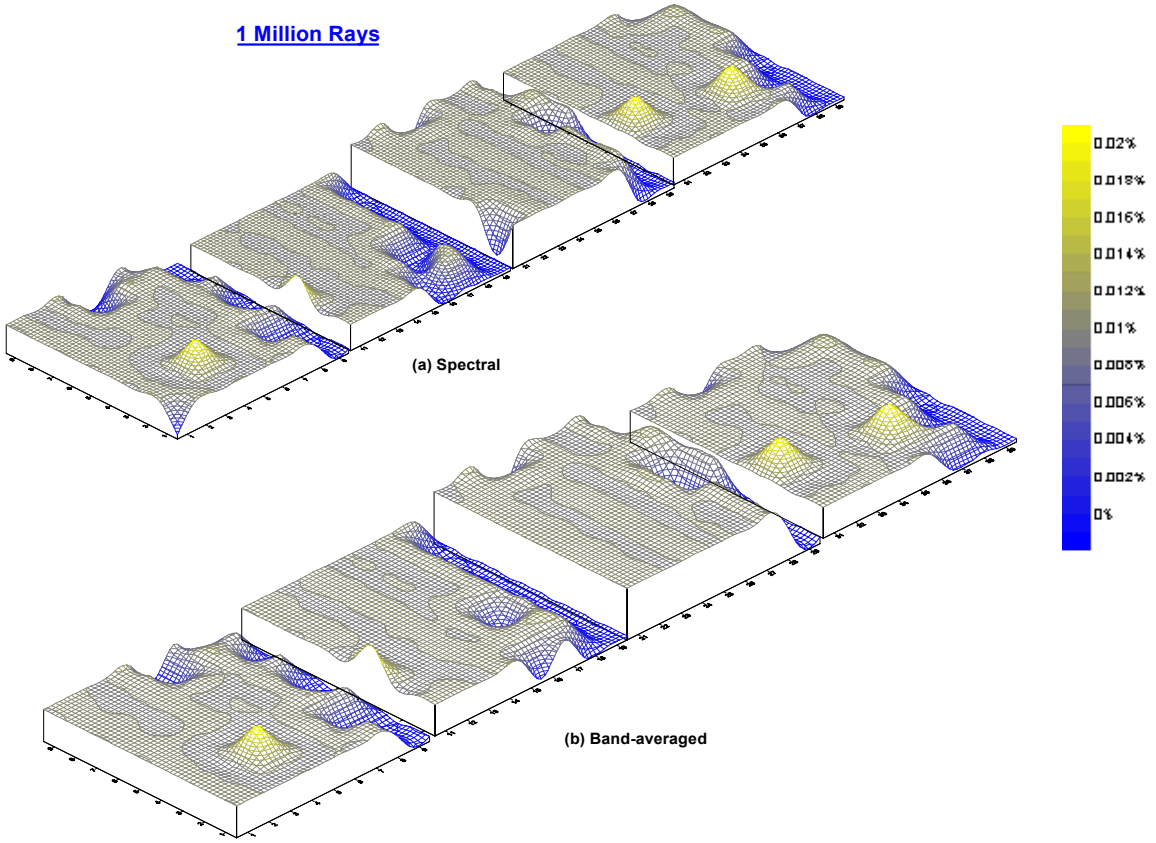

Figure 4.22. Three-dimensional view of the results of the 1 million ray simulation

The few differences observed between the spectral and the band-averaged simulation final layouts observed on Figure 4.21 fade away on Figure 4.22.

As a consequence of this and according to the results exposed along this section, the band-averaged MCRT version is concluded to be correct for the representation of the radiative effects of an absorbing, scattering, non-emitting media when a sufficiently large number of rays is traced.

The next topic to discuss according to the results presented in this chapter is the convergence of the MCRT method.

According to the weak law of large numbers convergence of the MCRT method is assured [Maltby, 1991]. For the experiments described above, convergence starts when a minimum of 250,000 rays have been launched. Yet, a million rays are necessary for the spectral and the band-averaged simulation to entirely match.

4.4 Conclusions

The conclusions drawn from the numerical experiments depicted along this chapter are:

- the microscopic MCRT method version described in Chapter 4 can correctly describe the radiative effects of a population of tropospheric aerosols on the solar radiative field
- by varying the value of the pcsr we have adjusted the monodisperse Mie scattering theory to accurately approximate the polydisperse Mie scattering results. The optimized value of pcsr is set to 900
- the results of the microscopic MCRT method applied to a participating media converge after 250,000 rays launched
- the band-averaged microscopic MCRT version simulation concurs with the spectral version for a large enough number of energy bundles traced. In this case, not less than a million
- for this research, the band-averaged version of the microscopic MCRT is considered correct and in benefit of time economy, it will be adopted for any further applications

The uniformity of scattering shown on these figures is not a reflection of reality; remember the relaxed conditions, imposed to the code, detailed at the beginning of the section. The purpose of these simulations is to ascertain the correctness of the band-averaged version of the MCRT, not yet to represent real atmospheric conditions.

Chapter 5 Practical Case

The purpose of this chapter is to illustrate the performance of the band-averaged microscopic MCRT method described in previous chapters. Two different simulations were performed to exemplify the effects on the solar radiative field of an absorbing, scattering, nonemitting media. Each of the simulations initialized the pseudo-random number generator with a different set of seeds to verify the independence of the results from the randomness of the pseudo-random number generator. We will refer to the first simulation as case A and to the second simulation as case B.

The chapter is structured so that, first, the conditions of the case are depicted. Then the results are analyzed, and finally they are compared with the theory.

5.1 Case description

The MCRT conditions were:

- a one-centimeter atmospheric cube with a particle density of 5000 cm^{-3} of clean continental aerosols whose sizes, ranging from 0 to 0.6 μm, adjust to a log-normal size distribution function
- the solar radiation is modeled as a collection of polychromatic, collimated and randomly polarized energy bundles whose wavelength bands range from 0.2 to 40 μm
- the seeds for the pseudo-random number generator are:
    - Case A: 21 for seed number 1 and 17546 for seed number 2
    - Case B: 6785 for seed number 1 and 5657 for seed number 2
- the number of rays traced is one million

The results obtained from the simulation are:

- the number of nonabsorbed nonscattered rays
- the number of rays rejected
- the number of rays absorbed
- the number of rays that exit through wall number 5
- the number of rays that exit through wall number 6 (backscattering)
- the number of rays absorbed as a function of the vertical location
- the number of rays absorbed as a function of the radius of the particles
- the number of rays scattered as a function of the radius of the particles
- the number of strikes per scattered ray

The number of nonabsorbed nonscattered rays refers to the total number of rays that traverses the cube without encountering any aerosols, therefore being neither scattered nor absorbed. These data allow us to calculate the efficiency of the MCRT code.

Some rays exit through a sidewall with an angle close to 90º. If these rays do not encounter any aerosols after being reentered through the opposite wall, it is probable that they start an endless loop where the ray keeps going out through a sidewall and being reentered without ever being scattered or absorbed or reaching the top or the bottom walls. To avoid this situation any ray that leaves the cube more than five times in a row without undergoing a scattering or absorption is rejected.

Another case of rays that may be skipped is the so-called orphan rays. Unluckily, some exiting rays might find that the distance from their origin point to two of the walls is the

same. To solve this problem, the smaller numbered wall is selected. For example, wall number 1 is preferred as an exiting wall over wall number 5.

Oddly, the search for a local system might fail. Due to the sensitivity of the programming language, small numbers are rounded to zero. If the distance between two scattering particles is sufficiently small, the code may eventually find a division by zero when calculating the magnitude of the ray vector. To avoid this inconsistency these rays are also skipped.

Every time a ray is absorbed the vertical plane in which absorption occurs and the radius of the absorbing aerosol are recorded. The number of absorbed rays as a function of the particle radius will be used to compare the performance of the MCRT code with the theory. The ultimate goal is to prove that the number of absorbed rays on the top of the cube is greater than the number of rays absorbed at the bottom. With this purpose, along the simulation, the number of rays absorbed at a certain vertical level is exited from the simulation.

Every time a ray is scattered the radius of the scattering aerosol is recorded. These data will allow us to compare the results of our simulation with theory.

The number of striking events of every scattered or absorbed ray is recorded. These rays are classified into bins according to the number of strikes they experience before being extinct. A ray with over five striking events is considered multiply scattered. In reality multiple scattering refers to more than one scattering event per ray, however, in this case we are interested on having a finer classification.

5.2 Results

Table 5.1 collects Case A and Case B results.

Table 5.1. Practical case general data

Number of rays that …	Case A	Case B
…are launched	1 million	1 million
…are skipped	55931	55806
…are not absorbed or scattered	436146	436708
…are absorbed	239035	238485
…are scattered out of the cube	268888	269001
… are backscattered	80189	79859

Out of a million rays launched, 5.59 percent have to be skipped in Case A and 5.58 percent of rays are left out in Case B. These percentages include the total launched rays that fall into an endless loop and the total number of rays that had to be passed over when the search for a local coordinate system failed. Future work to improve sensitivity of the local coordinate system search engine is required. The rays that fall into an endless loop are unavoidable; the correct approach to treat them is to consider them as neither absorbed nor scattered out the atmospheric cube rays.

The number of rays that undergo extinction represents 56.38 percent of the total in Case A and 56.32 percent in Case B. That is, on the average, 1 out of 1.77 launched energy bundles is either scattered or absorbed. This is a very good percentage. A lower efficiency will imply the need of higher number of traced rays in order to reveal the whole scattering phase range. The fact that we obtain such effectiveness reassures us on the correctness of the results presented.

The number of rays absorbed corresponds to 47.06 percent of the total extinct rays in Case A and 46.99 percent in Case B. The rest of the extinct rays are scattered out of the cube. In Case A, 29.82 percent of the scattered rays are backscattered. In case B, 29.68 percent of the scattered rays are backscattered. Backscattering means that the rays leave the cube through the top, wall number 6. Considering that in both cases more than 10 percent of the rays scattered out of the cube undergo multiple scattering, more than five strike events per scattered ray, this percentage of backscattered rays is not very high. This is in accordance with the theoretical scattering phase function as shown in Chapter 4.

The histogram in Figure 5.1 analyzes the results from Case A. The totality of rays scattered out of the cube is classified according to the number of scattering events they experienced before leaving the cube.

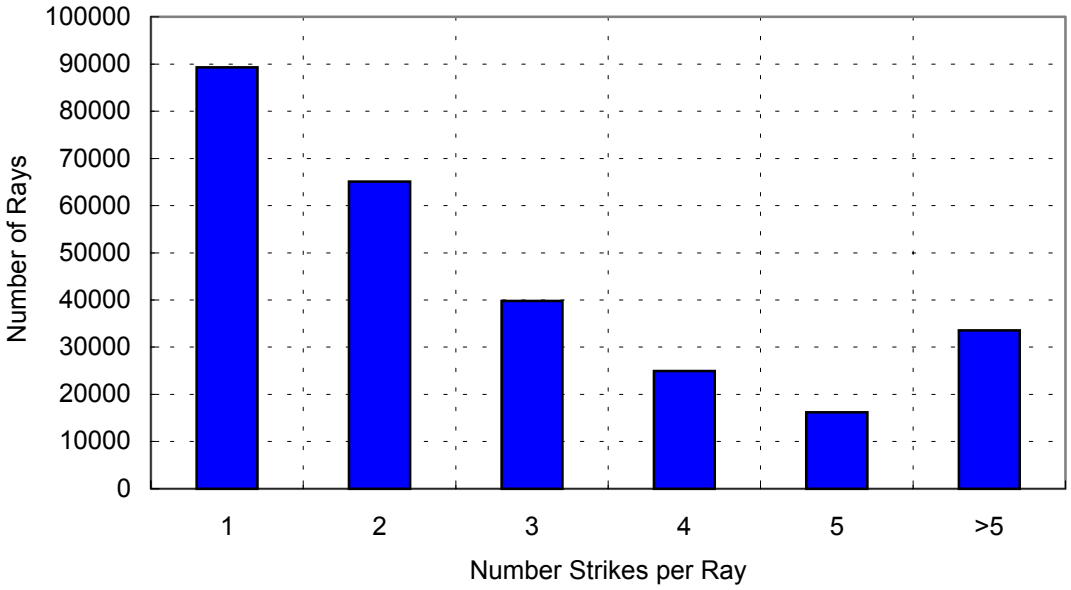

Figure 5.1. Total number of strikes per ray scattered out of the cube. Case A

The number of rays that experienced 1, 2…or over 5 scattering events before being scattered out of the cube determines the height of the bars.

The histogram in Figure 5.2 analyzes the results from Case B. This time, the total number of extinct rays is classified according to the number of scattering events that they undergone before they exited the cube, were absorbed or had to be skipped.

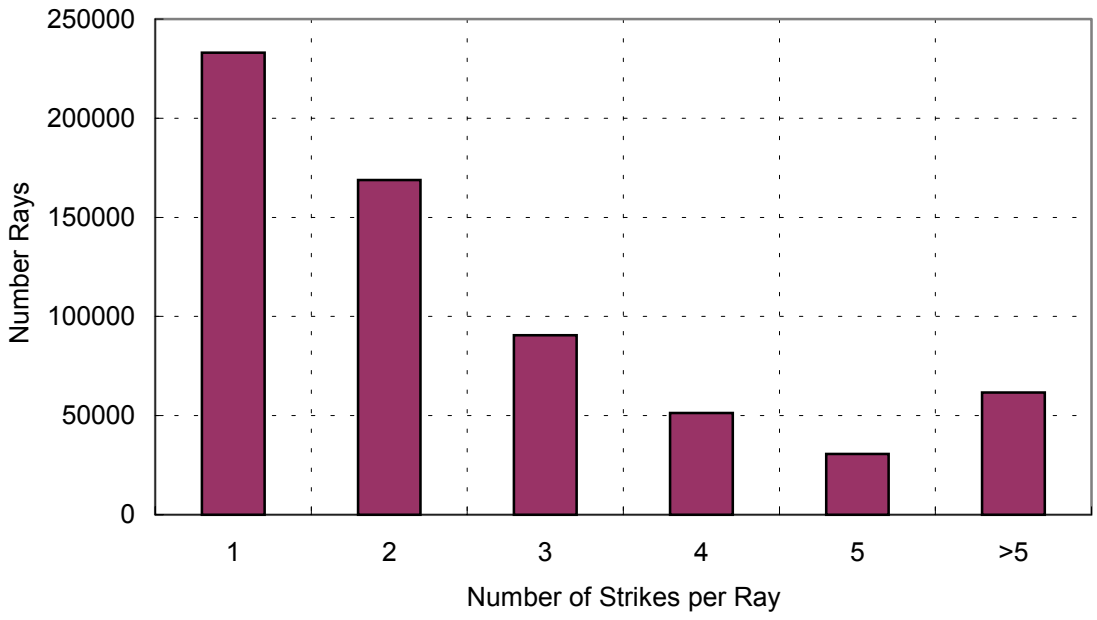

Figure 5.2. Total number of strikes per ray extinct. Case B

Both histograms show the same tendency. A majority of rays undergo single scattering and the percentage of rays that experience more than one scattering event decreases as the number of strikes per ray increases. However, a non-negligible portion of the launched rays experiences multiple scattering (over five strikes per ray).

Table 5.2 collects the percentages for each case.

Table 5.2. Percentage of extinct rays having n strikes

	Number of strikes per ray (percent)					
	1	2	3	4	5	>5
CASE A	33.20	24.21	14.79	9.28	6.02	12.48
CASE B	36.64	26.55	14.22	8.06	4.81	9.69

The analysis of the rate of absorbed rays as a function of height is used to verify the appropriateness of the hypothesis that motivated this research. It had been theorized that if a significant gradient exits between the number of rays absorbed at the top of an atmospheric column and the number of rays absorbed at the bottom, the growth rate of the photolytic secondary aerosols might be significantly dependent on vertical position.

The results drawn from Case A and Case B are remarkably coincident, thus confirming the randomness of the pseudo-random numbers generated.

In both cases an exponential increase with height of the number of rays absorbed is observed. The tendency line that best fits the results from Case A is

$$N_{abs}(z) = 16053e^{0.0687z} \tag{5.1}$$

where z is the vertical position and z equal to cero corresponds to the Earth's surface. The value of the R^2 statistic for Equation 6.1 is 0.92.

The tendency line that adjust the results from Case B is

$$Nr_{abs}(z) = 16028e^{0.0685z} \tag{5.2}$$

with an R^2 of 0.92 as well.

In Figure 5.3 the red solid line corresponds to Equation 5.1. In Figure 5.4 the red solid line corresponds to Equation 5.2.

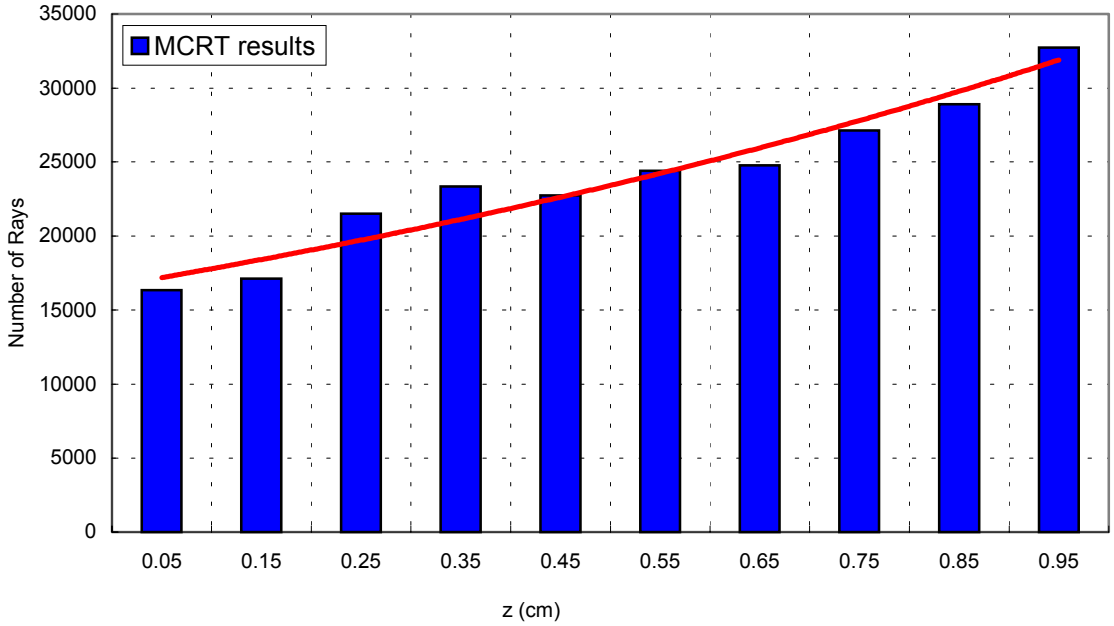

Figure 5.3. Absorbed rays versus vertical position. Case A

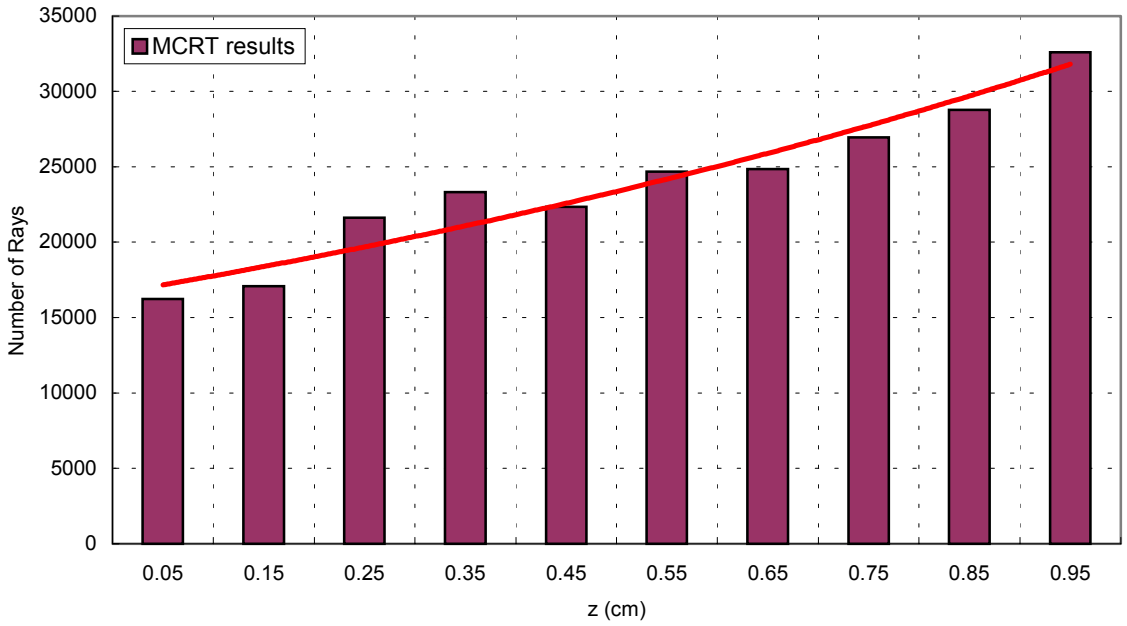

Figure 5.4. Absorbed rays versus vertical position. Case B

This exponential variability was predictable. The attenuation of the solar spectral flux as it traverses an absorbing media is

$$\frac{dL(x,\lambda)}{dx} = \frac{-\sigma_{abs}(\lambda)L(x,\lambda)}{\mu} \tag{5.3}$$

where $\sigma_{abs}(\lambda)$ is the spectral absorption coefficient and μ is the $\cos\theta$. Scientists usually refer to $1/\mu$ as the atmospheric mass. In our numerical simulations the incoming zenith angle θ, was cero; thus, μ equals unity.

Our numerical simulations where polychromatic; thus, we need to average Equation 5.3 over our wavelength range according to

$$\frac{\int_{\lambda_{min}}^{\lambda_{max}} \left[\frac{dL(x,\lambda)}{L(x,\lambda)}\right] i_{b\lambda}(\lambda)d\lambda}{\int_{\lambda_{min}}^{\lambda_{max}} i_{b\lambda}(\lambda)d\lambda} = \frac{-\int_{\lambda_{min}}^{\lambda_{max}} \sigma_{abs}(\lambda) i_{b\lambda} dx d\lambda}{\int_{\lambda_{min}}^{\lambda_{max}} i_{b\lambda}(\lambda)d\lambda} \tag{5.4}$$

where $i_{b\lambda}(\lambda)$ is the spectral solar radiance (W m^{-2} sr^{-1} μm^{-1}).

By definition,

$$\frac{\int_{\lambda_{min}}^{\lambda_{max}} \left[\frac{dL(x,\lambda)}{L(x,\lambda)}\right] i_{b\lambda}(\lambda)d\lambda}{\int_{\lambda_{min}}^{\lambda_{max}} i_{b\lambda}(\lambda)d\lambda} \equiv \frac{dL(x)}{L(x)} \tag{5.5}$$

and also by definition,

$$\frac{-\int_{\lambda_{min}}^{\lambda_{max}} \sigma_{abs}(\lambda) i_{b\lambda} dx d\lambda}{\int_{\lambda_{min}}^{\lambda_{max}} i_{b\lambda}(\lambda) d\lambda} \equiv -\sigma_{abs} dx \equiv -d\tau(x) \qquad (5.6)$$

where $\tau(x)$ is the optical thickness of the participating media.

Equation 5.3 becomes

$$\frac{dL(x)}{dx} = -\sigma_{abs} L(x) \qquad (5.7)$$

Integrating from x_1 to x_2, where x_1 corresponds to the top of the atmosphere (TOA) and is equal to cero, we obtain

$$L(x_2) = L(x_1 = x_{TOA}) e^{-\sigma_{abs} x_2} \qquad (5.8)$$

Equations 5.1, and 5.2 are equivalent to Equation 5.8 through this easy change of variables,

$$x = H - z \qquad (5.9)$$

where H is the total thickness of the atmosphere.

Introducing Equation 5.9 into Equations 5.1 and 5.2 we obtain

$$N_{abs}(H - x) = 16053 e^{0.0687 H} e^{-0.0687 x} \qquad (5.10)$$

for Equation 5.1 and

$$Nr_{abs}(H-x) = 16028e^{0.0685H}e^{-0.0685x} \tag{5.11}$$

for Equation 5.2.

According to the conditions of Case A and Case B, the theoretical polychromatic optical thickness is

$$\int_{x_1=0}^{x} d\tau(x) = \int_{x_1=0}^{x} \frac{\int_{0.2}^{40} \sigma_{abs}(\lambda) i_{b\lambda}(\lambda) dx d\lambda}{\int_{0.2}^{40} i_{b\lambda}(\lambda) d\lambda} dx = 0.0632x \tag{5.12}$$

The integral from Equation 5.12 is approximated by means of the trapezoidal rule, as the literature does not offer the absorption coefficient as an explicit function of the wavelength, but only some discrete data points for certain values of the wavelength.

The relative error between the theoretical exponent from Beer's hypothesis and the experimental averaged exponent is 7.8 percent.

5.3 Comparison of MCRT model result to theoretical data

Yet one more result needs to be compared with the theory before satisfactorily concluding this analysis. We are interested on checking if the absorption rate as a function of the particle radius agrees with our theoretical expectations.

The histogram in Figure 5.5 represents the number of rays absorbed by particles of a certain size according to the results of the Case A and Case B simulations. According to Figure 5.5, it seems that small particles absorb more rays than large particles. In the

figure, the peak of the histogram corresponds to the particles whose size ranges from 0.03 to 0.07 μm.

Although a decreasing tendency is clearly suggested, there are still some discordant points. For example, for particles of radius around 0.42 μm the number of absorbed rays is slightly greater than expected.

Recalling the characteristics of the size distribution function applied to generate the aerosols, 0.0285 μm corresponds to the mean radius, and the peak of the number density distribution. That is, there are more particles with radius around 0.03 μm than there are of any other size. Therefore it might be only logical that the number of absorbed rays by particles in that radius range is greatly superior than the number of absorbed rays by particles outside that radius range. More to the point, the conclusion that small particles absorb more energy than the big ones based on Figure 5.5 is invalid and unfounded.

It also may appear, according to Figure 5.5, that there is not absorption for certain sizes, such as 0.005 μm or between 0.54 and 0.56 μm. In reality, the cause of such small or inexistent values is that there are no particles with that radius.

Figure 5.6 represents the theoretical values of the scattering, absorption and extinction cross-sections (m^2) for a population of 5000 cm^{-3} clean continental aerosols as a function of the particle radius. The radius range represented in Figure 5.6 goes from 0 to 0.6 μm, matching the maximum and the minimum radius of the size distribution population attributed to Case A and Case B simulations. The theoretical data correspond to a monochromatic radiance of wavelength 0.5 μm.

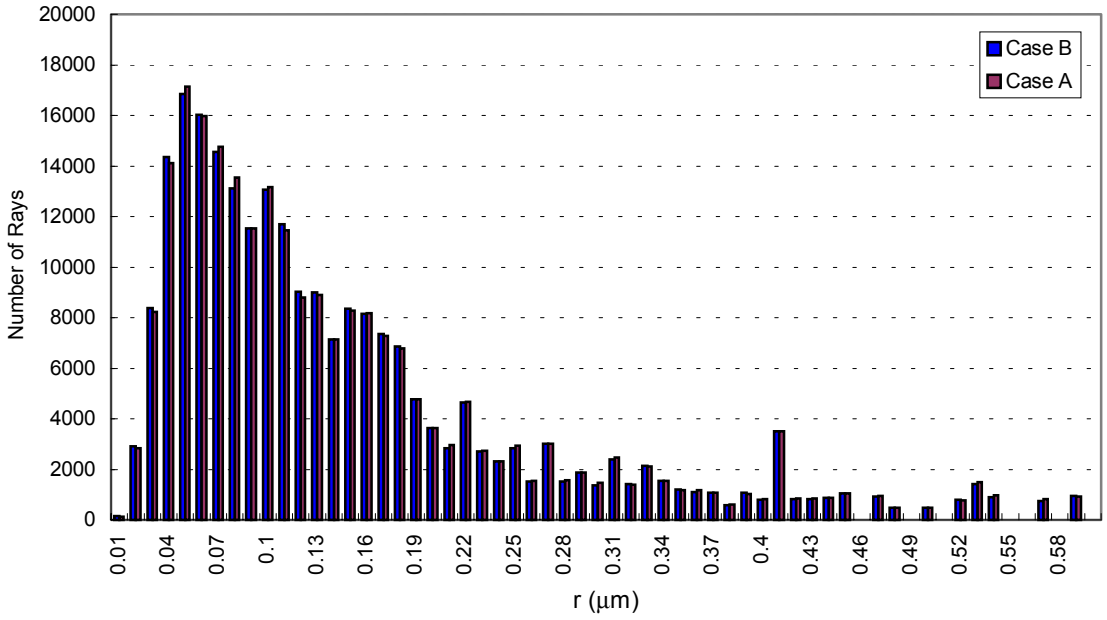

Figure 5.5. Number of rays absorbed versus particle radius

From Figure 5.6 the exact opposite conclusion is drawn. It seems that with such a small absorption cross-section, absorption will not be relevant until the particles reach a size over 0.3 μm.

Authors have reflected in the literature the ambiguity of considering the absorption rate a function of the particle radius.

> *Because these magnitudes* (when talking about the scattering and absorption efficiencies of spheres of various sizes) *change so radically from region to region, the single-scattering properties of the polydispersion –for example, their scattering albedo and absorption coefficient- change considerably, depending on the size range, dominant size, and proportion of small to large particles in the distribution. In this respect, errors of judgment are common in the literature* [Deirmendjian D., 1969, pp.33].

According to Figure 5.6, for r sufficiently small, where r refers to the radius of the aerosol, the absorption term is the main contribution to the extinction cross section. In this case, the absorption seems to be negligible for a wide range of sizes. For example, from 0.25 to 0.4 μm where the scattering is the main component of the extinction cross-section. Yet, as r tends to infinity we approach the condition of equal absorption and scattering efficiencies. This tendency is particular of rural aerosols, it cannot be generally applied to any kind of aerosols because the scattering contribution depends on the magnitude of the index of refraction of the particles.

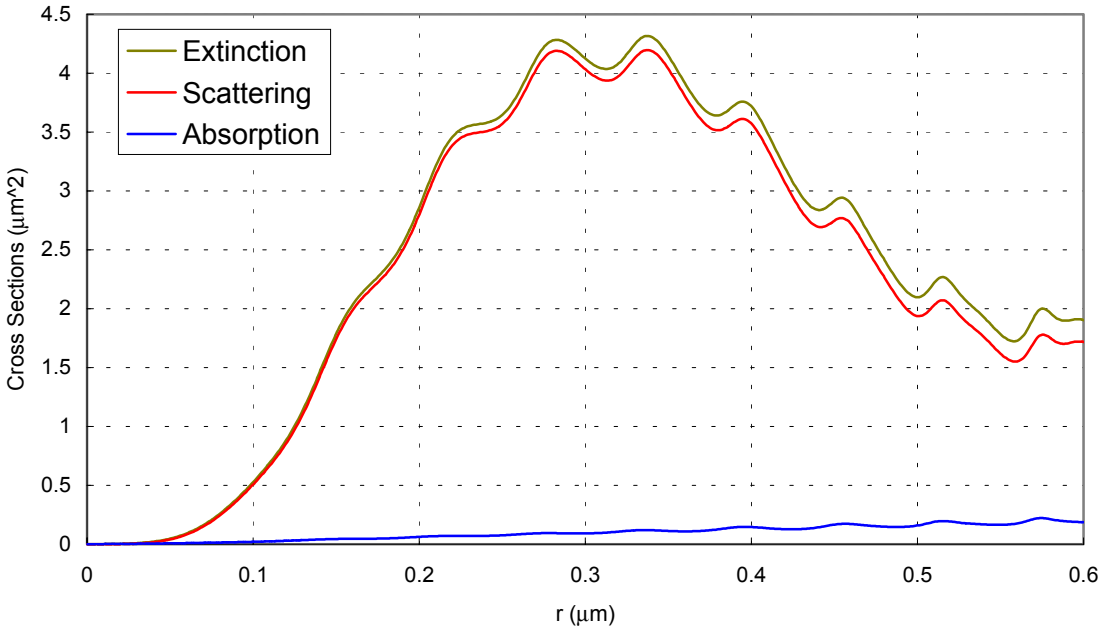

Figure 5.6. The extinction, scattering and absorption theoretical coefficients

A valid comparison between the theory and the MCRT results from Case A and Case B simulations would be the partial contribution of the scattering and absorption cross-sections to the extinction cross-section. That is to say, if absorption predominates over scattering for small particles, the results of the microscopic MCRT simulation should be such that the number of rays absorbed

by small particles would greatly exceed the number of rays scattered by these particles.

The ratio between the number of rays absorbed by particles of a given size range and the number of rays extinct by particles of that same range, is compared against the ratio between the absorption cross-section and the extinction cross-section theoretical values, in Figure 5.7. The values of the MCRT simulation results correspond to case B. Case A results were equally coincident and they are not reported in this thesis.

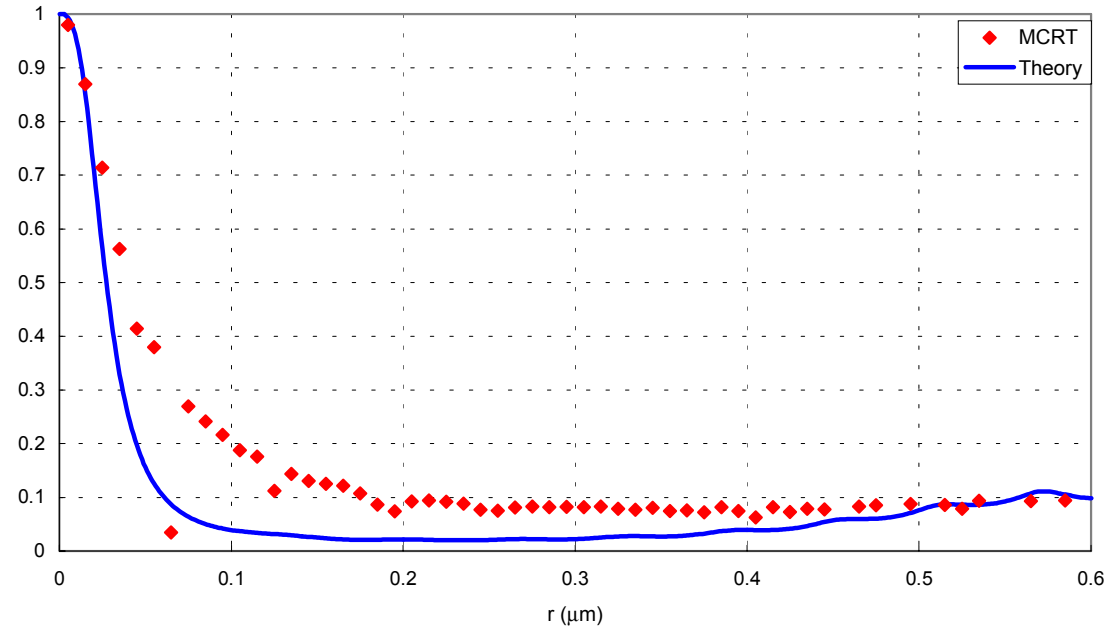

Figure 5.7. Comparison between theoretical cross-section values and the MCRT simulation results. Case B

The comparison between the theoretical cross-section data and the MCRT simulation results are very satisfying. The continuous blue line represents the theoretical data, and the red circles correspond to the MCRT values.

Discrepancies between both set of values are caused by two reasons. Firstly, the theoretical data correspond to monochromatic light with a wavelength of 0.5 μm, whereas the MCRT code simulates polychromatic solar radiation. However, the comparison among both set of values is valid, because 0.5 μm corresponds to the maximal and representative wavelength of the sun radiant power. Yet, it is still an approximation and it may induce errors.

And secondly, some parts of the radio range might be under exemplified.

The MCRT result tendency is the same as the proposed by the theory. Thus, we conclude that small particles of clean continental aerosols do in fact absorb more radiation than big particles do. Towards the end of the represented size range, we observe a recovery; as expected, absorption seems to trend to dominate extinction again as r trend to infinity.

After analyzing the results form these two simulation cases, we conclude that the performance of the microscopic design of a MCRT code, product of the effort reported in this thesis, is a truthful and efficient tool.

Chapter 6 Atmospheric Chemistry and Transport Models of Trace Species.

"It is not pollution that is harming the environment. It is the impurities in our air and water that are doing it."

(Dan Quayle).

Available atmospheric chemistry and transport models represent an effort to reproduce and forecast the behavior of the atmosphere. They are intended to ascertain the concentration of trace species over the atmosphere in a wide range of temporal and spatial scales. This chapter constitutes a historical survey of their algorithm evolution and of their accomplishments.

Dr. L. K. Peters' article, "The current state and future direction of Eulerian models in simulating the tropospheric chemistry and transport of trace species: a review", served as guideline for the bibliographic research [Peters L.K., 1995] summarized in this chapter. The final product of this bibliographic research is a documented file of articles, on file in the offices of the Thermal Radiation Group (TRG), in Randolph Hall, at Virginia Tech. An introductory software guide by the author of this research is also included in the file.

Also, in order to provide a background for members of the TRG future investigations, access to a first version of the second-generation model, MOZART (described later) and a data base to test it has been provided to the TRG. No testing of this program was carried out along this research as there was no special interest at the moment and it requires super-computer hardware support.

6.1 Description of the models

Transport and chemistry models describe the variation of concentration of chemical species in the atmosphere as a function of time and position.

Chemical compounds are released into the atmosphere from natural or from anthropogenic sources. Volcanoes, fires, lightning, desert dust and oceans are natural source examples. Anthropogenic emissions come mainly from industrial activities, such as fossil fuel combustion or nuclear energy production, and from biogenic wastes. Once in the atmosphere, these chemical compounds undergo physical and chemical reactions. They may be transported over large distances by winds or washed from the atmosphere by rain. They may drop to the Earth's surface or chemically react to generate new chemical species or aerosols. Finally, they may act as cloud condensation nuclei (CCN) and influence cloud coverage, and hence climate and meteorology.

Transport and chemistry models are intended to quantify these phenomena. Throughout the years, transport and chemistry models have seen increases in the complexity of their chemistry schemes, accounted for more physical processes, and progressively included feedback effects between climate, meteorology and chemistry. We will have the opportunity to briefly examine their evolution in the sections of this chapter dedicated to the chronological classification of the ChTMs.

Some of the main chemical reactions in the terrestrial atmosphere enclosed by ChTMs are briefly introduced next. Figure 6.1 does not intend to be a complete atmospheric chemical mechanism, its purpose is to depict the basis of the chemistry module of the ChTMs.

The Earth's atmospheric chemical composition is a consequence of the chemical compounds released by the biosphere. The most important reaction in the biosphere is the photosynthesis

$$CO_2 + H_2O \rightarrow CH_2O + O_2$$

Without the photosynthesis our atmosphere will evolve towards something similar to the atmospheres of planets like Venus or Mars. Oxygen (O_2), nitrogen (N_2) and other trace gases like methane (CH_4), nitrous oxide (N_2O), ammonia (NH_3), hydrogen chloride (HCl) or hydrogen (H_2) will vanish from our air. Photosynthesis is also a more efficient sink of CO_2 than the ultraviolet process because photosynthesis is a two-proton process.

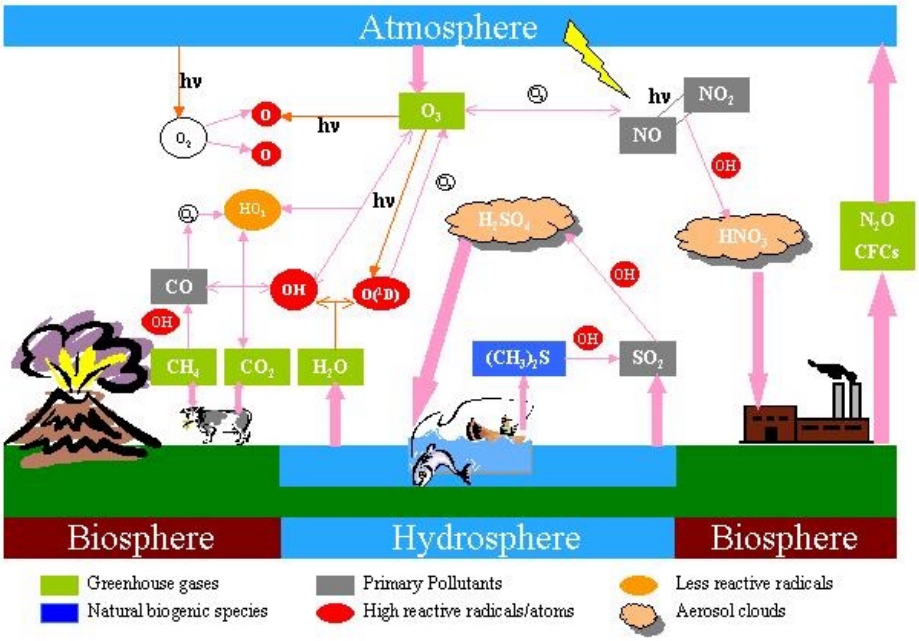

Figure 6.1 Simplified atmospheric chemistry scheme

6.1.1 Greenhouse gases

The main greenhouse gases, marked as green squares in Figure 6.1, are CH_4, CO_2, CFCs (such as CFC-11 or CFC-12) and N_2O. Water vapor is actually the most important greenhouse gas; nevertheless, as its concentration is highly dependent on temperature, it is not normally considered an independent parameter [Yung Y.L., 1999]. The temperature rise during the last century is attributed to an increase on the concentration of these gases. The increase of atmospheric CO_2 and CFCs is due to industrial activity, as CFCs do not have any known natural source. More to the point, CFCs have lifetime expectancy of the order of centuries; therefore, virtually all the released CFCs have remained in the atmosphere.

The main sources for CO_2 are combustion processes, such as industrial fossil fuel burning. The increase of CH_4 is mainly due to agricultural activities. The principal consequence of the increase of the concentration of greenhouse gases is a positive feedback on the Earth's Radiation budget by absorption of solar radiation.

6.1.2 Oxidants: OH

The principal oxidant in the atmosphere is the hydroxyl radical (OH). The precursor molecule is ozone (O_3). The photolysis of the ozone molecule yields an excited oxygen atom (O (^{1}D)) that, reacting with water, produces two molecules of the radical OH.

$$O_3 + h\nu \rightarrow O_2(^1\Delta) + O(^1D)$$

$$O(^1D) + H_2O \rightarrow OH + OH$$

The principal removal reaction for OH is

$$OH + CO \rightarrow H + CO_2$$

6.1.3 Ozone

Despite the fact that some stratospheric ozone is transported into the troposphere, the main source of tropospheric ozone is the oxidation of CO and CO_2.

$$\begin{aligned} &OH + CO \rightarrow H + CO_2 \\ &H + O_2 + M \rightarrow HO_2 + M \\ &HO_2 + NO \rightarrow OH + NO_2 \\ &NO_2 + h\nu \rightarrow NO + O \\ &O + O_2 + M \rightarrow O_3 + M \end{aligned}$$

$$\text{Net } CO + 2O_2 \rightarrow CO_2 + O_3$$

The ozone layer is located in the stratosphere. The origin of the stratospheric ozone is

$$\begin{aligned} &O_2 + h\nu \rightarrow O + O \\ &O + O_2 + M \rightarrow O_3 + M \end{aligned}$$

where M is a third body of reaction.

Stratospheric ozone absorbs the bulk of UV radiation by photolysis

$$O_3 + h\nu \rightarrow O_2 + O$$

6.1.4 Primary pollutants

NO_x, SO_x and CO are important atmospheric primary pollutants.

NO_x are mainly derived from anthropogenic industrial activities. Such nitrogen species have short lifetimes and do not reach the stratosphere. Approximately 10 percent of the NO_x of the atmosphere arises from the absorption of galactic cosmic rays.

NO_x also affect the ozone concentration. If NO_2 photolyzes via

$$NO_2 + h\nu \rightarrow NO + O$$

and NO reacts with O_3

$$NO + O_3 \rightarrow NO_2 + O_2$$

then the net reaction would be

$$O_3 + h\nu \rightarrow O_2 + O$$

where a molecule of ozone is destroyed yielding to the release of a molecule of oxygen and an oxygen radical.

There are a number of complex odd nitrogen compounds that derive from NO_x. For instance,

$$NO_2 + OH + M \rightarrow HNO_3 + M$$

The former reaction is a sink of HO_x radicals. Nitric acid (HNO_3) is water-soluble; it will eventually be washed from the atmosphere by rain, contributing to the so-called acid rain effect.

The bulk of terrestrial sulfur resides in the oceans as sulfate. By means of physical processes described on Chapter 3, sulfur is released into the atmosphere. The largest natural source of sulfur, in spite of volcanic sporadic eruptions, is DMS ($(CH_3)_2S$). The ultimate fate of reduced sulfur species such as DMS is oxidation to SO_2, followed by oxidation of the SO_2 to SO_3. By absorption of a water molecule, SO_3 becomes sulfate (H_2SO_4), which is also washed off the atmosphere by rain, contributing to the above-mentioned effect, the acid rain.

The following sections classify the ChTMs according to three different criteria. Namely, Eulerian or Lagrangian, on-line or off-line and, a more specific chronological classification.

6.2 Eulerian versus Lagrangian classification

The chemistry and transport models are classified according to different criteria. For instance, they may be divided between Eulerian or Lagrangian models, depending on the way position within a field is defined.

In the Lagrangian approach the concentration of a species is described for a particular fluid element as it travels with the flow. The coordinates are dependent variables [Peters L. K., 1995]. However, the Eulerian approach describes the concentration of a species at a given point and time, with the coordinates fixed in space and time.

Even though the Lagrangian approach requires less computational resources to simultaneously solve differential equations systems, most of the papers recovered for the TRG deal with Eulerian models. Therefore, most of the works reported in this summary focus on the description of the Eulerian approach over the Lagrangian approach.

The grid-based Eulerian models provide a pollutant distribution over the entire modeling region rather than along trajectories. The mathematical equation describing the time-averaged concentration of an inert species using the Eulerian approach is given by:

$$\frac{\partial \bar{c}}{\partial t} + \nabla(\bar{v}\bar{c}) = -\nabla(\overline{v'c'}) + \bar{S} \qquad (6.1)$$

where $\bar{v}$ is the velocity vector, $\bar{c}$ is the species concentration, and $\bar{S}$ is the source term. The overbar indicates time averaging over a period τ to eliminate turbulent fluctuations. The primed quantities, v' and c' represent the turbulent fluctuations of the velocity and concentration relative to their averaged values, and the first term on the right-hand of the Equation 6.1 represents turbulent transport of the trace species [Peters L.K., 1995].

However, some of the trace species of interest are chemically reactive. The basic equation of models that account for chemical reactive species is:

$$\frac{\partial \bar{c}}{\partial t} + \nabla(\bar{v}\bar{c}) = -\nabla(\overline{v'c'}) + \bar{S} + \bar{R} \qquad (6.2)$$

where $\bar{R}$ is the rate of formation by chemical reaction. The reaction term is calculated with mean concentrations. The introduction of this term introduced a major difference between models, as one of the goals became to create codes capable of including more and more species, in order to generate simulations closer to a real atmospheric situation. Thus, an important part of the early investigation of the ChTMs addressed the search for atmospheric chemistry systems.

6.3 Off-line and on-line classification

Depending on the mode of operation, the Chemistry and Transport Models can be classified in off-line models or on-line models.

An off-line model works with decoupled atmospheric chemistry and atmospheric dynamics modules. That is to say, meteorological fields (winds and temperature profiles), water fields (rain percentage and cloud coverage) and radiative fields are introduced as inputs to the code. As a result, off-line models have very little capability for detailed feedback analysis between atmospheric chemical perturbations and climate impacts. Most of the FGM and SGM are off-line models.

An on-line model is a model that contains both chemical and meteorological components but allows interaction between the two of them. Most third generation models seek to evaluate the relevance of different feedback processes; therefore an on-line operational mode is more appropriate for them. However an on-line model is more complex and computational limits may apply.

6.4 Chronological classification

How the idea of a feedback between the chemical dynamics of the atmosphere and the solar radiation was conceived, will be more understandable by means of a chronological arrangement of the evolution of the chemistry and transport models.

The first chemistry and transport models were programmed in the early seventies. We can divide ChTMs in three groups:

- First Generation Models (FGM)
- Second Generation Models (SGM)
- Third Generation Models (TGM), currently under development

6.4.1 First generation models

The industrial revolution during the 19th century started a new chapter for the atmospheric chemistry. The effects of human activities on the environment would suppose a set of environmental changes and problems. Some examples of these human-induced chemical perturbations are acid deposition, increasing greenhouse gas concentrations, stratospheric ozone depletion, direct and indirect climatic response to anthropogenic sulfur, and increasing tropospheric ozone concentration.

The first generation of Chemistry and Transport Models reflected the concern of the scientific community about this situation. The FGM mainly intended to simulate the effects of alternative emission controls strategies by studying the effects of pollutants concentration.

In March of 1973, Dr. Steven D. Reynolds and his team published the first of three papers in the journal *Atmospheric Environment (Pergamon Press)*, describing the first working Eulerian grid-based urban model [Reynolds S. D., 1973]. The first article, published in March dealt with the formulation of the Model. The second, published in May, gave a deeper description of the model and an inventory of pollutant emissions. Finally, the third, published in June of the same year, consisted of an evaluation of the model over the urban airshed of Los Angeles (California).

This first model included the processes of transport, emissions and gas-phase chemistry, but not the cloud effects or the dry deposition processes. The homogeneous gas-phase

chemical mechanism consisted of eleven species involved in fifteen reactions. The focus of their work was the prediction of carbon monoxide (CO), nitric oxide (NO), nitrogen dioxide (NO_2), hydrocarbons and ozone (O_3) concentrations. Also sulfur dioxide (SO_2) and aerosol concentrations were of interest but they did not pursue their study in their researches. For the other five species the steady-state approximation was applied.

Although a very simple model, as far as the feedback processes are concerned, this early work already shows concern about the radiative feedbacks in the atmosphere. It is assumed that the presence of pollutants in the atmosphere does not affect the meteorology, however citing textually from the article:

> *An important exception is the attenuation of incoming radiation by photochemically generated haze, a common occurrence, for example, in the Los Angeles area during the summer and autumn months. While the variation in pollutant concentrations may, in this way, alter the energy input to the system, and thus affect both the energy and momentum equations, it is possible to incorporate this effect in the equations of continuity alone (by treating measured intensities as data) if it is not of interest to predict temperature and velocity. Thus, the equations of continuity can be solved independently of the coupled Navier-Stokes and energy equation*.

Their limited hardware and software resources held them from installing any dynamic energy input system in their model. Instead the radiative field was part of the meteorological data module, as well as the wind speed and the wind direction. The time step of the energy input changes was assumed to be small enough with respect to the characteristic temporal scale for changes in the rate of generation or depletion of species by chemical reaction.

If we remember that at that time the meteorological data came from manual drafting and translation of hand drawn maps to punched cards, it is easy to understand what a big

constraint for the applicability and reliability of model results this was. The need of further research about the time dependence of the energy changes on photochemical reactions was stated.

Some earlier results had suggested that nitrate formation might occur on particle surfaces. Thus another reaction was included in the model, despite the ignorance about aerosols and atmospheric species feedbacks:

$$NO_2 + \text{Particle} \rightarrow \text{Nitrate} \qquad (6.3)$$

to account for the observed effect.

Nevertheless, the kinetic mechanism employed by Dr. Reynolds, had a number of fundamental shortcomings, and Dr. Reynolds himself referred to another improved mechanism published shortly after these articles as a better choice [Hecht and Seinfeld, 1974].

In 1979, Dr. Leonard K. Peters and Dr Athanasios A. Jouvanis published a paper describing their numerical simulation of the transport and chemistry of methane and carbon monoxide in the troposphere. It consisted of a global model, with a twenty-reaction gas-phase chemical mechanism describing the behaviour of nine species. Only CH_4 and CO were treated as transported species. The pseudo steady-state approximation was applied to the rest of the species, whose concentration was assumed to be able to be reliably specified.

The novelty of this model was that, first of all, an initial concentration of CH_4 and CO was specified. And second of all, it included a proper interpretation of oceans, lands and stratospheric leakage as sources and/or sinks of the particular species. Up to that moment, only a few analyses had dealt with these species.

For instance, Kwok, Langlois and Ellefsen work, in 1971, initialised their model with a CH_4 and CO empty atmosphere, included only anthropogenic CH_4 and CO sources, and treated CO as an inert species [Kwok H.C.W. et al, 1971]. Also, Wofsy developed in 1976 a model employing CH_4 and CO concentration data [Wofsy S.C., 1976]. Neither of these models accounted for the complicated processes included in Dr. Peters and Dr. Jouvanis later achievement.

Other important contribution to the first steps of the Chemistry and Transport Models were STEM-I and ROM. STEM-I was the first operational regional-scale Eulerian model designed to study sulfur air pollution [Carmichael et al., 1984]. The regional oxidant model (ROM) was designed to study the ozone production and destruction as well [Lamb R.J., 1983]. Both models, STEM-I and ROM, handled simple chemistry mechanisms and ROM did not account for dry deposition processes. Meteorological fields and emission inventories were treated as input files and the feedbacks of the chemistry and the atmospheric dynamics were not taken into account.

6.4.2 Second generation models

In the late 1970s and early 1980s the development of most of the atmospheric chemistry and transport models currently in use started. They are the so-called Second Generation Models (SGMs).

The coding took two different paths. On the one hand there were the regional and meso-scale models, and on the other hand the less sophisticated global-scale models.

The main difference between FGM and SGM is the treatment of both gas- and aqueous-phase chemistry, and cloud and precipitation scavenging processes [Peters L. K., 1995]. First Generation Models used highly parameterized formulations for the chemical transformation, using both gas- and aqueous-phase reactions lumped into one overall transformation rate, and ignored cloud-scavenging processes. Second Generation Models

however, employ more extensive chemical mechanisms and improved treatments of physical and chemical processes within and below the clouds.

Regional SGMs

STEM-II

Carmichael published in 1986 a Second Generation version of their regional-scale Eulerian model STEM-I, STEM-II [Carmichael et al. 1986]. This second version of STEM included boundary layer-free troposphere exchange in both cloud-free and cloudy environments, and in-cloud and below-cloud wet removal and chemistry processes were described more adequately.

STEM-II works in a modular structure. It can be driven by observed or modeled meteorological data. This work includes a module of heterogeneous chemistry with two processes. First process is the direct deposition of species on aerosol surfaces and the second process is the interactions between aerosol composition and the gas-phase concentrations of NH_3, HNO_3 and H_2SO_4. For that second part, the analysis of Luther and Peters was adopted, treating the mass exchange between the gas-phase and aerosol-phase by kinetic theory for very small particles and by continuum theory for the larger particles [Luther C.J. et al., 1982]. In either case, characterization of the physico-chemical interactions was only approximately known, leading to some uncertainties. A set of aerosol chemistry that had been reasonably well studied by that time was the NH_3-HNO_3-H_2SO_4-NH_4NO_3-$(NH_4)_2SO_4$ system [Stelson et al. 1979]. The point on highlighting STEM-II model is to emphasize the inclusion of a heterogeneous chemistry module in a Chemistry and Transport Model for the first time. According to their results, the relative importance of heterogeneous removal is conditioned by the radiation, having minimum influence during the mid-afternoon period.

ADOM

Another representative regional-scale SGM is ADOM [Venkatram A. et al., 1988]. ADOM stands for Acid Deposition and Oxidant Model; it was developed by ERT and MEP Co. in Canada. Simultaneously there was a similar model being developed in the State University of New York, RADM [Chang et al., 1987]. Once again the authors of these models recognize their limitations due to a lack of understanding of the most relevant processes, and a hardware resources restraint.

Urban SGMs

Morris and Myers created in 1990 one of the most important second-generation urban-scale models, which represented the second-generation development of the original work of Reynolds et al. in 1973 described in the First generation model section of this chapter [Morris R.E. et al., 1990]. The formulation for the urban Airshed model can be found in McRae G. J. et al. (1982) and [McRae G.J. et al., 1983].

The photochemical reaction mechanism employed by Morris' model was very innovative. It focused on the photolysis of species such as nitrogen dioxide (NO_2), formaldehyde (HCHO) and nitrous acid (HONO) for the formation of smog. Their model incorporated also the latest numerical solution techniques and objective analysis procedures including among others a Lagrangian trajectory and a three dimensional grid. The photochemical mechanism adopted in their work was based on [Falls A.H. et al., 1978; Falls A.H. et al., 1979].

The radiative transfer model (RTM) designed by Peterson in 1976 was used to ascertain the actinic irradiance as a function of zenith angle. The RTM accounted for aerosol

scattering and absorption, Rayleigh scattering, and ozone absorption [Peterson J.T., 1976].

Global-scale SGMs

The validity of these models depends on their accuracy to reality. To evaluate their precision, model results are compared with measurement inventories of the pertinent species. By combining high performance models with authoritative and reliable emissions inventories, it is possible to predict the concentrations of major products. Through this activity, the capability of making confident predictions on future consequences of anthropogenic emissions is achieved. There was an article by J. E. Penner presented during the 37th OHOLO conference that focused on comparing the IGAC recommended emissions inventories for reactive nitrogen and sulfur dioxide to those that had been used previously [Penner et al., 1993]. The results from the global-scale model GRANTOUR were also presented in that article. Next, GRANTOUR and several other second generation global-scale models are briefly described.

GRANTOUR

GRANTOUR is a global-scale three-dimensional atmospheric chemistry model from the Lawrence Livermore National Laboratory (LLNL) [Walton et al., 1988]. GRANTOUR results showed how emissions of anthropogenic NO_x might potentially affect tropospheric ozone and OH concentrations and how emissions of anthropogenic sulfur increased sulfate aerosol loadings [Penner J. E. et al., 1993]. Further information about GRANTOUR chemistry gas phase can be found in [Lurmann F.W. et al., 1986]. About the sulfur cycle results provided by GRANTOUR for the Troposphere in [Erickson III D.J. et al., 1991]. About the cycle of reactive nitrogen in the troposphere in [Penner J.E. et al., 1991.a]. And about the climate forcing by smoke aerosols produced by biomass burning [Penner J.E. et al., 1991. b].

GRANTOUR is part of the group of chemical tropospheric tracer models developed during the eighties that are currently in use. These models common factor is that they were used to establish the global distribution of nearly passive tracers such as CO_2, CH_4 or the isotopes ^{222}Rn and ^{210}Pb and ^{85}Kr.

MOGUNTIA

The Max-Planck Institute for Chemistry in Mainz (Germany) developed the MOGUNTIA model for the study of ^{85}Kr transport. ^{85}Kr is an exclusively anthropogenic radioactive noble gas, released by nuclear fuel recycling plants, very suitable for computing testing as its sources and sinks are rather well-known [Zimmermann P. H. et al., 1989]. MOGUNTIA has also been applied to the study of the global sulfur cycle [Langner J. et al., 1991].

Harvard University's chemical tracer model

Harvard University's global-scale Chemical Tracer Model (CTM) was also applied to the simulation of the transport ^{85}Kr [Jacob D.J. et al., 1987], as well as other trace species such as chlorofluorocarbons [Prather et al., 1987], other noble gases such as ^{222}Rn [Jacob D.J. et al., 1990; Balkanski Y.J. et al., 1990; Balkanski Y.J. et al., 1992], and heavy metals such as ^{210}Pb [Balkanski Y.J. et al., 1993].

Los Alamos national laboratory chemical tracer model

Los Alamos national laboratory CTM can be found on the following reference [Tie X. et al., 1991]. It has been used for the multi-year simulations of long-lived species, such as CH_4, CFC-11 and CH_3CCl_3.

The Pacific Northwest laboratory

Finally, the Pacific Northwest Laboratory developed The Global Chemistry Model (GChM) to estimate the long-range transport of sulfur from North America and Europe to the North Atlantic [Luecken D.J. et al., 1991]; and more recently to study mid-tropospheric carbon monoxide [Easter R.C. et al., 1993].

Hybrid Models

To obtain more realistic results, hybrid models are very recommendable. As a matter of fact, as the software and the computer support evolve, an increasing number of such models are being generated. One remarkable work fitting into this category is the Multiscale Modelling of Pollutant Transport and Chemistry by Mehmet T. Odman, in 1991 [Mehmet T.O. et al., 1991]. This work compasses urban emissions with regional oxidant formation to accurately resolve pollutant dynamics during transition from urban to regional areas.

As well as the scale of the models (urban and global), and numerical analysis mode (Lagrangian and Eulerian), this hybridization process is also affecting the vertical limits of the grids. Currently, many only-tropospheric models and many only-stratospheric models are being extended to account for upper-troposphere or lower-stratosphere leakage effects. Third Generation Models will recapitulate all of these advances.

Other SGMs

As the coding of the chemistry and transport models improved and involved more atmospheric phenomena and feedbacks, the objectives of these studies became more specialized.

Two interesting cites concerning this matter are [John J. Walton et al., 1991; Zhang Renjian et al., 2000].

J. J. Walton worked on a model capable of addressing the question of whether anthropogenic sources of sulfur are significant enough as to impact meteorology and climate [Walton J.J. et al., 1991]. Sulfur plays a major role as a source of condensation nuclei (CN). An increasing number of CN has been speculated to be responsible for an increased number of cloud droplets [Bates T.S. et al., 1987] and therefore for an enhancement of the cloud albedo (cloud reflectivity and hence cooling effect on the climate [Twomey S.A., 1974]). Over the continents, industrial emissions of SO_2 are believed to be the major source of sulfur; over the marine surfaces, biogenic dimethylsulfide (DMS). The model was applied to investigate if anthropogenic sulfur transported from continents might impact the total amount of CN over the oceans. This model consisted on a global-scale three-dimensional Lagrangian model, including a simplified treatment of the atmospheric sulfur cycle (it included only conversion of SO_2 and DMS to form the condensate SO_4^{-2}), transport, convective and eddy mixing, removal of SO_2 and SO_4^{-2} by dry deposition, and wet deposition of SO_4^{-2}.

Zhang Renjian presented a global-scale two-dimensional model stable for long time integrations, hence suitable to study the long-term trends of atmospheric species such as CH_4, CO and NO_x [Zhang R., 1997; Zhang R. et al., 1999].

Special case: MOZART

In 1998, Dr. Brasseur and his team released information about a new chemical transport model called MOZART aimed to study the global budget of ozone and its precursors.

The author would like to thank once more Dr. Brasseur kindness and Stacey Walters (MOZART software developer) inestimable help on behalf of the Thermal Radiation

Group, for putting at our disposition a first version of MOZART and facilitate future access to a second updated version of the model.

MOZART was created at the National Center for Atmospheric Research (NCAR), Colorado, (United States) by the Atmospheric Chemistry Division. MOZART stands for Model of Ozone Research in the Troposphere. It is a three-dimensional global-scale off-line chemical transport model that provides the distribution and the seasonal evolution of 56 chemical constituents. MOZART was initially used to help plan field campaigns.

To solve the equation of mass conservation for the concentration of each species, MOZART accounts for the advective, convective and diffusive transport of the species, as well as surface and in situ emissions, photochemical conversions, and wet and dry deposition. MOZART introduces the concept of volume mixing ratio, $q_i(t)$ as a function of time. This review does not intend to fully reproduce the description of the model. For further information about its code, the reader is referred to Brasseur et al., 1998.

The chemical scheme of MOZART includes 107 gas phase reactions, 5 heterogeneous reactions and 28 photochemical reactions. Emphasis is placed on the processes affecting tropospheric ozone and its precursors. Heterogeneous reactions cover N_2O_5 and NO_3 processes on sulfate aerosol surfaces, believed to provide an important loss mechanism for NO_x during nighttime. Its simulation extends from the planetary surface to the upper stratosphere.

The access to MOZART that NCAR Climate and Global Dynamics Division has provided to the Thermal Radiation Group supposes a tremendous time saver. An identification name and a password were provided to the author of this project, to access the codes of MOZART on line and permission was confirmed for her to freely download them. For confidential reasons these data are not included in this memory. Thanks to the kindness of Dr. Brasseur's team the model is now available for the TRG.

The architecture of the model is based on a front-end processor that interprets a user input file to form a Fortran® 90 source code and input data files for a complete simulation. Therefore the model is flexible allowing the user to control over basic processes such as advection, convection, diffusion, chemistry, grid and time spacing, and numerical method parameterization.

Super computer hardware support for the running of the code is crucial. MOZART is a highly vectorized, multitasked code that typically runs at 95% efficiency. A full year input data from the Community Climate Model (CCM) needs approximately 15 Gb of storage space, and a one year run of the code generates about 20 Gb of output data, a powerful Mass Storage System is consequently required. A one-year run of MOZART, with a 41 trace gases on the chemical module, a 144-point grid and a T42 spatial grid performs in approximately 200 CPU hours, consuming 60% of the computing time on the chemistry module and the remainder for transport of the 50 tracers.

6.4.3 Third generation models

Although SGM have been continuously updated, their codes are still unable to address the features currently required from chemistry and transport models. Third Generation Models (TGM) will restructure SGM codes to accommodate parallel computing architectures, utilize recent developments in numerical methods, handle cloud physics and precipitation chemistry more effectively, and address interactive processes.

In this section, a resume of some of the possible modifications and enhancements to be included in a TGM are introduced.
First of all, the chemistry module should be able to represent the chemistry regimes encountered worldwide. And second of all, the code needs to be robust enough to encompass the changes in atmospheric chemistry that would result from changes in meteorological and climate attributes, such as temperature, moisture concentration in the air, cloud coverage, solar actinic flux and localized trace gas emission. Since the

chemical mechanism supporting data require a massive storage system, and the majority of computing time is consumed by the integration of the chemical concentration rate equations, it is critical to evaluate the relevance of the processes to be included in the module.

Nowadays, the photochemical oxidant cycle is a very active research field. The peroxyl (HO_2 and RO_2) and hydroxyl (OH) radicals are the primary oxidants of the atmosphere. They are key for the balance of the nitrogen oxides (NO and NO_2) that control ozone concentration. TGM should improve the ability to predict these radicals concentration.

Reactive Hydrocarbons, (RHCs), are decisive in the generation and recycling of oxidant radicals, but their analysis is obsolete for two reasons. On the one hand, the RHCs compounds are grouped according to their structure or reactivity. Commonly, RHCs are lumped into alkanes, alkenes, aromatics and carbonyls. This generalization simplifies calculations but disguises the effectiveness of the results of the ozone depletion control techniques. And on the other hand, the codes are accommodated to predict ozone concentration based on out-of-date RHC to NO_x ratios. Nowadays, the RHC to NO_x ratios are significantly lower. What hydrocarbon species to include and up to what extend, are important questions for a TGM.

Chlorine chemistry lacks evaluation of relevance studies and a good source retrieval system.

Heterogeneous reaction importance was already highlighted when developing FGM [Reynolds S. D., 1973]. Research on this area focuses on alternatives to homogeneous aerosol formation reactions and on heterogeneous reactions on aerosol surfaces. TGM will evaluate the convenience of allowing simultaneous treatment of aerosol physics and thermodynamics, aqueous-phase chemistry on wetted particles, and mineral-composed aerosols in their codes.

Going on with heterogeneous chemistry, there are three applicable processes concerning the aqueous-phase chemistry. First, the possible dependence between cloud and rain water composition and water droplet size distribution suggested by Ogren [Ogren J.A. et al., 1989]. Second, the photochemistry within the clouds and rain droplets. And third, organic acids, such as formic or acetic acids should be taken into account. Despite the fact that these are minor pollutant gases, in comparison with nitric or sulfuric acids, they may be significant in remote regions.

Concerning aerosols, TGM should improve the treatment of the aerosol scattering function and optical properties, as well as the interactions and feedbacks between aerosols and clouds. These enhancements concern to aerosol dynamics, gas-to-particulate conversion and Cloud Condensation Nuclei (CCN).

As explained in Chapter 3, aerosols scatter and absorb short wavelength radiation from the sun. They are responsible for visibility factors and climate effects. A good size distribution simulation is required.

Aerosol dynamics concerns coagulation, condensational growth, evaporative loss and settling. Homogeneous nucleation and CCN processes need an optimal estimation of aerosol size distribution and composition that should be enhanced by TGM.

The role played by aerosols in gas-to-particulate conversion has been introduced earlier when talking about heterogeneous chemistry.

Finally, Chemistry and Transport Models have treated, so far, only inorganic aerosols; any complete TGM should consider the inclusion of organic aerosols as well.

Cloud studies are another of the most active research arenas in atmospheric science. Clouds participate in the chemistry of the atmosphere in several ways. Of course wet removal is sink of many species. Clouds provide the aqueous medium for aqueous-phase

chemical reactions. There is vertical transport of species within a cloud. Lastly, clouds modify radiative fields of the atmosphere and therefore the photolysis rate of the photochemical reactions. As a whole, clouds suppose the most complicated ensemble of feedbacks reported in the Chemistry and transport models.

SGMs worked with a simplifying concept, the scavenging coefficient, which represented the loss rate of species. This coefficient was proportional to the precipitation rate, and was estimated from empirical studies. The proposal for the TGM is to work with cloud modules. The way a cloud module works is once the model receives the information that there are clouds in that position and at that time, the cloud module would generate a vertical profile of the composition of the cloud according to the meteorological information and the profiles of trace gases and aerosols.

Cloud modules do not represent the cloud processes in a completely realistic way either. The case of non-precipitating clouds and the need for coupled processes between clouds microphysics, aerosols and the radiative field still remain unstudied. Another problem arises if we consider that clouds are not fixed in space or time, and that sometimes, a cloud is smaller than the smallest grid size employed by any model. A probabilistic approach, proposed for cloud water only, to develop a parameterisation of subgrid cloud variability might be the solution [Smith R.N.O., 1990].

Dry deposition processes were already included in the earliest Chemistry and Transport Models. Nevertheless, some shortcomings about surface exchange processes still remain. Some of these shortcomings are the following. Treating dry deposition processes as boundary conditions ignores reversibilities, surface saturation problems, aging, conditioning and time lags. Sometimes, a horizontal atmospheric grid subdivision will cover different Earth's surface classes, for instance a soil terrain with a river crossing along. In addition to this, the field data to validate dry deposition rates are scarce. These effects could be easily overcome in a TGM. A feedback treatment between meteorology,

temperature, relative humidity, surface type, air composition and the characteristics of species exchange will provide a self-consistent dry deposition flux.

SGM estimated meteorology either from observational input files as in the STEM-I model or from atmospheric circulation models performing a decoupled chemistry circulation and meteorological simulation. Up to this point it appears obvious the convenience of a coupled meteorological system and the atmospheric chemical composition module. Temperature and relative humidity are a function of the concentration of chemical species in the air. Consider the influence of the scattering aerosol distribution on the atmospheric albedo, on the cloud coverage and consequently on the climate.

Turbulent mixing, overall at the boundary layer, and vertical mixing are some other points that the meteorological module needs to realistically address in a TGM. As they have already been described in previous sections, they will not be discussed any further here.

There is a tendency on the late SGM to blur the limits between only-tropospheric models and only-stratospheric models. Instead stratospheric-tropospheric models started being contemplated. The concern with NO_x and ozone species being concentrated on the upper limit of the troposphere initiated this tendency [Kasibhatla P.S. et al., 1991].

Based on Andrews' 1987 article, TGM should evaluate the pertinence of including six different processes at the troposphere-stratosphere limit. These will be: large-scale radiatively driven circulations, tropopause folding during upper-level cyclogenesis, transverse secondary circulations associated with jet streams, penetration of cumulonimbus clouds intro the stratosphere, cloud top radiative cooling near the tropopause, and turbulent mixing due to gravity-wave breaking or shear instabilities at the tropopause [Andrews D.G. et al., 1987].

Remember from the description of the FGM that the radiative transfer module was an input coming from look-up tables of clear sky actinic flux calculated off-line (observational data) and stored as a function of wavelength, solar zenith angle, and altitude (or pressure), with the effects of clouds accounted on line [Peters L. K., 1995]. The handicap of this approach is that it is impracticable for global-scale models or atmospheric columns with a varying amount of photochemical reactant or oxidant species like the ozone.

Cloud optical properties are assumed to be independent of the wavelength, thus to consider their influence as a dependence of the clear sky to cloudy sky ratio is acceptable. The aerosol case, however, is different. Scattering processes by aerosols are wavelength dependent. More to the point, absorption coefficient is also a function of aerosol composition. Hence a feedback between aerosol size distribution and composition, and the radiative transfer module becomes apparent. Solutions that a TGM may apply could be either a more complete off-line look-up table or an on-line radiative transfer and aerosol module. The first solution may create manageable problems when dealing with such a big table. This research is aimed at the evaluation of the second solution feasibility evaluation.

Corroboration of the performance of the model is indispensable to advance in its development. When a model is going to be used to evaluate control techniques, its validation is a requirement.

As the models become more and more comprehensive, the straightforward model evaluation becomes more impractical. Straightforward model evaluation refers to the technique applied to FGM and SGM evaluation, consisting on varying one or two parameters and comparing outputs. It has been suggested that TGM should incorporate their specific sensitivity coefficients or develop an automatic differentiation technology [Griewank A., 1989; Griewank A. et al., 1994].

One last remark to conclude this discussion. Flexible TGM are also very appealing. A model capable of running either on-line or off-line mode could be used to validate theories or observational data. If the simulation were based on observational meteorology (off-line), field measurements would be validated by the model. If the simulation were based on simulated meteorology (on-line), the model performance could be used as a forecast.

Chapter 7 Conclusions and Future Work

This research is a required preliminary step to evaluate the feedback mechanism between photolytic aerosols and the solar radiative field in order to estimate the convenience of including it in a third generation chemistry and transport model. This thesis deals with the evaluation of the impact on the solar radiative field of an absorbing, scattering, nonemitting media.

The physical characterization of the participating media was established in accordance with aerosol field retrievals reported in the literature. The optical properties of the participating media were ascertained by means of the Mie scattering theory. Finally, the MCRT method was applied to model the radiation heat transfer.

This analysis was applied to one-centimeter atmospheric cubes, this size being sufficiently large to ensure that the cube contains a statistically meaningful number of aerosol scattering centers, yet sufficiently small to permit a finely resolved vertical structure in the atmosphere. The sun was modeled as a polychromatic, collimated, nonpolarized radiative source. A population of 5000 spherical-shaped rural aerosols was uniformly distributed within the cube. The population of rural aerosols was assumed to be composed purely of water-soluble particles, such as nitrates, sulfates, DMS and water-soluble organic substances. Humidity is zero. Scattering divergence is cancelled.

The novelty of the MCRT method developed by this research is its capability to physically characterize and locate every aerosol individually. It consists of a microscopic analysis of the effects of a participating media in the solar radiative field. This feature was required for future coupling with a chemistry kinetics module.

A new parameter, pcsr, was introduced to enable the application of the MCRT. The pcsr parameter was optimized according to theoretical results, and the results provided by the microscopic MCRT method were validated by comparison with the literature. The optimum value of pcsr was proved to be 900.

Prior to the modeling portion of this work a library of available chemistry and transport models and literature about these models was provided to the thermal radiation group of Virginia Tech. Access to a second-generation model, MOZART, and a database for its execution was provided by the author to this group.

The conclusions drawn from this research are:

- the proposed microscopic MCRT method is a truthful and correct tool to model the radiative part of the above-cited feedback mechanism
- a band-averaged version of the microscopic MCRT method is selected for the simulations as an accurate and more time economical analytical resource
- the absorption of solar radiation by atmospheric aerosols decreases exponentially as it penetrates the atmosphere
- the small clean-continental aerosols absorb more efficiently than the larger aerosols

The MCRT model designed in this thesis opens endless research possibilities. The author recommends further work addressing the improvement of the local coordinate system generator to eliminate or significantly reduce the 5 percent of rays the program is forced to reject for problems described along Chapter 5.

It would be interesting as well, to study analytically the dependency of the accuracy of the band-averaged model based on the precision of the particle radius and wavelength discretization.

The relationship between the optimum value of pcsr and optics could also an interesting discussion.

Future work on this subject will be dedicated to the coupling of the radiative module with a dynamic chemical kinetic module to model the growth rate of the photolytic aerosols as a function of the radiative field.

References

Andrews D. G., Holton J. R. and Leovy C. B. *Middle Atmosphere Dynamics*, pp. 489. Academic Press New York. 1987.

Balkanski Y. J. and Jacob D. J. *Transport of continental air to the Subantarctic Indian Ocean.* Tellus. **Vol**. 42B, pp. 62-75. 1990.

Balkanski Y. J., Jacob D. J., Arimoto R. and Kritz M. A. *Long range transport of Radon-222 over the North Pacific Ocean: implications for continental influence.* Journal atmos. Chemistry. **Vol**. 14, pp. 353-374. 1992.

Balkanski Y. J., Jacob D. J., Gardner G. M., Graustein W. C. and Turekian K.K. *Transport and residence times of tropospheric aerosols inferred from a global three-dimensional simulation of ^{210}Pb*. Journal geophysics research. **Vol**. 98, pp. 20,573-20,586. 1993.

Barrie L. A., Hoff R. M. *Five years of air chemistry observations in the Canadian Arctic*. Atmospheric Environment., **Vol**. 19, pp. 1995-2010. 1985.

Barrie L.A., Hoff R. M., Daggupaty S.M. *The influence of mid-latitudinal pollution sources on haze in the Artic.* Atmospheric Enviroment, **Vol**. 15. pp. 1407-1419. 1981.

Bates T. S., Charlson R. J. and Gammon R. H. *Evidence for the climatic role of marine biogenic sulphur*. Nature, **Vol**. 329, pp. 319-321. 1987.

Blanchard D. C., and Woodcock A. E. *The production, concentration and vertical distribution of the sea salt aerosol.* Ann. N. Y. Acad. Sci., **Vol**. 338, pp. 330-347. 1980.

Bongiovi R. P. *A parametric Study of the Radiative and Optical Characteristics of a Cassegrain Telescope Scanning Radiometer for Earth Radiation Budget Applications Using the Monte-Carlo Method*. Master of Science, Mechanical Engineering Department. Virginia Polytechnic Institute and State University. Blacksburg, Virginia, U.S.A., 1993.

Brasseur G. P., Hauglustaine D. A., Walters S., Rasch P. J., Müller J. F., Granier C. and Tie X. X. *MOZART, a global chemical transport model for ozone and related chemical tracers 1. Model description*. Journal of geophysical research. **Vol**. 103, No. D21, pp. 28,265-28,289. November 20, 1998.

Brewster M. Q. *Thermal radiative transfer and properties*. John Wiley & sons, Inc. Wiley-Interscience Publication. 1992.

Brewster M.Q. and Tien C.L. *Radiative Transfer in packed fluidized beds: dependent versus Independent scattering*. Journal of Heat Transfer, **Vol**. 104, No. 4, pp. 573-579. November, 1982.

Cameron, A. G. W. *Elementary and nuclidic abundances in the solar system, in: Essays in Nuclear Astrophysics* (C. A. Barnes, D. D. Clayton, and D. N. Schramm, eds.), Cambridge University Press, Cambridge, England. 1981.

Carmichael G. R., Peters L. K. [a], *An Eulerian transport/transformation/removal model for SO_2 and sulfate-I. Model development*. Atmospheric Environment, **Vol**. 18, 937-952. 1984.

Carmichael G. R., Peters L. K. [b], *An Eulerian transport/transformation/removal model for SO_2 and sulfate. Model calculation of SO_x transport in the eastern United States*. Atmospheric Environment, **Vol**. 18, 953-967. 1984.

Carmichael G.R., Peters L.K. and Kitada T. *A second-generation model for regional-scale chemistry/transport /deposition*. Atmospheric Environment, **Vol**. 20, 173-188. 1986.

Carnicero Domínguez B. A. *Preliminary design of an Airborne Tracking Aureolemeter for studying Atmospheric Aerosols.* Proyecto fin de carrera. Centro Politécnico Superior. Universidad de Zaragoza. Zaragoza. Spain, 1999.

Chang J. S., Brost R. A., Isaksen I. S. A., Madronich S., Middleton P., Stockwell W. R. and Walcek C.J. *A three-dimensional Eulerian acid deposition model: physical concepts and formulation.* Journal Geophysics Research, **Vol**. 92, pp. 14,681-14,700. 1987.

Chapman D.D. A Monte-Carlo-Based Simulation of Jet Exhaust Nozzle Thermal Radiative Signatures. Master of Science, Mechanical Engineering Department. Virginia Polytechnic Institute and State University. Blacksburg, Virginia, U.S.A., 1992.

Coffey K. L. *Next generation Earth Radiation Budget Instrument Concepts*. Master of Science, Mechanical Engineering Department. Virginia Polytechnic Institute and State University. Blacksburg, Virginia, U.S.A., 1998.

D'Almeida G. A. *On the variability of desert-dust radiative characteristics*. Journal Geophysics Research, **Vol**. 92, pp. 3017-3026. 1987.

D'Almeida G. A., Koepke P., Shettle E. P. *Atmospheric Aerosols, global climatology and Radiative Characteristics*. A. Deepak Publishing; Hampton, Virginia, USA. 1991.

Davies C.N. *Size distribution of atmospheric particles,* Journal of Aerosol Science, **Vol**. 5, pp. 293-300. 1974.

Deirmendjian D. *Electromagnetic Scattering on Spherical Polydispersions*. American Elsevier Publishing Company, INC. New York. 1969.

Desalmand F., Podzimek J., and Serpolay R. [a], *A continental well-aged aerosol in the Guinea savannah at the level of a through along the ICTZ*. Journal Aerosol Science, Vol. 16, pp. 19-28. 1985.

Desalmand F., Serpolay R., and Podzimek J. [b], *Some specific features of the aerosol particle concentrations during the dry season and during a bush fire event in West Africa.* Atmospheric Environment, **Vol**. 9, pp. 1535-1543. 1985.

Easter R. C., Saylor R. D. and Chapman E. G. *Analysis of mid-tropospheric carbon monoxide data using a three-dimensional global atmospheric chemistry numerical model.* Proc. 20th Int. Tech. Meeting on Air Pollution Modeling and its Application, 29 November-3 December, 1993, Valencia, Spain.

Erickson III. D. J., Walton J. J., Ghan S. J., and J. E. Penner. *Three-dimensional modeling of the global atmospheric sulfur cycle: A first step*. Atmospheric Environment, **Vol**. 25A, 2513-2520. 1991.

Eskin L. D. *Application of the Monte Carlo Method to the Transient Thermal Modeling of a Diffuse-Specular radiometer Cavity.* Master of Science, Mechanical Engineering Department. Virginia Polytechnic Institute and State University. Blacksburg, Virginia, U.S.A., 1986.

Falls A. H. and Seinfeld J. H. *Continued development of a kinetic mechanism for photochemical smog*. Environmental Technology, **Vol**. 12, pp. 1398-1406. 1978.

Falls A. H., McRae G. J. and Seinfeld J. H. *Sensitivity and uncertainty of reaction mechanisms for photochemical air pollution*. Int. Journal Chemical Kinetics, **Vol**. 11, pp. 1137-1162. 1979.

Fleck J. A. *The calculation of nonlinear radiation transport by a Monte Carlo Method*. Technical report UCRL-7838, Lawrence Radiation Laboratory. 1961.

Gibbons J. D., and Chakraborti S. *Nonparametric Statistical Inference*. Third Edition, Mercel Dekker Incorporated, New York, NY. 1992.

Griewank A. and Corliss G. *Automatic Differentiation of Algorithms: Theory, Implementation, and Application*. SIAM, Philadelphia, PA. 1991.

Griewank A. *On automatic differentiation. In Mathematical Programming: Recent Developments and Applications.* Edited by Iri M. and Tanabe K, pp. 83-108. Kluwer, Dordrecht. 1989.

Griewank A., Juedes D. and Utke J. *ADOL-C: a package for the automatic differentiation of algorithms written in C/C++*. ACM Trans. Math. Software, in press. 1994.

Haeffelin M. *A study of Earth Radiation Budget Radiometric Channel Performance and Data Interpretation Protocols*. Ph. D. Dissertation, Mechanical Engineering Department. Virginia Polytechnic Institute and State University. Blacksburg, Virginia, U.S.A., 1997.

Hammersley J. M. and Handscomb D. C. *Monte Carlo Methods*. John Wiley $ Sons, New York. 1964.

Harshvardhan, Arking A., King M.D., and Chou M. D. *Impact of the El Chichon stratospheric aerosol layer on northern hemisphere temperatures*. *Aerosols and their Climatic Effects*. (H.E. Gerber and A. Deepak, eds.). A. Deepak Publishing, Hampton, VA, USA, pp. 251-273. 1984.

Hecht T. A. and Seinfeld J. H. *Further development of a generalized kinetic mechanism for photochemical smog*. Environmental Science Technology, In Press. 1974.

Hess M., P. koepke, and I. Schult, May. *Optical properties of Aerosols and Clouds: The Software package OPAC. Meteorologisches Institut der Universität München. München, Germany.* Available from the Bulletin of the American Meteorological Society. **Vol**. 79, No. 5, pp.831-844. 1998.

Hidy G. M. *Aerosol, an industrial and environmental science*. Academic Press, Orlando, Florida. Page 774. 1984.

Howell J. R. and Perlmutter M. *Monte Carlo solution of thermal transfer through radiant media between gray walls*. ASME Journal of heat transfer, **Vol**. 86, No.1, pp. 116-122. 1964.

Jacob D. J. and Prather M. J. *Radon-222 as a test of convective transport in a general circulation model*. Tellus. **Vol**. 42B, pp. 118-134. 1990.

Jacob D. J. and Prather M. J., Wofsy S. C. and McElory M. B. *Atmospheric distribution of ^{87}Kr simulated with a general circulation model. Journal geophysics research*. **Vol**. 92, pp. 6,614-6,626. 1987.

James, F. *Review of pseudorandom number generator*. Computer physics communications, **Vol**. 60, pp. 329-344. 1990.

Junge C.E. *Gesetzmäßigkeiten in der Größenverteilung atmosphärischer Aerosole über dem kontinent.* Ber. D. Wetterd. US-Zone, **No**. 35, pp. 261-277. 1952.

Kasibhatla P. S., Levy H. II, Moxim W. J. and Chameides W. L. *The relative impact of stratospheric photochemical production on tropospheric NO_y levels: a model study*. Journal of geophysics research. **Vol**. 96, pp. 18,631-18,646. 1991.

Kwok H. C.W., Langlois W.E. and Ellefsen R.A. *Digital simulation of the global transport of carbon monoxide*. IBM J. Research Development. **Vol**. 15, 3-9. 1971.

Lamb R.J. *A regional-scale (1000 km) model of photochemical air pollution-I. Theoretical formulation.* EPA Report EPA-600/3-83-035. 1983.

Landgraf J. and Crutzen P.J. *An efficient method for online calculations of photolysis and heating rates*. Journal of Atmospheric Science. **Vol**. 55, pp. 863-878. 1998.

Langner J. and Rodhe H. *A global three-dimension model of the tropospheric sulfur cycle.* Journal of Atmospheric Chemistry, **Vol**. 13, pp. 225-263. 1991.

Lenoble J. *Atmospheric radiative transfer*. A. Deepak Publishing; Hampton, VA, USA. 1993.

Luecken D. J., Berkowitz C. M. and Easter R. C. *Use of a three-dimensional cloud-chemistry model to study the transatlantic transport of soluble sulfur species*. Journal geophysics research. **Vol**. 96, pp. 22,477-22,490. 1991.

Lurmann F. W., Lloyd A. C. and Atkinson R. *A chemical mechanism for use in long-range transport/acid deposition computer modeling*. Journal of Geophysics Research. **Vol**. 91, pp. 10,905-10,936. 1986.

Luther C.J. and Peters L.K. *The possible role of heterogeneous aerosol processes in the chemistry of CH4 and CO in the troposphere*. In Heterogeneous Atmospheric Chemistry, Edited by Schryer D.R. Geophysical Monograph 26, American Geophysical Union, Washington, pp. 264-273. 1982.

Mahan J. R. *Radiation Heat Transfer*. Class notes manuscript. Virginia Tech. 2001.

Mahan J. R. *Radiation Heat Transfer: a Statistical Approach*. John Wiley & Sons, Inc. New York. 2002.

Maltby J. D. and Burus P. J. *Performance, accuracy and convergence in a three-dimensional Monte Carlo radiative heat transfer simulation*. Numerical Heat Transfer, Part B. **Vol**. 19, pp. 191-209. 1991.

McRae G. J. and Seinfeld J. H. *Development of a second-generation mathematical model for urban air pollution. II. Evaluation of model performance*. Atmospheric Environment, **Vol**. 17, pp. 501-522. 1983.

McRae G. J., Goodin W. R. and Seinfeld J. H. *Development of a second-generation mathematical model for urban air pollution. I. Model formulation*. Atmospheric Environment, **Vol**. 16, pp. 679-696. 1982.

Meekinsm J. L. *Optical Analysis of ERBE Scanning Thermistor Bolometer Radiometer using the Monte-Carlo Method.* Master of Science, Mechanical Engineering Department. Virginia Polytechnic Institute and State University. Blacksburg, Virginia, U.S.A., 1990.

Mehmet T. O. and Armistead G. R. *Multiscale Modeling of Pollutant Transport and Chemistry.* Journal of Geophysical Research, **Vol**. 96, No. D4, pp. 7363-7370. April 20, 1991.

Meszaros A. *On the size distribution of atmospheric aerosol particles of different composition.* Atmospheric Environment, **Vol**. 11, pp. 1075-1081. 1977.

Mie G. *Optics of turbid media*. Annalen der Physik, **Vol**. 25, No. 3, pp. 377-445.1908.

Modest M. F. *Radiative heat transfer*. McGraw-Hill, Inc. 1993.

Morris R. E. and Myers T. C. *User's guide for the Urban Airshed Model, Vol. 1, User's manual for UAM (CB-IV)*, *U.S.EPA Report EPA/450/4-90/007A*. National Technical Information Service, Springfield, Virginia, Document PB91-1312227/REB. 1990.

Nguyen T. K. *Optimization of Radiometric Channel Solar Calibration for the clouds and the Earth's Radiant Energy System (CERES) using the Monte-Carlo method*. Master of Science, Mechanical Engineering Department. Virginia Polytechnic Institute and State University. Blacksburg, Virginia, U.S.A., 1994.

Ogren J. A., Heintzenberg J., Zuber A., Noone K. J. and Charlson R. J. *Measurements of the size-dependence of solute concentrations in cloud droplets.* Tellus **Vol**. 41B, pp. 24-31. 1989.

Parungo F., Bodhaine B., Bortniak J. *Seasonal variation in Antarctic aerosols*. Journal Aerosol Science, **Vol**. 17. pp. 491-504. 1981.

Parungo F., Harris J., Rosenwasser B., and Ruhnke L. *Analyses of aerosol and precipitation samples collected during a transatlantic research cruise*. NOAA-Technical Memorandum, ERL ESG-5, Boulder, Co., USA, pp. 62. 1984.

Penner J. E., Atherton c. S. and Graedel T. E. *Global emissions and models of photochemically active compounds.* In 37th OHOLO Conf. Series (edited by Slinn A.) Plenum, New York. 1993.

Penner J. E., Atherton C. S., Dignon J., Ghan S. J., Walton J. J. and Hameed S. [a], *Tropospheric nitrogen: A three-dimensional study of sources, distribution, and deposition*. Journal of Geophys. Res., **Vol**. 96, 959-990. 1991.

Penner J. E., Ghan S. J., and Walton J. J. [b], *The role of biomass burning in the budget and cycle of carbonaceous soot aerosols and their climate impact, in Global Biomass Burning*. Edited by J. Levine, MIT press, Cambridge, MA, pp. 387-393. 1991.

Peters L. K. and Jouvanis A.A. *Numerical simulation of the transport and chemistry of CH_4 and CO in the troposphere*. Atmospheric Environment **Vol**. 13, pp. 1443-1462. 1979.

Peters L. K., Berkowitz C. M., Carmichael G. R., Easter R. C., Fairweather G., Ghan S. J., Hales J. M., Leung L. R., Pennell W. R., Potra F. A., Saylor R. D. and Tsang T. T. *The current state and future direction of Eulerian models in simulating the tropospheric chemistry and transport of trace species: a review*. Atmospheric Environment (Pergamon Press), **Vol**. 29, No. 2, pp. 189-222. 1995.

Peterson J. T. *Calculated Actinic Fluxes (290-700 nm) for Air Pollution Photochemistry Application.* U.S. Environmental Protection Agency Report EPA-600/4-76-025, 63 pp. 1976.

Planck M. *Über das Gesetz der Energievertheilung im Normalspektrum*. Annalen der Physik. **Vol**. 4, pp. 553-563. 1901.

Podzimek J. *Physical properties of aerosol in rural and forested areas. Aerosols and Climate* (P.V. Hobbs and M. P. McCormick, eds.), A. Deepak Publishing, Hampton, VA, USA, pp. 153-164. 1987.

Priestly K. J. *Use of First-Principle Numerical Models to enhance the Understanding of the Operational Analysis of Space-Based Earth Radiation Budget Instrument.* Master of Science, Mechanical Engineering Department. Virginia Polytechnic Institute and State University. Blacksburg, Virginia, U.S.A., 1997.

Reist P. C. *Aerosol Science and Technology*. McGraw-Hill, Inc. 1984.

Reynolds S. D., Liu M. K., Hecht T. A., Roth P. M. and Seinfeld J. H. *Modeling of photochemical air pollution-III. Evaluation of the model*. Atmospheric Environment **Vol**. 8, pp. 563-596. 1974.

Reynolds S. D., Roth P. M., and Seinfeld J. H. *Mathematical modeling of photochemical air pollution-I. Formulation of the model.* Atmospheric Environment Pergamon Press, **Vol**. 7, pp. 1033-1061. 1973.

Sánchez M. C. *Optical Analysis of a Linear-Array Thermal Radiation Detector for Geostationary Earth Radiation Budget Applications*. Master of Science, Mechanical Engineering Department. Virginia Polytechnic Institute and State University. Blacksburg, Virginia, U.S.A., 1998.

Schütz L. *Long range transport of desert dust with special emphasis on the Sahara*. Ann. N.Y. Acad. Sci., **Vol**. 338, pp. 515-532. 1980.

Shaw G.E. *Considerations on the origin and properties of the Antarctic aerosol.* Rev. Geophys. Space Phys., **Vol**. 8, pp. 1983-1998. 1979.

Shettle E. P., and Fenn R. W. *Models for the aerosols of the lover atmosphere and the effects of humidity variations on their optical properties.* AFGL-TR-79-0214, Environmental Research Paper **No**. 675, NTIS ADA 085951. 1979.

Shettle E. P., Fenn R.W. *Models of atmospheric aerosols and their optical properties*. AGARD Conference Proceedings **No**. 183, Optical Properties in the Atmosphere AGARD-CP-183, NTIS, ADA 028615. 1976.

Siegel R. and Howell J. R. *Thermal radiation heat transfer*. Hemisphere Publishing Corporation. McGraw-Hill Book Company. 1981.

Smith R. N. O. *A scheme for predicting layer clouds and their water content in a general circulation model*. Q. J. R. met. Soc. **Vol**. 116, pp. 435-460. 1990.

Stelson A. W., Freidlander S.K. and Seinfeld J.H. *A note on the equilibrium relationship between ammonia and nitric acid and particulate ammonium nitrate.* Atmospheric Environment **Vol**. 13, pp. 369-371. 1979.

Tie X., Alyea F. N., Cunnold D. M. and kao C. Y. *Atmospheric methane: A global three-dimensional model study*. Journal geophysics Research, **Vol**. 96, pp. 17,339-17,348. 1991.

Turk J. A. *Acceleration Techniques for the Radiation Analysis of General Computational Fluid Dynamics Solutions Using Reverse Monte Carlo Ray Tracing.* Ph. D. Dissertation, Mechanical Engineering Department. Virginia Polytechnic Institute and State University. Blacksburg, Virginia, U.S.A., 1994.

Twomey S. A. *Pollution and the planetary albedo*. Atmospheric Environment. **Vol**. 8, pp. 1251-1256. 1974.

Van de Hulst H. C. *Light scattering by small particles*. Dover Publications, Inc. New York. 1981.

Venkatram A., Karamachandani P. K. and Misra P. K. Testing a comprehensive acid deposition model. Atmospheric Environment, **Vol.** 22, pp. 737-747. 1988.

Villeneuve P. V. *A Numerical Study of the Sensitivity of Cloudy-Scene Bi-directional Reflectivity Distribution Functions to Variations in Cloud Parameters*. Ph. D. Dissertation, Mechanical Engineering Department. Virginia Polytechnic Institute and State University. Blacksburg, Virginia, U.S.A., 1996.

Walkup M. D., *A Monte Carlo Optical Workbench for Radiometric Imaging System Design.* Master of Science, Mechanical Engineering Department. Virginia Polytechnic Institute and State University. Blacksburg, Virginia, U.S.A., 1996.

Walton J. J., Ghan S. J. and Penner J. E. *Three-dimensional modeling of the global atmospheric sulfur cycle: a first step.* Atmospheric Environment. **Vol**. 25A. No. 11, pp. 2513-2520. 1991.

Walton J. J., McCracken M. C. and Ghan S. J. *A global-scale Lagrangian trace species model of transport, transformation, and removal processes*. Journal of Geophysics Research, **Vol**. 93, pp. 8339-8354. 1988.

Wofsy S.C. *Interactions of CH4 and CO in the Earth's atmosphere*. In Annual Review of Earth and Planetary Sciences 4, edited by F. A. Donath, F.G. Stehli, and G.W. Wetherill, pp. 441-469. Annual Reviews, Palo Alto, CA. 1976.

World Climate Programme, WCP-112. *A preliminary cloudless standard atmosphere for radiation computation*, WMO/TD-No. 24. World Meteorological Organization, Geneva. 1986.

World Climate Programme, WCP-55. *Report of the expert meeting on aerosols and their climatic effects* (A. Deepak and H. E. Gerber, eds.), World Meteorological Organization, Geneva. 1983.

Yung Y.L. and DeMore W.B. *Photochemistry of planetary atmospheres*. Oxford University Press, New York. 1999.

Zhang Renjian and Wang Mingxing. *Modeling the sudden decrease in CH4 growth rate in 1992*. Advances in Atmospheric Science, Vol. 16(2), 242-250. 1999.

Zhang Renjian, Wang Mingxing and Zeng Quingeun. *Global two-Dimensional chemistry model and simulation of atmospheric chemical composition.* Advances in Atmospheric Science. **Vol**. 17, No. 1, pp. 72-82. February 2000.

Zhang Renjian. *A global two-dimensional chemistry model and methane increasing in atmosphere*, Ph.D. dissertation (in Chinese). Institute of Atmospheric Physics, Chinese Academy of Sciences, 126 pp. 1997.

Zimmerman P. H., Feichter J., Rath H. K., Crutzen P. J. and Weiss W. *A global three-dimensional source receptor model investigation using ^{85}Kr.* Atmospheric Environment, **Vol**. 23, pp. 25-35. 1989.

Zimmerman P. R., Chatfield R. B., Fishman J., Crutzen P. J., and Hanst P. L. *Estimates of the production of CO and H2 from the oxidation of hydrocarbon emission from vegetation*. Geophysics research Letters, **Vol**. 5, pp. 679-682. 1978.

Internet Web Cites

http://www.scd.ucar.edu/zine/96/spring/articles/SC95/home.html

http://www.acd.ucar.edu/

http://www.ucar.edu

http://www.tau.ac.il/geophysics/staff/colin/chemistry.htm

http://www.meteo.physik.uni-muenchen.de/

http://www.lrz-muenchen.de/~uh234an/www/radaer/gads.html

http://www.lrz-muenchen.de/~uh234an/www/radaer/opac.html

http://www.nasa.gov

http://nssdc.gsfc.nasa.gov/images/solar/eit_sl_171.jpg

http://www.ucar.edu/learn/1_3_1.htm

http://www.ucar.edu/learn/1_1_1.htm

http://www.ucar.edu/learn/1_1_1.htm

Appendix

Supporting Computer Codes

THIS IS THE BAND-AVERAGED PROGRAM FORTRAN® 90 CODE

```
****************************************
*     MAIN PROGRAM BAND-AVERAGED       *
****************************************
      PROGRAM Band-Averaged

C     This program launches a ray vertically downwards from a square
      imaginary surface placed on the atmospheric cube top imaginary
      surface.

*     Subroutine "Shooting Point" assigns a shooting point in
Gl.coord.sys.
*     Subroutine "Sol" assigns a wavelength to the ray.
*     Subroutine "IndexRefraction" looks for the corresponding
      complex index of refraction as a function of wavelength.



c           Iz_axis  !  / !
c           I       ! /  !
c           I       !/   !
c           I            !
c           I            !
c           I            !
c           I____________________
c           /                   y_axis
c          /
c         /
c        /x_axis



C     First two random numbers are used to randomly position the
*     energy bundle on the source surface (x0, y0). Taking the
*     left back corner of the atmospheric cube as the origin of
*     coordinates, the value of z0 is constant *an equal to 1 cm.
*
*     The origin where an energy bundle strikes on an aerosol is
*     approximated the center of the aerosol.

C     The parameter "pcsr" represents the probability cross section.
*     A ray is represented by the MCRT method as a line whose
diameter is
*     infinitively small, it is almost impossible that the ray
strikes on
*     any aerosol. However, in reality, the energy bundle behaves as
a
*     wave, and it has a finite diameter. The "pcsr" parameter
compensates *     this effect.


*---------------------------------------*
*     Description of variables          *
*---------------------------------------*

C     The real variables are:
*           OriPG(x, y, z)=position the aerosol within the cube (cm).
*           DesPG(x, y, z) (cm).
*           CosDir=Direction Cosines -array(3).
*           lam=wavelength
```

```
*           rm=real part of the index of refraction, wavelength
dependent
*           ri=imag. part of the index of refraction, wavelength
dependent
*           scs=scattering cross section (microns**2)
*           ecs=extinction cross section (microns**2)
*           PhaseF=array containing the scat.Pha.Func. from MieMono.
*           Theta=array containing the Theta angles from MieMono
(degrees)
*           Zenith=zenith angle (radians)
*           Azimuth=azimuth angle (radians)
*           X/Y/ZLocAxis
*           Aerodata=(5000x4) matrix containing the data of each
aerosol
*           Absorption=(5000x3) matrix containing the 1st-height (cm)
*           the 2nd-rad (μm) the absorbing aerosol, and 3-the number
of
*           absorbed rays.
*           Strikes(NRays,2)=1st col. Aerosol height (cm)//2nd column
*           #Strikes.

*     The integer variables are:
*           i=counter for the aerosols.
*           RayCounter=are the distribution factor for the cube
imaginary
*                 surfaces.
*           Nray=Total # of rays
*           Nwall=the number of the wall [1:6]
*           Naer=the number of the aerosol [1:5000]
*           NTotalAbs=total number of absorptions.
*           Dimensions=the dimensions of the cube [1cm]
*           irow and icol=the bins for the output point.
*           OutRays=#rays that outgo through wall number 5 for 1st
column
*                 and through wall number 6 for 2nd column.
*           exits=counter for the number of exits per ray.(maximum=4)


*     The logical variables are:
*           jj=1.TRUE the ray hits an aerosol
*           absor=1.TRUE the ray is absorbed by the aerosol
*           SkipVal=1.TRUE the ray is skipped.
*
*-----------------------------------------------------------------*
*     USE DFPORT
      REAL pp,CDsum,scs,ecs,PhaseF(1:200)
      INTEGER seed1,seed2,Nray,NWall,NAer,ii,jj,k,
     &RayCounter(6,10,10),irow,icol,absor,NaerTotal,
     &NTotalAbs,OutRays(2),exits,SkipVal
      DIMENSION Dimensions(3)
      DOUBLE PRECISION strikes(500000,2)
      DOUBLE PRECISION rad,Azimuth,Zenith,Theta(1:200),CosDir(3),
     &OriPG(3),DesPG(3),
     &XLocAx(3),YLocAx(3),ZLocAx(3),T,lam,rm,im,AeroData(5000,4),
     &Absorption(5000,3)
      DATA OutRays,Absorption,strikes,RayCounter,CosDir,Dimensions
     &/1015604*0,-1,3*1/
      PARAMETER (PI=3.1415926535897932385)

C     This is a call to the CPU clock to record the
*     the starting time.
```

```
      character*8 char_time

      DO 1 j=1,181
      Theta(j)=j-1
   1  CONTINUE

      OPEN(UNIT=80,FILE='Clock82.txt',STATUS='new')
      call TIME(char_time)
      WRITE(80,*)'Starting time: ', char_time

C     This is the start of the Band-Averaged code.
      skipVal=0
      seed1=***
      seed2=***
      Nray=***
      NTotalAbs=0
      NaerTotal=5000

C     CHECK!! The sum of the square direction cosines MUST be one.
C     CHECK!! The absolute value of the direction cosine must be [-
1,1].
C     CHECK!! The Origin point must be within the limits of the cube.

      CALL rmarin(seed1,seed2)
      CALL AerosolData(NaerTotal,AeroData)

      DO 15 j=1,Nray
      exits=0

      CALL ShootingPoint(OriPG)
      CALL Sol(lam)

      CosDir(1)=0
      CosDir(2)=0
      CosDir(3)=-1

   3  CDsum=CosDir(1)**2+CosDir(2)**2+CosDir(3)**2

      IF ( CDsum.NE.1)  THEN
         write(*,*)
         write (*, *) ' The sum of the cosine directors'
         write (*, *) ' is not equal to one.'
         write (*, *) 'Stopping...'
         STOP
      END IF

      CALL InitialShot(NaerTotal,AeroData,OriPG,CosDir,
     &jj,DesPG,rad,NAer)


      IF (jj.EQ.1) THEN
            exits=0
*           strikes(j,1)=AeroData(Naer,4)
            strikes(j,2)=strikes(j,2)+1
            CALL LookUpTable(lam,rad,scs,ecs,PhaseF)
            CALL Decision(scs,ecs,absor)
            IF (absor.EQ.1) THEN
                  write(*,*) 'This ray is absorbed'
                  Absorption(NAer,3)=Absorption(NAer,3)+1
                  Absorption(NAer,2)=AeroData(NAer,1)
```

```
                  Absorption(NAer,1)=AeroData(NAer,4)
                  NTotalAbs=NtotalAbs+1
                  GO TO 15
            ELSE IF (absor.EQ.0) THEN
                  write(*,*) 'This ray is scattered'
                  CALL Angles(Theta,PhaseF,Zenith,Azimuth)
                  CALL
Local(OriPG,DesPG,XLocAx,YLocAx,ZLocAx,skipVal)
                  if (skipVal.EQ.1) then
                        go to 15
                  else if (Skipval.EQ.0) then
                        CALL
NewRay(Zenith,Azimuth,XLocAx,YLocAx,ZLocAx,CosDir)

                        IF (CosDir(1).GT.1 .or. CosDir(1).LT.-1 .or.
     S                  CosDir(2).GT.1 .or. CosDir(2).LT.-1 .or.
     S                  CosDir(3).GT.1 .or. CosDir(3).LT.-1) THEN
                              write(*,*)
                              write(*,*) 'The cosine directors must
                        have'
                              write(*,*) ' a value between -1 and 1.'
                              write(*,*) ' Stopping...'
                              STOP
                        END IF

                        DO 20 n=1,3
                              OriPG(n)=DesPG(n)
  20                    CONTINUE

                        IF (OriPG(1).GT.1 .or. OriPG(1).LT.0 .or.
     S                  OriPG(2).GT.1 .or. OriPG(2).LT.0 .or.
     S                  OriPG(3).GT.1 .or. OriPG(3).LT.0) THEN
                              write(*,*)
                              write(*,*) ' This point is beyond the '
                              write(*,*) ' the limits of the cube.'
                              write(*,*) 'Stopping...'
                              STOP
                        ELSE
                              DO 21 n=1,3
                                    DesPG(n)=OriPG(n)+CosDir(n)
  21                          CONTINUE
                        END IF

                        GO TO 3

                  end if
            END IF

       ELSE IF (jj.EQ.0) THEN
            CALL Walls(OriPG,CosDir,NWall,T)

            if (Nwall.NE.5 .and. Nwall.NE.6) then
                  DesPG(1)=OriPG(1)+T*CosDir(1)
                  DesPG(2)=OriPG(2)+T*CosDir(2)
                  DesPG(3)=OriPG(3)+T*CosDir(3)
                  CALL OpPoint(NWall,DesPG,OriPG)
                  exits=exits+1
                  if (exits.LE.5) then
                        go to 3
                  else
                        GO TO 15
```

```
                  end if
            end if

            if (Nwall.EQ.5) then
                  OutRays(1)=OutRays(1)+1
            else if (Nwall.EQ.6) then
                  OutRays(2)=OutRays(2)+1
            end if

            CALL Point(Nwall,OriPG,CosDir,T,irow,icol)
*           write(*,*)'Exit through #Wall/ #row/
            #col',Nwall,irow,icol
*
      RayCounter(Nwall,irow,icol)=RayCounter(Nwall,irow,icol)+1
      END IF

  15  CONTINUE

      IF (Nray-NTotalAbs.LE.0) THEN
            WRITE(*,*) 'The number of scattered rays'
            write(*,*) 'is < or = 0'
            write(*,*) 'Stopping....'
            STOP
      END IF

      DO 22 j=1,2
            CALL
WriteWindData(j+94,NTotalAbs,Nray,RayCounter,OutRays)
  22  CONTINUE

      CALL Files(NaerTotal,Nray,Absorption,strikes,RayCounter)

  10  FORMAT (F7.4,3X,F7.4,3X,F7.4)
  11  FORMAT (F7.2,6X,F7.2)
  12  FORMAT (2X,I4)
  13  FORMAT (I5,2x,I5,2x,I5,2x,I5,2x,I5,2x,I5,2x,I5,2x,I5,2x,
     +            I5,2x,I5,2x)
  16  FORMAT(6X,F7.4,6X)

C     This is the final call to the CPU clock to evaluate the
*     performance required time.

      call TIME(char_time)
      WRITE(80,*)'Finishing time: ', char_time
      CLOSE(UNIT=80)

      END
*_____________________________________________________________*
**********************************************
*      1.SUBROUTINE Generate New Starting Point *
**********************************************

      SUBROUTINE ShootingPoint(OriP)

C     This subroutine generates a shooting point randomly distributed
within
*     the source plane in global coordinates.

*--------------------------------------*
*     Description of variables         *
*--------------------------------------*
```

```
C     The real variables are:
*           - OriP(3)= the shooting point global coordinates.
*           - Dimensions(3)= the dimensions of the atmospheric
*                        cube (cm).
*-----------------------------------------------------------------------

      DOUBLE PRECISION OriP(3),Dimensions(3)
      DATA Dimensions /3*1/

      OriP(1)=ranmar()
      OriP(2)=ranmar()
      OriP(3)=1

      END
*_______________________________________________________________________*

************************************************************************
****
*     2.SUBROUTINE Integrate Solar Radiation Distribution Function
      *
************************************************************************
****

      SUBROUTINE Sol(lambda)

C     This subroutine integrates the Planck's blackbody radiation
distribution
*     function "SolRad" by means of the trapezoidal rule.
*     It returns as Int the integral of "SolRad" between the points
x_1 and x_2.
*
*     The objective is to find the wavelength of a ray within the
range
*     [0,60] (microns), according to its distribution function,
"SolRad".
*     The value is stored in a real variable called "lambda".
*     It has a precision of 1E-3, very good.
*

*-----------------------------*
*  Description of variables   *
*-----------------------------*

C     The only integer variable is i, a counter.
*     The real variables are:
*           a and b for the limits of the aerosol radius range.
*           Dl for the step size of the probability algorithm search.
*           Int and sum for the integral values, (i) and (i-1) step
of the
*                 calcul.
*           Rr to store the random number.
*           SolRad for the Solar Radiation distribution function.
*           pr1 and pr2 for the possible wavelength limits of each
*           iteration
*           (microns).
*           lambda for the final value of the wavelength (microns).


C     This part of the code approximates the value of Int to the
random
```

```
*     number assigned, Rr.


      DOUBLE PRECISION h,co,pi,k,n,lambda,SolRad,T,a,sum,Dl,Int,Rl
      INTEGER i
      PARAMETER (pi=3.1415926535897932385,h=0.66262E-
33,co=0.2997924E09,
     +k=0.1380662E-22,n=1.0,T=5777.0,TotalRadiance=63110800.0)

      SolRad(lambda)=(2*pi*h*(co**2)*0.1E25)/(n**2*lambda**5
     S*(EXP(h*co*0.1E7/(n*lambda*k*T))-1))


      sum=0.0
      a=0.1
      Dl=0.00001
      i=0
      Rl=ranmar()

      Int=0.5*Dl*(SolRad(a)+SolRad(a+Dl))/TotalRadiance
      sum=Int


   3  IF (Int.LT.Rl) THEN
      i=i+1
      Int=sum+(((0.5*Dl*(SolRad(a+i*Dl)+SolRad(a+(i+1)*Dl))))/TotalRa
dia
     Snce)
        sum=Int
        GO TO 3
      END IF

C     This part of the code is a fixed-point routine to find the
exact value of *  the wavelength "lambda".

      pr1=a+i*Dl
      pr2=a+(i+1)*Dl
      sum=Int-(0.5*Dl*(SolRad(pr1)+SolRad(pr2)))

   4  IF (Int.NE.Rl) THEN
            Int = sum+0.5*Dl*(SolRad(pr1)+SolRad(0.5*(pr1+pr2)))
      IF (Int.GT.Rl) THEN
         pr2=0.5*(pr1+pr2)
         lambda=pr2
      ELSE
        IF (Int.LT.Rl) THEN
           sum=sum+0.5*Dl*(SolRad(pr1)+SolRad(0.5*(pr1+pr2)))
           pr1=0.5*(pr1+pr2)
           lambda=pr1
          GO TO 4
        END IF
      END IF
      END IF

      END
*_____________________________________________________________________*
**************************************
*     3.SUBROUTINE Get Aerosol Data *
**************************************

      SUBROUTINE AerosolData(AerN,AerDat)
```

```
C     This subroutine stores the aerosol radius (μm)
*     and the aerosol position coordinates [x, y, z] (cm)
*     in the matrix AerDat (Aerosol Data) with 10,000 rows and
*     4 columns.

*---------------------------------------*
*     Description of variables          *
*---------------------------------------*

C     AerDat is a matrix of real numbers:
*           -FIRST column= radius (μm)
*           -SECOND column= x (cm)
*           -THIRD column= Y (cm)
*           -FOURTH column= Z (cm)
*
*---------------------------------------------------------------------

      DOUBLE PRECISION AerDat(5000,4)
      INTEGER AerN

      OPEN (UNIT=70, FILE='cuatro',STATUS='Old')

      DO 1 i=1,AerN
      READ(70,*) AerDat(i,1),AerDat(i,2),AerDat(i,3),AerDat(i,4)
   1  CONTINUE
      CLOSE (UNIT=70)

      END
*_____________________________________________________________________*
*****************************************
*     4.SUBROUTINE Shot of Rays     *
*****************************************

      SUBROUTINE InitialShot(NtotalAer,AerDat,OriP,CD,j,DesP,r,AerN)


C     This subroutine shoots a ray and it checks if the ray hits an
aerosol.
*     It looks for the closest one.
*
*           If the ray strikes on an aerosol, it gives back:
*                 - a j=1
*                 - the distance between launching point (OriP) and
*                       the aerosol position (DesP).
*                 - the number of the aerosol stroke.
*           If the ray does not strike on aerosol, it gives back:
*                 - a j=0
*                 - i=0

*---------------------------------------*
*     Description of variables      *
*---------------------------------------*

C     The real variables are
*           AerDat(5000,4)=matrix containing the aer. data:
*                 -r=radius of the aerosol (μm).
*                 -rcm=radius of the aerosol (cm).
*                 -a, b, c= position the aerosol within the cube
(cm).
*           pcsr probability cross section radius.
```

```
*           OriP= the ray origin pointG.
*           DesP= the ray destine pointG.
*     The integer variables are
*           i=counter for the aerosols.
*           k=counter for the rays.
*           j=true or false for "strike on an aerosol".
*
*-----------------------------------------------------------------------
      INTEGER i,NTotalAer,j,PosNaer,AerN
      DIMENSION rcm(10000),Rr(10000),Aa(10000),Bb(10000),
     &Cc(10000),BbB(10000),CcC(10000)
      DOUBLE PRECISION OriP(3),DesP(3),CD(3),pcsr,PosT,T,Test,r,
     &AerDat(5000,4)

      pcsr=***
      j=0
      AerN=1
      T=11
      PosNaer=0
      PosT=11

      DO 6 i=1,NTotalAer
      rcm(i)=AerDat(i,1)*0.0001
   6  CONTINUE



      DO 8 i=1,NTotalAer
      Aa(i)=OriP(1)-AerDat(i,2)
      Bb(i)=OriP(2)-AerDat(i,3)
      Cc(i)=OriP(3)-AerDat(i,4)
      Rr(i)=(rcm(i)**2)*((1+pcsr)**2)
      BbB(i)=2*(Aa(i)*CD(1)+Bb(i)*CD(2)+Cc(i)*CD(3))
      CcC(i)=Aa(i)**2+Bb(i)**2+Cc(i)**2-Rr(i)
      Test=BbB(i)**2-4*CcC(i)
            IF (Test.GE.0) THEN
            IF (OriP(1).EQ.AerDat(i,2) .AND. OriP(2).EQ.AerDat(i,3)
.AND.
     S            OriP(3).EQ.AerDat(i,4)) THEN
                  GO TO 8
            ELSE
                  j=1
                  PosNaer=i
                  PosT=(-BbB(i)+SQRT(Test))/2
                  IF (PosT.LT.T .AND. PosT.GT.0) THEN
                        T=PosT
                        AerN=PosNaer
                  END IF
                  go to 8
            END IF
            else if (Test.LT.0) then
                  go to 8
            END IF
   8  CONTINUE

      r=AerDat(AerN,1)
      DesP(1)=AerDat(AerN,2)
      DesP(2)=AerDat(AerN,3)
      DesP(3)=AerDat(AerN,4)

      END
```

```
*_____________________________________________________________________*
**************************************
*     5.SUBROUTINE LookUpTable       *
**************************************

      SUBROUTINE LookUpTable(lambda,radius,ScCS,ExCS,phase)

C     This subroutine opens the corresponding file according
*     to the radius (μm) and reads the corresponding ScatCS, ExtCS
*     and Single Scat. Albedo according to the wavelength (μm).
*--------------------------------------------------------------------
*

      DOUBLE PRECISION lambda,radius,lmin,rmin,Datos(31,6)
      REAL Dlam,Drad,Phase(200),ScCS,ExCS
      INTEGER UnitN,EmptyRead

      rmin=0.0001
      lmin=0.2
      Dlam=0.1
      Drad=0.01

      UnitN=DNINT((radius-rmin)/Drad)+7

      IF (lambda.LE.lmin) THEN
            EmptyRead=2
      ELSE
            EmptyRead=DNINT((lambda-lmin)/Dlam)*32+2
      END IF

      OPEN(UNIT=UnitN,STATUS='old')

      DO 1 j=1,EmptyRead
            Read(UnitN,*)
   1  CONTINUE

      DO 2 irow=1,31
            READ(UnitN,10) (Datos(irow,jcol),jcol=1,6)
   2  CONTINUE

      ControlL=DABS(Lambda-Datos(1,1))
      IF (ControlL.GE.Dlam) THEN
            write(*,*) 'The subroutine LookUpTable'
            write(*,*) 'is reading the wrong values'
            write(*,*) ControlL,lambda,Datos(1,1)
            write(*,*) 'Stopping...'
             STOP
      END IF

      ScCS=Datos(1,2)
      ExCS=Datos(1,3)
      phase(1)=Datos(1,4)
      phase(2)=Datos(1,5)
      phase(3)=Datos(1,6)

      DO 3 irow=1,30
        DO 4 jcol=1,6
            phase((irow-1)*6+3+jcol)=Datos(irow+1,jcol)
   4    CONTINUE
   3  CONTINUE
```

```
  10   FORMAT(1X,F9.5,2X,F9.5,2X,F9.5,2X,F9.5,2X,F9.5,2X,F9.5)
       CLOSE(UNIT=UnitN)

       END
*_____________________________________________________________________
_*
*********************************
*     6.SUBROUTINE Decision     *
*********************************

       SUBROUTINE Decision(sCrSe,eCrSe,absor)

C      This subroutine draws a random number (Rabs) and compares it to
the
*      ratio between the scattering and extinction cross sections:
*            -Rabs>(1-sCrSe/eCrSe) then the ray is scattered (absor=0)
*            -Rabs< or equal then the ray is absorbed (absor=1)

*--------------------------------------*
*     Description of variables      *
*--------------------------------------*
C      The real variables are
*            sCrSe=scattering cross section
*            eCrSe=extinction cross section
*            Rabs=random number
*      The integer variable is
*            absor=logical variable
*                  -1=TRUE (absorbed)
*                  -0=FALSE (scattered)
*----------------------------------------------------------------------

       REAL sCrSe,eCrSe,Rabs
       INTEGER absor

       Rabs=ranmar()

       IF (Rabs.LE.1-(sCrSe/eCrSe)) THEN
             absor=1
       ELSE
             absor=0
       END IF

       END
*_____________________________________________________________________*
*****************************************************
*     7.SUBROUTINE Scattering Angles                *
*****************************************************
       SUBROUTINE Angles(Zenith,INT,ThetaAngle,PhiAngle)

C      OUTPUT of this subroutine is the corresponding scattering
angles:
*            -ThetaAngle=(zenith) found by the ThetaSum subroutine
*            -PhiAngle=(azimuth) uniformly distributed azimuth angle.
*

*-----------------------------*
*  Description of variables   *
*-----------------------------*
C      The real variables are (double precision):
*            ThetaAngle and PhiAngle (radians)
*            Norm=the normalization denominator
```

```
*           Rphase=random number to determine scat.phase func. val.
*-----------------------------------------------------------------

      DOUBLE PRECISION PhiAngle,ThetaAngle,Zenith(1:200)
      REAL INT(1:200)
      PARAMETER (PI=3.1415926535897932385)

      CALL ThetaSum(Zenith,INT,ThetaAngle)
      PhiAngle=Ranmar()*2*PI

      END
**-----------------------------------------------------------------
      SUBROUTINE ThetaSum(ThetaVal,PhaseVal,Theta)

C     This subroutine looks for the value of the zenith angle
throughout
*     a list of values (ThetaVal) from MieMono.
*     It estimates it applying the trapezoidal rule to the cumulative
*     scattering phase function (PhaseVal), from MieMono as well.

      INTEGER i
      DOUBLE PRECISION ThetaVal(1:200),Theta,Phase,Norm
      REAL PhaseVal(1:200)
      PARAMETER (PI=3.1415926535897932385)

      DO 80 i=1,90

      Norm=Norm+(PhaseVal(i+1)+PhaseVal(i))*(DCos(ThetaVal(i)*PI/180)
-
     &       DCos(ThetaVal(i+1)*PI/180))
   80 CONTINUE

      Rphase=ranmar()
      Phase=(PhaseVal(2)+PhaseVal(1))*(DCos(ThetaVal(1)*PI/180)-
     &      DCos(ThetaVal(2)*PI/180))/Norm

      i=1
   82 IF (Rphase.GT.Phase) THEN
            i=i+1

      Phase=Phase+((PhaseVal(i+1)+PhaseVal(i))*(DCos(ThetaVal(i)*
     &        PI/180)-DCos(ThetaVal(i+1)*PI/180))/Norm)
            GO TO 82
      ELSE
            Theta=ThetaVal(i)*PI/180
      END IF

      END
*_________________________________________________________________*
****************************************
*     8.SUBROUTINE Local Coordinates    *
****************************************
      SUBROUTINE Local(OriP,DesP,XlAxis,YlAxis,ZlAxis,skip)

C     This program receives the origin and the destination point
*     of the ray as an input and generates the LOCAL axis.
*-------------------------------------*
*     Description of variables      *
*-------------------------------------*
C     The real (double precision) variables are:
*           OriP(3)=Origin Point G stored in an array.
```

```
*           DesP(3)=Destination Point G stored in an array.
*           (XlAxis,YlAxis,ZlAxis)= the local coordinate system axis
*           (IgAxis,JgAxis,KgAxis)= the global coordinate system axis
*           RotMatrix(3,3)= the Rotation Matrix
*
*           Mag(-)= The magnitude of a vector.
*           DOvector= the coordinates of the vector
*                 defined by D and O points.
*
*-----------------------------------------------------------------------

      DOUBLE PRECISION DesP(3),OriP(3),IgAxis(3),JgAxis(3),KgAxis(3),
     SXlAxis(3),YlAxis(3),ZlAxis(3),RotMatrix(3,3),DOvector(3),
     SCrossValue(3),MagValue
      integer skip
      DATA IgAxis,JgAxis,KgAxis /1,2*0,0,1,0,2*0,1/

C     ------Z LOCAL AXIS------- (ZlAxis).
*     ZlAxis is parallel to the incoming ray.

      skip=0
      DO 1 i=1,3
            DOvector(i)=DesP(i)-OriP(i)
   1  CONTINUE

      CALL Magnitude(DOvector,MagValue)

      IF (MagValue.EQ.0) THEN
            write(*,*)
            write (*, *) ' 1.The search for a local system'
            write (*, *) ' failed.'
            write (*, *) 'Skip this ray.'
            skip=1
            go to 5
      END IF

      DO 2 i=1,3
      ZlAxis(i)=DOvector(i)/MagValue
   2  CONTINUE

C     -------Y LOCAL AXIS------- (YlAxis).
*     This axis is perpendicular to the plane defined by the
*     z local axis and the x global axis (IgAxis [1,0,0]).
*

C     CHECK!! That the magnitude of the cross product
*           between the z local axis and the x global
*           axis is not zero. If so, choose the y global
*           axis (JgAxis [0,1,0])

      CALL CrossProduct(ZlAxis,IgAxis,CrossValue)
      CALL Magnitude(CrossValue,MagValue)

      IF (MagValue.EQ.0) THEN
            CALL CrossProduct(ZlAxis,JgAxis,CrossValue)
            CALL Magnitude(CrossValue,MagValue)
      END IF

      IF (MagValue.EQ.0) THEN
            write(*,*)
            write (*, *) '2.The search for a local system'
```

```
            write (*, *) ' failed.'
            write (*, *) 'Skip this ray'
            skip=1
            go to 5
      END IF

      DO 3 i=1,3
      YlAxis(i)=CrossValue(i)/MagValue
   3  CONTINUE

C     -------X LOCAL AXIS------- (XlAxis).
*     This axis is perpendicular to the plane defined by the
*           z local axis and the y local axis.

      CALL CrossProduct(ZlAxis,YlAxis,CrossValue)
      CALL Magnitude(CrossValue,MagValue)

      IF (MagValue.EQ.0) THEN
            write(*,*)
            write (*, *) '3.The search for a local system'
            write (*, *) ' failed.'
            write (*, *) 'Skip this ray'
            skip=1
            go to 5
      END IF

      DO 4 i=1,3
      XlAxis(i)=CrossValue(i)/MagValue
   4  CONTINUE

   5  END
**--------------------------------------------------------------------
      SUBROUTINE Magnitude(vector,Mag)

C     This subroutine calculates the magnitude of the vector defined
*     by the points "OP" (Origin) and "DP" (Destine), the value is
*     stored in the variable "Mag".

      DOUBLE PRECISION vector(3),Mag,sum

      sum=0

      DO 1 i=1,3
            sum=sum+(vector(i))**2
   1  CONTINUE

      Mag=SQRT(sum)

      END
**--------------------------------------------------------------------
      SUBROUTINE CrossProduct(A,B,cross)

      DOUBLE PRECISION A(3),B(3),cross(3)

      cross(1)=A(2)*B(3)-A(3)*B(2)
      cross(2)=A(3)*B(1)-A(1)*B(3)
      cross(3)=A(1)*B(2)-A(2)*B(1)

      END
*_____________________________________________________________________*
**********************************
```

```
*     9.SUBROUTINE New Ray            *
*************************************
      SUBROUTINE NewRay(Theta,Phi,XlAxis,YlAxis,ZlAxis,IncG)

C     This subroutine generates the new scattered ray. It calculates
*     the direction cosines of the scattered ray.
*     The inputs for this program are:
*            - the angles (from subroutine "Angles") referenced
*                 to the local coord. system (from the subroutine
*                 "Local") (radians).
*            - The origin point, referenced to the global coordinate
*                 system.

*---------------------------------------*
*     Description of variables          *
*---------------------------------------*

C     The real (double precision) variables are:
*           IncG(3)=Destination Point in GLOBAL coord. system.
*           IncL(3)=Destination Point in LOCAL coord. system.
*           (XlAxis,YlAxis,ZlAxis)= the local coordinate system axis
*           (IgAxis,JgAxis,KgAxis)= the global coordinate system axis
*           (Theta,Phi)= the cone (zenith) and the clock (azimuth)
angles.
*-----------------------------------------------------------------------
     DOUBLE PRECISION IncG(3),IncL(3),IgAxis(3),JgAxis(3),
     SKgAxis(3),XlAxis(3),YlAxis(3),ZlAxis(3),
     STheta,Phi,DirCos(3)

C     ------DESTINATION LOCAL POINT------
      IncL(3)=COS(Theta)
      IncL(1)=SIN(Theta)*COS(Phi)
      IncL(2)=SIN(Theta)*SIN(Phi)
      CALL LocalToGlobal(IncL,IncG)

      END
**-----------------------------------------------------------------------
      SUBROUTINE GlobalToLocal(GPoint,LPoint)

C     This program transform a point from GLOBAL coordinates
*     to LOCAL coordinates.
*     The local axis are inputs to the program.

*---------------------------------------*
*     Description of variables          *
*---------------------------------------*
C     The real (double precision) variables are:
*           - RotMatrix(3,3)= the rotation matrix from LOCAL
*                to GLOBAL.
*           - LPoint(3)= the point in LOCAL coordinates.
*           - GPoint(3)= the point in GLOBAL coordinates.
*           - (XlAxis,YlAxis,ZlAxis)= the LOCAL axis.
*-----------------------------------------------------------------------

      DOUBLE PRECISION RotMatrix(3,3),LPoint(3),GPoint(3),XlAxis(3),
     S      YlAxis(3),ZlAxis(3)
      DATA XlAxis,YlAxis,ZlAxis /-1,3*0,-1,3*0,-1/

      DO 1 i=1,3
      RotMatrix(1,i)=XlAxis(i)
      RotMatrix(2,i)=YlAxis(i)
```

```
      RotMatrix(3,i)=ZlAxis(i)
   1  CONTINUE

      DO 2 i=1,3
      LPoint(i)=RotMatrix(i,1)*GPoint(1)+
     S              RotMatrix(i,2)*GPoint(2)+
     S              RotMatrix(i,3)*GPoint(3)
   2  CONTINUE

      END
**--------------------------------------------------------------------
      SUBROUTINE LocalToGlobal(LPoint,GPoint)

C     This program transform a point from LOCAL coordinates
*     to GLOBAL coordinates.
*     The local Axis are inputs to the program.

*---------------------------------------*
*     Description of variables          *
*---------------------------------------*
C     The real (double precision) variables are:
*           - RotMatrix(3,3)= the rotation matrix from LOCAL
*                to GLOBAL.
*           - LPoint(3)= the point in LOCAL coordinates.
*           - GPoint(3)= the point in GLOBAL coordinates.
*           - (XlAxis,YlAxis,ZlAxis)= the LOCAL axis.
*
*--------------------------------------------------------------------

      DOUBLE PRECISION RotMatrix(3,3),LPoint(3),GPoint(3),XlAxis(3),
     S      YlAxis(3),ZlAxis(3)
      DATA XlAxis,YlAxis,ZlAxis /-1,3*0,-1,3*0,-1/

      DO 1 i=1,3
            RotMatrix(i,1)=XlAxis(i)
            RotMatrix(i,2)=YlAxis(i)
            RotMatrix(i,3)=ZlAxis(i)
   1  CONTINUE

      DO 2 i=1,3
            GPoint(i)=RotMatrix(i,1)*LPoint(1)+
     S              RotMatrix(i,2)*LPoint(2)+
     S              RotMatrix(i,3)*LPoint(3)
   2  CONTINUE

      END
*____________________________________________________________________*
**************************
*     10.SUBROUTINE Walls *
**************************
      SUBROUTINE Walls(OPG,CD,WallN,shortT)

C     This subroutine receives as inputs the origin point and
*     the direction cosines of a ray that does not strike on an
*     aerosol. The subroutine finds what wall does the ray go
*     out through (the closest).

*---------------------------------------*
*     Description of variables          *
*---------------------------------------*
C     The real variables are
```

```
*           OPG(3)= the origin point in global coordinates (cm).
*           CD(3)= the cosine directors.
*           Dimension(3)= the atmospheric cube dimensions (cm).
*           T(6)= an array containing the distances to the six walls.
*           shortT= the shortest distance.
*     The integer variables are
*           WallN= the number of the closest wall.
*-----------------------------------------------------------------------
      DOUBLE PRECISION OPG(3),CD(3),Dimensions(3),T(6),shortT
      INTEGER WallN
      DATA Dimensions,T /3*1,6*20/

      WallN=5
      shortT=20

      IF (CD(1).NE.0) THEN
            T(1)=-OPG(1)/CD(1)
            T(2)=(Dimensions(1)-OPG(1))/CD(1)
      ELSE IF (CD(1).EQ.0) THEN
            T(1)=20
            T(2)=20
      END IF
      IF (CD(2).NE.0) THEN
            T(3)=-OPG(2)/CD(2)
            T(4)=(Dimensions(2)-OPG(2))/CD(2)
      ELSE IF (CD(2).EQ.0) THEN
            T(3)=20
            T(4)=20
      END IF

      IF (CD(3).NE.0) THEN
      IF (OPG(3).LT.1) THEN
            T(5)=-OPG(3)/CD(3)
            T(6)=(Dimensions(3)-OPG(3))/CD(3)
      ELSE IF (OPG(3).EQ.1) THEN
            T(5)=-OPG(3)/CD(3)
            T(6)=20
      END IF
      ELSE IF (CD(3).EQ.0) THEN
            T(5)=20
            T(6)=20
      END IF

      DO 1 i=1,6
            IF (T(i).LT.shortT .and. T(i).GE.0) THEN
                  shortT=T(i)
                  WallN=i
            ELSE
                  GO TO 1
            END IF
  1   CONTINUE

      END
*_______________________________________________________________________*
*******************************
*     11.SUBROUTINE Point     *
*******************************
      SUBROUTINE Point(WallN,OPG,CD,shortT,row,col)

C     This subroutine receives as inputs the origin point and
*     the cosine directors of a ray that leaves the cube.
```

```
*     The subroutine finds the exact point the ray go
*     out through.

*--------------------------------------*
*     Description of variables         *
*--------------------------------------*
C     The real variables are
*           OPG(3)= the origin point in global coordinates (cm).
*           CD(3)= the cosine directors.
*           shortT= the distance between origin and the out point.
*           P(3)= the output point.
*-----------------------------------------------------------------------

      DOUBLE PRECISION OPG(3),CD(3),P(3),shortT
      INTEGER WallN,row,col

      P(1)=OPG(1)+shortT*CD(1)
      P(2)=OPG(2)+shortT*CD(2)
      P(3)=OPG(3)+shortT*CD(3)

      IF (WallN.EQ.1 .or. WallN.EQ.2) THEN
            row=IDINT(P(3)*10)+1
             col=IDINT(P(2)*10)+1
      ELSE IF (WallN.EQ.3 .or. WallN.EQ.4) THEN
            row=IDINT(P(3)*10)+1
            col=IDINT(P(1)*10)+1
      ELSE IF (WallN.EQ.5 .or. WallN.EQ.6) THEN
            row=IDINT(P(1)*10)+1
            col=IDINT(P(2)*10)+1
      END IF

      END
*_______________________________________________________________________*
```

```
*****************************************************************
*   12.Subroutine Pseudo-Random Number Generator                *
*****************************************************************
      SUBROUTINE rmarin(ij, kl)

C     This is the initialization routine for the PRG ranmar().
*     The seed variables can have values between:
*            0 <= IJ <= 31328
*            0 <= KL <= 30081
C     The random number sequences created by these two seeds are of
*     sufficient length to complete an entire calculation width. For
*     example, if several different groups are working on different
*     parts of the same calculation, each group could be assigned its
*     own IJ seed. This would leave each group with 30000 choices for
*     the second seed. That is to say, this random number generator
can
*     create 900 million different subsequences -- with each
*     subsequence having a length of approximately 10^30.

C     Use IJ = 1802 & KL = 9373 to test the random number generator.
*     The subroutine ranmar should be used to generate 20000 random
*     numbers.  Then display the next six random numbers generated
*     multiplied by 4096*4096.  If the random number generator is
*     working properly, the random numbers should be:
*           6533892.0  14220222.0  7275067.0
*           6172232.0  8354498.0   10633180.0

C      implicit real*8 (a-h, o-z)
      real*8 u(97), c, cd, cm, s, t
      integer ii, i, j, ij, jj, k, kl, l, m, i97, j97
      logical test
      common /raset1/ u, c, cd, cm, i97, j97, test
      test = .false.

      if( IJ .lt. 0  .or.  IJ .gt. 31328  .or.
     +    KL .lt. 0  .or.  KL .gt. 30081 ) then
         write (*, *) ' The first random number seed must have a'
         write (*, *) ' value between 0 and 31328.'
         write (*, *)
         write (*, *) ' The second seed must have a value between 0'
         write (*, *) ' and 30081.'
         write (*, *) 'Stopping...'
         stop
      endif

      i = mod(IJ/177, 177) + 2
      j = mod(IJ    , 177) + 2
      k = mod(KL/169, 178) + 1
      l = mod(kl,     169)

      do 2 ii = 1, 97
         s = 0.0
         t = 0.5
         do 3 jj = 1, 24
            m = mod(mod(i*j, 179)*k, 179)
            i = j
            j = k
            k = m
            l = mod(53*l+1, 169)
```

```
            if (mod(l*m, 64) .ge. 32) then
               s = s + t
            endif
            t = 0.5 * t
 3     continue
         u(ii) = s
 2    continue

      c = 362436.0 / 16777216.0
      cd = 7654321.0 / 16777216.0
      cm = 16777213.0 /16777216.0

      i97 = 97
      j97 = 33

      test = .true.

      return
      end


      real*8 function ranmar()

C     This is the random number generator proposed by George
Marsaglia
*     in Florida State University Report: FSU-SCRI-87-50

C       implicit real*8 (a-h, o-z)
      real*8 u(97), uni, c, cd, cm
      integer i97, j97
      logical test
      common /raset1/ u, c, cd, cm, i97, j97, test

      if(.not.test) then
         write (*, *)
         write (*, *) 'ranmar error #1: must call the'
         write (*, *) 'initialization routine rmarin before'
         write (*, *) 'calling ranmar.'
         write (*, *) 'Stopping...'
         stop
      endif

      uni = u(i97) - u(j97)
      if( uni .lt. 0.0 ) uni = uni + 1.0
      u(i97) = uni
      i97 = i97 - 1
      if(i97 .eq. 0) i97 = 97
      j97 = j97 - 1
      if(j97 .eq. 0) j97 = 97
      c = c - cd
      if( c .lt. 0.0 ) c = c + cm
      uni = uni - c
      if( uni .lt. 0.0 ) uni = uni + 1.0

      ranmar = uni

      return
      end
*_____________________________________________________________________*

**************************************
```

```
*     13.SUBROUTINE     Opposite Point    *
*****************************************
      SUBROUTINE OpPoint(WallN,Point,OpP)

      DOUBLE PRECISION Point(3),OpP(3)
      INTEGER WallN

      if (WallN.EQ.1) then
            Point(1)=1
      else if (WallN.EQ.2) then
            Point(1)=0
      else if (WallN.EQ.3) then
            Point(2)=1
      else if (WallN.EQ.4) then
            Point(2)=0
      end if

      do 1 j=1,3
      OpP(j)=Point(j)
  1   continue

      END
*_____________________________________________________________________*
*****************************************
*     14.SUBROUTINE     DATAforWINDSURF   *
*****************************************
      SUBROUTINE WriteWindData(WallN,Abs,Rays,Raycount,RaysOut)

      integer WallN,RayCount(6,10,10),Abs,Rays,RaysOut(2)
      real perc,num,den

      den=Rays-Abs

      OPEN(UNIT=WallN,STATUS='new')

      write(WallN,*)'_____________________________________'
      write(WallN,*)' x(mm) / y(mm) / #Rays / %Rays '
      write(WallN,*)'_____________________________________'

      WRITE(WallN,*)'*----------------------------*'
      WRITE(WallN,*)'         Nwall',WallN-90
      WRITE(WallN,*)'*----------------------------*'

c      IF (WallN.EQ.91) THEN
c           DO 1 col=1,10
c           DO 2 row=1,10
c                 num=RayCount(1,col,row)
c                 perc=num/den
c                 WRITE(WallN,17) (col-1)+0.5,(row-1)+0.5,
c     &                 RayCount(1,col,row),
c     &                 perc
c
c   2       CONTINUE
c   1    CONTINUE
c
c      ELSE IF (WallN.EQ.92) THEN
c           DO 3 col=1,10
c           DO 4 row=1,10
c                 num=RayCount(2,col,row)
c                 perc=num/den
c                 WRITE(WallN,17) (col-1)+20.5,(row-1)+0.5,
```

```
c     &                 RayCount(2,col,row),
c     &                 perc
c   4       CONTINUE
c   3    CONTINUE
c
c      ELSE IF (WallN.EQ.93) THEN
c           DO 5 col=1,10
c           DO 6 row=1,10
c                 num=RayCount(3,col,row)
c                 perc=num/den
c                 WRITE(WallN,17) (col-1)+30.5,(row-1)+0.5,
c     &                 RayCount(3,col,row),
c     &                 perc
c   6       CONTINUE
c   5    CONTINUE
c
c      ELSE IF (WallN.EQ.94) THEN
c           DO 7 col=1,10
c           DO 8 row=1,10
c                 num=RayCount(4,col,row)
c                 perc=num/den
c                 WRITE(WallN,17) (col-1)+10.5,(row-1)+0.5,
c     &                 RayCount(4,col,row),
c     &                 perc
c   8       CONTINUE
c   7    CONTINUE
c
      IF (WallN.EQ.95) THEN
            write(WallN,*)'The total number of rays that'
            write(WallN,*)'Exit through wall number',WallN-90
            write(WallN,*)'is',RaysOut(1)
            DO 9 col=1,10
            DO 10 row=1,10
                  num=RayCount(5,col,row)
                  perc=num/den
                  WRITE(WallN,17) (col-1)+0.5,(-1)*row+0.5,
     &                 RayCount(5,col,row),
     &                 perc
  10        CONTINUE
   9    CONTINUE

      ELSE IF (WallN.EQ.96) THEN
            write(WallN,*)'The total number of rays that'
            write(WallN,*)'Exit through wall number',WallN-90
            write(WallN,*)'is',RaysOut(2)
            DO 11 col=1,10
            DO 12 row=1,10
                  num=RayCount(6,col,row)
                  perc=num/den
                  WRITE(WallN,17) (col-1)+0.5,(row-1)+10.5,
     &                 RayCount(6,col,row),
     &                 perc
  12        CONTINUE
  11    CONTINUE
      END IF
  17  FORMAT(2X,F4.1,2X,F4.1,2X,i4,4x,f6.4)
      CLOSE(UNIT=WallN)

      END
*                                                                      *
************************************
```

```
*   15.SUBROUTINE OutPutFiles        *
*************************************
      SUBROUTINE
Files(AerN,RayN,AbsorptionCount,StrikeCount,RayCount)

C     This subroutine writes the output data in three .txt files.
*           -File(100): WALLS, matrix(6x2) 6 walls, and the distri-
*                 bution factors of the scattered outgoing rays.
*           -File(98): ABSORPTION, matrix(5000x2) 5000 aerosoles,
*                 their height (z,cm) and the # of rays absorbed
*                 by each of them.
*           -File(97): STRIKES, array(Nrays), the number of strikes
*                 correspondant to each ray. To assure single
*                 scattering (pcsr).

*--------------------------------------*
*     Description of variables      *
*--------------------------------------*
C     The real variables are
*           RayCount
*           AbsorptionCount
*           StrikeCount
*-----------------------------------------------------------------------

      INTEGER RayCount(6,10,10),AerN,RayN
      DOUBLE PRECISION AbsorptionCount(5000,3),strikecount(500000,2)

C-------First let's write the file WALLS.-------------
      OPEN (UNIT=100,FILE='Wall',STATUS='new')

      DO 1 l=1,6
            write(100,*) '_____________________________'
            write(100,*) '    Wall number    ',l
            write(100,*) '_____________________________'

      DO 2 m=1,10
            write(100,13) RayCount(l,m,1),RayCount(l,m,2),
     +            RayCount(l,m,3),RayCount(l,m,4),RayCount(l,m,5),
     +            RayCount(l,m,6),RayCount(l,m,7),
     +      RayCount(l,m,8),RayCount(l,m,9),RayCount(l,m,10)
   2    continue
      WRITE(100,*)
   1  continue

  10  FORMAT (F7.4,3X,F7.4,3X,F7.4)
  11  FORMAT (F7.2,6X,F7.2)
  12  FORMAT (2X,I4)
  13  FORMAT (I5,2x,I5,2x,I5,2x,I5,2x,I5,2x,I5,2x,I5,2x,I5,2x,
     +I5,2x,I5,2x)

C--------SECOND let's create ABSORPTION--------------
      OPEN (UNIT=98,FILE='AbsorHeight82',STATUS='new')
      write(98,*) '_____________________________'
      write(98,*) '   Absorption vs Height  '
      write(98,*) '-------------------------'
      write(98,*) '  Height  /  # Abs. Rays '
      write(98,*) '_____________________________'

      DO 3 j=1,AerN
            write(98,14) AbsorptionCount(j,1),AbsorptionCount(j,3)
    3 CONTINUE
```

```
      OPEN (UNIT=99,FILE='AbsorRad82',STATUS='new')
      write(99,*) '_____________________________'
      write(99,*) '   Absorption vs Rad.    '
      write(99,*) '-------------------------'
      write(99,*) '  Rad (mi) / # Abs. Rays '
      write(99,*) '_____________________________'

      DO 4 j=1,AerN
            write(99,14) AbsorptionCount(j,2),AbsorptionCount(j,3)
    4 CONTINUE

   14 FORMAT(2X,F6.4,4X,F5.1)

C--------THIRD the last output file STRIKES.-----------
      OPEN(UNIT=97,FILE='Strikes82',STATUS='new')
      write(97,*)'____________________'
      write(97,*)'      STRIKES        '
      write(97,*)'------------------'
      write(97,*)'  Ray#/ #strikes '
      write(97,*)'____________________'

      DO 7 j=1,RayN
      write(97,15) j,strikecount(j,2)
   7  CONTINUE
  15  FORMAT(1X,I7,3x,f3.0,2x)

C--------Closing statements------------
      CLOSE(UNIT=97)
      CLOSE(UNIT=98)
      CLOSE(UNIT=99)
      CLOSE(UNIT=100)
      END
*_____________________________________________________________________________*
```

THIS IS AN EXAMPLE OF ONE OF THE TABLES THAT FEED THE BAND-AVERAGED CODE

This is a detail of table number 9, corresponding to the optical properties of a rural aerosol spherical particle of radius 0.024 micrometers for an incoming energy bundle of wavelength 0.2 micrometers.

The first value is the wavelength in micrometers.
The second value is the Scattering Cross section (μm^2)
The third value is the Extinction Cross section (μm^2)
The rest are the values of the scattering phase function from Mie Monodisperse.

Radius (mi) 0.0239999997

L (mi) / ScatCS / ExtCS / Phase /					
0.20000	0.08276	0.21490	1.92653	1.92618	1.92512
1.92337	1.92091	1.91776	1.91392	1.90940	1.90419
1.89831	1.89177	1.88457	1.87672	1.86824	1.85913
1.84941	1.83909	1.82818	1.81671	1.80467	1.79210
1.77900	1.76539	1.75130	1.73673	1.72171	1.70626
1.69040	1.67414	1.65751	1.64053	1.62322	1.60560
1.58770	1.56953	1.55112	1.53249	1.51366	1.49465
1.47550	1.45622	1.43683	1.41735	1.39782	1.37825
1.35866	1.33907	1.31952	1.30001	1.28057	1.26122
1.24199	1.22288	1.20393	1.18515	1.16656	1.14818
1.13003	1.11212	1.09447	1.07710	1.06002	1.04325
1.02680	1.01069	0.99493	0.97954	0.96452	0.94989
0.93566	0.92183	0.90842	0.89544	0.88290	0.87079
0.85914	0.84794	0.83720	0.82692	0.81712	0.80778
0.79893	0.79055	0.78265	0.77523	0.76829	0.76182
0.75584	0.75034	0.74531	0.74075	0.73666	0.73303
0.72987	0.72716	0.72490	0.72308	0.72171	0.72076
0.72024	0.72013	0.72044	0.72114	0.72223	0.72371
0.72556	0.72777	0.73033	0.73324	0.73648	0.74004
0.74391	0.74808	0.75254	0.75728	0.76228	0.76753
0.77302	0.77874	0.78468	0.79083	0.79716	0.80368
0.81036	0.81720	0.82418	0.83130	0.83853	0.84586
0.85330	0.86081	0.86839	0.87604	0.88372	0.89145
0.89919	0.90695	0.91471	0.92246	0.93018	0.93787
0.94552	0.95312	0.96065	0.96811	0.97548	0.98276
0.98993	0.99700	1.00394	1.01075	1.01742	1.02395
1.03032	1.03653	1.04257	1.04843	1.05410	1.05959
1.06487	1.06996	1.07483	1.07949	1.08392	1.08813
1.09211	1.09585	1.09936	1.10262	1.10563	1.10839
1.11090	1.11316	1.11515	1.11688	1.11835	1.11955
1.12049	1.12116	1.12156	1.12170	0.00000	0.00000

THIS IS A DETAIL OF THE PREPROCESSED AEROSOL DATA

This is a detailed of 'AerRadLoc', the text file containing the preprocessed data for the aerosol size, represented by its radius, and its location within the control volume.

RADIUS (μm)	x(cm)	y(cm)	z(cm)
0.0208549984	0.96484679	0.882970393	0.420486867
0.0541249998	0.577386141	0.942340136	0.243162394
0.0604049973	0.689230263	0.476426423	0.962395668
0.0394949988	0.0614917874	0.103925645	0.0876287818
0.14961499	0.782492518	0.731956303	0.762118518

THIS IS A DETAIL OF THE INDEX OF REFRACTION LOOK-UP TABLE

This is a portion of the look-up table for the complex index of refraction 'IndexRefractionData' of rural aerosols as a function of wavelength. The data come from Guillaume A. D'Almeida and Eric P. Shettle 1991 book, **Atmospheric Aerosols. Global Climatology and Radiative Characteristics**, published by A. Deepak Publishing, Hampton, (VA), USA. Table 4.3. Page 57. For water-soluble aerosols.

The first value is the wavelength in micrometers.
The second value is the real coefficient of the index of refraction.
The third value is the imaginary coefficient of the index of refraction.

L (μm)	mr	mi
0.200	1.530	-7.00E-02
0.250	1.530	-3.00E-02
0.300	1.530	-8.00E-03
0.350	1.530	-5.00E-03
0.400	1.530	-5.00E-03
0.450	1.530	-5.00E-03
0.500	1.530	-5.00E-03
0.550	1.530	-6.00E-03
0.600	1.530	-6.00E-03
0.650	1.530	-7.00E-03
0.700	1.530	-7.00E-03
0.750	1.530	-8.50E-03
0.800	1.520	-1.00E-02
0.900	1.520	-1.15E-02
1.000	1.520	-1.55E-02
1.250	1.510	-1.90E-02
1.500	1.420	-2.25E-02
1.750	1.420	-1.75E-02

THESE ARE THE MIE THEORY CODES

These codes where developed at Laboratoire d'Optique Atmosphérique de la Université des Science et Technologie de Lille (France).

UNO

```
************************************************
*           Monodisperse Mie scattering        *
************************************************
      PROGRAM uno

c Programme de Mie pour des spheres monodispersees
      character*6 fich
      OPEN (2,FILE='donuno.dat')
 1    format(a6)
      OPEN (1,FILE='resuno')
      CALL PPPP
      CLOSE (1)
      CLOSE (2)
      STOP
      END
*-------------------------------------------------------------------*
      SUBROUTINE PPPP

      IMPLICIT DOUBLE PRECISION (A-H,O-Z)
C     CE PROGRAMME CALCULE POUR UNE VALEUR DE RAYON, LES FACTEURS
EFFICACES
C     D'EXTINCTION ET DE DIFFUSION, AINSI QUE I(MU),Q(MU) POUR NBMU
VALEURS
C     DE L'ANGLE DE DIFFUSION (NBMU MAX EST DE 200).
C     LA VALEUR MAX DE ALPHA EST DE 250....MAIS PEUT ETRE
AUGMENTEE...
C     LA PARTIE IMAGINAIRE DE L'INDICE DOIT ETRE ENTREE  < 0
C
      INTEGER UN,TEST
      DOUBLE PRECISION K1,K2,IA,IB,IN,IGNA,IDNB,IBETA
C
      DIMENSION CNA(-1:900),RGNA(-1:900),IGNA(-1:900),
     &RDNA(0:900),RA(0:900),RB(0:900),IA(0:900),IB(0:900),
     &RDNB(0:900),IDNB(0:900),SNA(-1:900),RMU(1:200)
C
      COMMON/A/PI,RMU,RA,IA,RB,IB,ALPHA,RN,IN,K1,K2,RLAM,NBMU,N2
      PI=3.141592653585
      CALL ZERO(CNA,902)
      CALL ZERO(RGNA,902)
      CALL ZERO(IGNA,902)
      CALL ZERO(RDNB,901)
      CALL ZERO(SNA,902)
      CALL ZERO(IDNB,901)
      CALL ZERO(RDNA,901)

C               DONNEES
C  LAMBDA=LONGUEUR D'ONDE EN MICRONS
C  RN=PARTIE REELLE DE L'INDICE
C  IN=PARTIE IMAGINAIRE DE L'INDICE (NEGATIVE)
C  R0=RAYON DE LA SPHERE EN MICRONS
c
      read(2,*)rlam,rn,in,r0
      ALPHA=2*PI*R0/RLAM
```

```
      WRITE(1,51)
      WRITE(1,52)RLAM,RN,IN,R0
      READ(2,*)NBMU
      READ(2,*)(RMU(J),J=1,NBMU)
      RBETA=RN*ALPHA
      IBETA=IN*ALPHA
      N1=DINT(ALPHA+ALPHA+20)
      N2=DINT(ALPHA+ALPHA+5)
      N2P1=N2+1
      CNA(-1)=-DSIN(ALPHA)
      RGNA(-1)=0
      RGNA(0)=0
      CNA(0)=DCOS(ALPHA)
      IGNA(-1)=0
      IGNA(0)=-1
      DO 25 I=1,N2
         CNA(I)=(2*I-1)*CNA(I-1)/ALPHA-CNA(I-2)
         X=RGNA(I-1)
         Z=I/ALPHA
         Y=IGNA(I-1)
         W=((Z-X)*(Z-X)+(Y*Y))
         RGNA(I)=(Z-X)/W-Z
         IGNA(I)=Y/W
         IF(CNA(I).LT.1E+35) GO TO 100
           N2=I
           N2P1=I+1
           N1=I+15
  100    CONTINUE
   25 CONTINUE
      RDNA(N1)=0
      RDNB(N1)=0
      IDNB(N1)=0
      X1=RBETA*RBETA+IBETA*IBETA
      X2=RBETA/X1
      X3=IBETA/X1
      SNA(N1)=0
      SNA(N1-1)=1
      DO 30 KK=1,N1
         I=N1-KK
         X=RDNB(I+1)
         Y=IDNB(I+1)
         Z=X+(I+1)*X2
         W=Y-(I+1)*X3
         X4=Z*Z+W*W
         RDNB(I)=(I+1)*X2-Z/X4
         IDNB(I)=-(I+1)*X3+W/X4
         Z=(I+1)/ALPHA
         X=RDNA(I+1)
         RDNA(I)=Z-1/(X+Z)
         SNA(I-1)=(2*I+1)*SNA(I)/ALPHA-SNA(I+1)
         IF (SNA(I-1).LE.1D+60) GOTO 40
             TEST=I-1
             X=SNA(TEST)
             DO 35 J=TEST,N2
   35    SNA(J)=SNA(J)/X
   40    CONTINUE
   30 CONTINUE
      Q=-SNA(0)/CNA(-1)
      DO 45 I1=1,N2P1
   45 SNA(I1-1)=SNA(I1-1)/Q
      TEST=0
```

```
      UN=1
      DO 50 I=1,N2
         X1=SNA(I)
         X2=CNA(I)
         X3=RDNB(I)
         X4=IDNB(I)
         X5=RDNA(I)
         X6=RGNA(I)
         X7=IGNA(I)
         Y1=X3-RN*X5
         Y2=X4-IN*X5
         Y3=X3-RN*X6+IN*X7
         Y4=X4-RN*X7-IN*X6
         Y5=RN*X3-IN*X4-X5
         Y6=IN*X3+RN*X4
         Y7=RN*X3-IN*X4-X6
         Y8=IN*X3+RN*X4-X7
         X4=Y2*Y3-Y1*Y4
         X3=Y1*Y3+Y2*Y4
         X5=X1*X1+X2*X2
         X6=Y3*Y3+Y4*Y4
         X7=Y5*Y7+Y6*Y8
         X8=Y6*Y7-Y5*Y8
         X9=Y7*Y7+Y8*Y8
         Q=(I+I+1.)/I/(I+1.)*UN
         Y1=X1*(X1*X3+X2*X4)/X5/X6
         Y2=X1*(X1*X4-X2*X3)/X5/X6
         Y3=X1*(X1*X7+X2*X8)/X5/X9
         Y4=X1*(X1*X8-X2*X7)/X5/X9
         RA(I)=Y2*Q
         IB(I)=Y3*Q
         Q=-Q
         RB(I)=Y4*Q
         IA(I)=Y1*Q
         UN=-UN
   50 CONTINUE
      RA(0)=0
      IA(0)=0
      RB(0)=0
      IB(0)=0
      RA(N2P1)=0
      IA(N2P1)=0
      RB(N2P1)=0
      IB(N2P1)=0
C
C     CALCUL DE KMAT1 ET KMAT2
C
      K1=0
      K2=0
      J=-1
      DO 55 N=1,N2
         K1=K1+N*(N+1)*J*(IA(N)-IB(N))
         L1=N*N
         A2=(N+1.)*(N+1.)
         X=RA(N)
         Y=IA(N)
         Z=RB(N)
         T=IB(N)
         K2=K2+L1*A2/(N+N+1.)*(X*X+Y*Y+Z*Z+T*T)
         J=-J
   55 CONTINUE
```

```
      W6=2/ALPHA/ALPHA
      K1=W6*K1
      K2=W6*K2
      CALL CALCUL
  301 CONTINUE
   51 FORMAT(/,1x,'lambda (mic.)',5x,'rn',9x,'in',10x,'r (mic.)')
   52 FORMAT(F7.3,10x,F6.3,3x,E10.3,5x,F7.2/)
 9999 RETURN
      END

      SUBROUTINE ZERO(IT,N)
      DOUBLE PRECISION IT(1)
      DO 1 I=1,N
    1 IT(I)=0
      RETURN
      END

      SUBROUTINE CALCUL
      IMPLICIT DOUBLE PRECISION (A-H,O-Z)
      IMPLICIT INTEGER*4 (I-N)
      DOUBLE PRECISION KMA1,KMA2,IA,IB,IN,IMS1,IMS2
      REAL INT,AY1,AY2,AY3,Q
      DIMENSION RMU(1:200),RA(0:900),RB(0:900),IB(0:900),IA(0:900),
     1INT(1:200),Q(1:200)
      COMMON/A/P,RMU,RA,IA,RB,IB,ALPHA,RN,IN,KMA1,KMA2,RLAM,NBMU,N2
      AY1=ALPHA
      RR=AY1*RLAM/2/P
      AY2=KMA1
      AY3=KMA2
      COEF=2./KMA2/ALPHA**2
      DO 1 J=1,NBMU
         X=-DCOS(RMU(J)*P/180.)
         PIM=0.
         PI=1.
         TAU=X
         RES1=0
         RES2=0
         IMS1=0
         IMS2=0
         DO 2 N=1,N2
            AI=IA(N)
            BI=IB(N)
            AR=RA(N)
            BR=RB(N)
            RES1=RES1-AI*PI-BI*TAU
            RES2=RES2+AI*TAU+BI*PI
            IMS1=IMS1+AR*PI+BR*TAU
            IMS2=IMS2-AR*TAU-BR*PI
            PIP=((2*N+1)*X*PI-(N+1)*PIM)/N
            PIM=PI
            PI=PIP
            TAU=(N+1)*X*PI-(N+2)*PIM
    2 CONTINUE
      Y1=RES1**2+IMS1**2
      Y2=RES2**2+IMS2**2
      INT(J)=COEF*(Y1+Y2)
      Q(J)=COEF*(Y2-Y1)
    1 CONTINUE
      WRITE(1,110)
      WRITE(1,111)AY1,AY2,AY3
      WRITE(1,112)
```

```
      WRITE(1,113)(RMU(J),INT(J),Q(J),J=1,NBMU)
  110 FORMAT(3x,'ALPHA',8x,'QEXT',8x,'QDIF')
  111 FORMAT(3(F8.3,4x))
  112 FORMAT(/,5x,'Theta',7x,'I',12x,'Q')
  113 FORMAT(2x,F7.2,3x,E12.5,3x,E12.5)
      RETURN
      END
*---------------------------------------------------------------*
```

DONUNO.DAT

The data are introduced to 'uno' from 'donuno'.
This is an example of 'donuno' format.
RLAM is the wavelength in micrometers.
rn and **in** are the real and imaginary components of the index of refraction.
r0 is the radius of the particle in micrometers.
nbmu is the number of scattering angle divisions for which the scattering phase
function is to be computed, in our simulations 181.
The rest are the values of **rmu(j)**, the zenith scattering angle for which
scattering phase function is to be computed.

L(μm)	**mr**	**mi**	**r**(μm)
0.5	1.530	-.6E-02	1

nbmu
181

```
  0   1   2   3   4   5   6   7   8   9
 10  11  12  13  14  15  16  17  18  19
 20  21  22  23  24  25  26  27  28  29
 30  31  32  33  34  35  36  37  38  39
 40  41  42  43  44  45  46  47  48  49
 50  51  52  53  54  55  56  57  58  59
 60  61  62  63  64  65  66  67  68  69
 70  71  72  73  74  75  76  77  78  79
 80  81  82  83  84  85  86  87  88  89
 90  91  92  93  94  95  96  97  98  99
100 101 102 103 104 105 106 107 108 109
110 111 112 113 114 115 116 117 118 119
120 121 122 123 124 125 126 127 128 129
130 131 132 133 134 135 136 137 138 139
140 141 142 143 144 145 146 147 148 149
150 151 152 153 154 155 156 157 158 159
160 161 162 163 164 165 166 167 168 169
170 171 172 173 174 175 176 177 178 179
180
```

RESUNO

The results obtained from uno are written in an output file called 'resuno'. This is an example of the format of resuno.

ALPHA is the size parameter (dimensionless)
QEXT is the extinction coefficient (μm^{-1})
QDIF is the scattering coefficient (μm^{-1})
Theta is the scattering zenith angle in local coordinates (deg).
I is the scattering phase function.
Q is the polarization degree.

RLAM (μm)	**rn**	**in**	**r0** (μm)
0.500	1.530	-0.600E-02	1.0000

ALPHA	**QEXT**	**QDIF**
12.56637	2.01104	1.71467

Theta	**I**	**Q**
0.00	0.97517E+02	0.00000E+00
2.00	0.91386E+02	0.12476E+00
4.00	0.74796E+02	0.43633E+00
6.00	0.52459E+02	0.77722E+00
8.00	0.30208E+02	0.97193E+00
10.00	0.12929E+02	0.91201E+00
12.00	0.30737E+01	0.60806E+00
14.00	0.29384E+00	0.18420E+00
16.00	0.21784E+01	-0.18053E+00
18.00	0.56096E+01	-0.33475E+00
20.00	0.80734E+01	-0.22181E+00
22.00	0.84121E+01	0.98188E-01
24.00	0.68450E+01	0.47908E+00
26.00	0.44338E+01	0.75555E+00
28.00	0.23532E+01	0.81521E+00
30.00	0.13214E+01	0.64426E+00
32.00	0.13891E+01	0.32741E+00
34.00	0.20846E+01	0.37441E-02
36.00	0.27627E+01	-0.20019E+00
38.00	0.29518E+01	-0.22737E+00
40.00	0.25409E+01	-0.10978E+00
42.00	0.17540E+01	0.58179E-01
44.00	0.96719E+00	0.17523E+00

(data for theta from 45 to 176 degrees are not included)

176.00	0.75934E+00	0.16332E+00
178.00	0.10287E+01	0.49396E-01
180.00	0.11443E+01	0.32571E-12

MIE POLIDISPERSE. PRI

```
*************************************************
*           Polydisperse Mie scattering         *
*************************************************
      PROGRAM pri
c ********************************************************************
c
c calculs de mie sur 192 mu de gauss
c ----------------------------------
c
c ici: granulometrie log-normale :
c nr=a*exp(-(log10(r)-alri)**2/2.0/b**2)/r
c
c entrees sur fichier lu en read(5) :
c - nom du fichier qui stockera les resultats ;
c - lambda, rn, in <0 ;
c |||
c - le alpha final (<10000) (alphmax = 2*pi*rmax/lambda).
c |||||
c - les parametres de la granulometrie (rn0, a, b).
c - le rayon maximum (si r>rmax, n(r)=0.0)
c
c parametres imposes dans le programme mais pouvant etre changes :
c - le alpha initial (0.05).
c - les pas en alpha.
c
c
c ********************************************************************
*
      parameter (ialfmx=10000,ialfmx2=2*ialfmx,nmumax=97)

      implicit double precision (a-h,o-z)
      character*20 par1
      double precision in,ia,ib,k1,k2,k3,int,q,u,igna,idnb
      double precision kmat1,kmat2,kmat3,np,it,i1
      dimension rmu(-nmumax:nmumax),chr(-nmumax:nmumax),
     &int(-nmumax:nmumax),q(-nmumax:nmumax),u(-nmumax:nmumax)
      dimension
ra(0:ialfmx2),rb(0:ialfmx2),ia(0:ialfmx2),ib(0:ialfmx2),
     &cna(-1:ialfmx2),rgna(-1:ialfmx2),igna(-
1:ialfmx2),rdna(0:ialfmx2),
     &rdnb(0:ialfmx2),idnb(0:ialfmx2),sna(-1:ialfmx2)
     dimension i1(-nmumax:nmumax),q1(-nmumax:nmumax),it(-
nmumax,nmumax)
      common /c/ int, q, u
      common /g/ nbmu,rmu,chr
      common /l/ rlam,rn,in
      common /cpi/pi,cons
      common /p/pas
      common /d/ pl,pol,beta,gamma,alp,zeta,delta,it,qt,ut
      common /r/ kmat1,kmat2,kmat3,i1,q1,u1,np

      pi=dacos(-1.0d+00)
      cons=dsqrt(2*pi)

      open(4,file='nmu192')
      nbmu=nmumax
      read(4,222)(rmu(j),chr(j),j=nbmu,-nbmu,-1)
      lll=2*nbmu+1
```

```
      read(5,*)rn0,aa,bb,rmin,rmax
      aaa=rn0/bb/alog(10.0)/cons
      alri=dlog10(aa)

    1 continue
      read(5,*,end=999)rlam,rn,in
      rnu=10000.0/rlam
      inu=rnu+0.1
      write(par1,150)inu
  150 format('redl',i5.5)
      open(8,file=par1)
      af=2.0*pi*rmax/rlam
      alphao=2.0*pi*rmin/rlam
c alphaf augmente de 10 (petite securite...)
      alphaf=dint(af+10.)
c write(6,*)'alpha final = ',alphaf
c write(6,*)
      call zero(ra,ialfmx2+1)
      call zero(rb,ialfmx2+1)
      call zero(ia,ialfmx2+1)
      call zero(ib,ialfmx2+1)
      call zero(cna,ialfmx+2)
      call zero(rgna,ialfmx+2)
      call zero(igna,ialfmx+2)
      call zero(rdnb,ialfmx2+1)
      call zero(sna,ialfmx2+1)
      call zero(idnb,ialfmx2+1)
      call zero(rdna,ialfmx2+1)

      call zero(beta,2*nmumax+11)
      call zero(gamma,2*nmumax+11)
      call zero(alp,2*nmumax+11)
      call zero(zeta,2*nmumax+11)
      call zero(delta,2*nmumax+11)
      call zero(i1,2*nmumax+1)
      call zero(q1,2*nmumax+1)
      call zero(u1,2*nmumax+1)
      call zero(it,2*nmumax+1)
      call zero(qt,2*nmumax+1)
      call zero(ut,2*nmumax+1)

      np=0.0
      kmat1=0.0
      kmat2=0.0
      kmat3=0.0

      if(alphao.gt.alphaf)goto301
      alpha=alphao
      pas=0.001
 7777 alpha1=alpha
c-----------------------------
c definition des pas :
c-----------------------------
      if(alpha.ge.0.01)pas=0.005
      if(alpha.ge.0.05)pas=0.01
      if(alpha.ge.10)pas=0.05
      if (alpha.ge.50)pas=0.1
      if(alpha.gt.100)pas=0.5
      if(alpha.gt.500)pas=1.0
      if(alpha.gt.1000)pas=5.0
c-----------------------------
```

```
c
c write(6,*)'alpha :',alpha
c
      call pp1
      call pp2
c
      alpha=alpha+pas
      if (alpha.le.alphaf+pas/100.0) goto 7777
  301 continue
c
      do 55 j=-nbmu,nbmu
      i1(j)=i1(j)/kmat2
      q1(j)=q1(j)/kmat2
      u1(j)=u1(j)/kmat2
   55 continue
c
c facteur d'assymetrie non tronque, sections ext/dif, pizero :
c
      sext=kmat1/np
      scatt=kmat2/np
      gasym=kmat3/kmat2
      piz=kmat2/kmat1
c
C write(6,100) rn0,r0,aa,bb,ggam,rmax
      write(8,*) rn0,aa,bb,rmax
c write(8,156)rlam
c write(8,158)rn,in
      write(8,22)np
      write(8,21)sext,scatt,piz,gasym
c write(8,155)
c write(8,154)
c write(8,155)
      write(6,159)

      do 444 j=-nbmu,nbmu
c write(6,157)j,rmu(j),dacos(rmu(j))*180/pi,i1(j),q1(j),u1(j),
c &q1(j)/i1(j)
      write(6,157)dacos(rmu(j))*180/pi,i1(j),q1(j)/i1(j)
  444 continue

c write(8,155)
c write(8,*)
c write(8,*)
c
c stockage des intensites et des taux de polarisation :
c
      write(8,*) rlam,inu,np
      write(8,*)sext,scatt,piz,gasym
      write(8,*)
      write(8,203)(i1(j),j=-nbmu,nbmu)
c write(8,*)
c write(8,204)(q1(j)/i1(j),j=-nbmu,nbmu)
c
  888 continue
c write(6,*)
c write(6,*)
      goto 1
  999 continue
      stop
c
c -------------------------------------------------------
```

```
c
  222 format(2d21.14)
  203 format(5(2x,e14.7))
  204 format(8(2x,f8.5))
  100 format(5x,'granulometrie : rn = ',f4.1,'.r**',f4.1,'.exp(-',
     &f6.3,'*r)',' pour r < ',f4.0,' mic.',/,5x,70(1h=),/,/)
  154 format(2x,'
j',8x,'mu',8x,'teta',8x,'i',13x,'q',13x,'u',12x,'q/i')
  155 format(1x,78(1h-))
  156 format(20x,'longueur d,onde :',f7.3,'
microns'/,20x,32(1h=),/,/)
c 157 format(1x,i4,3x,f8.5,3x,f7.2,1x,3(e12.5,2x),2x,f8.5)
  157 format(1x,f7.2,1x,2(e12.5,2x))
  159 format(3x,'Theta',7x,'p11',9x, '-p12/p11')
  158 format(5x,'indice reel',f10.5,5x,
     &'indice imaginaire:',1e12.5,/,/,/)
   21 format(7x,'Sections d`extinction et de diffusion ramenees a',
     &' une particule :',/,7x,64(1h-),/,5x,'extinction : ',
     &e12.5,' mic**2',5x,'diffusion : ',e12.5,' mic**2',/,/,
     &5x,'pizero : ',f8.6,17x,'facteur d`assymetrie :',f8.5,/,/,/)
   22 format(10x,'nombre de particules :',e13.5,/,/)
      end
c
c*********************************************************************
*
c
      subroutine pp1
c
c calcul des series de Mie, facteurs de diffusion et d'extinction,
c et facteur d'assymetrie pour un parametre de Mie alpha donne :
c

      parameter (ialfmx=10000,ialfmx2=2*ialfmx,nmumax=97)
      implicit double precision (a-h,o-z)
      integer un,r1,test
      double precision k1,k2,k3,ia,ib,in,igna,idnb,ibeta

      dimension cna(-1:ialfmx2),rgna(-1:ialfmx2),igna(-1:ialfmx2),
     &rdna(0:ialfmx2),ra(0:ialfmx2),rb(0:ialfmx2),ia(0:ialfmx2),
     &ib(0:ialfmx2),rdnb(0:ialfmx2),idnb(0:ialfmx2),sna(-1:ialfmx2),
     &rmu(-nmumax:nmumax),chr(-nmumax:nmumax)
      common/a/ra,ia,rb,ib,alpha,k1,k2,k3,n2
      common /b/ cna,rgna,igna,rdna,rdnb,idnb,sna
      common /g/ nbmu,rmu,chr
      common /l/ rlam,rn,in
      common /cpi/pi,cons

      r1=20
      rbeta=rn*alpha
      ibeta=in*alpha
      n1=dint(alpha+alpha+r1)
      n2=dint(alpha+alpha+5)
      n2p1=n2+1
      rsurl=alpha/2.0/pi+1.0d-10
      irl=dint(rsurl)
      frc=rsurl-irl*1.0d00
      if(frc.lt.1.0d-08) alpha=alpha*(1.+1.0d-08)
      cna(-1)=-dsin(alpha)
      rgna(-1)=0
      rgna(0)=0
      cna(0)=dcos(alpha)
```

```
      igna(-1)=0
      igna(0)=-1
      do 25 i=1,n2
      cna(i)=(2*i-1)*cna(i-1)/alpha-cna(i-2)
      x=rgna(i-1)
      z=i/alpha
      y=igna(i-1)
      w=((z-x)*(z-x)+(y*y))
      rgna(i)=(z-x)/w-z
      igna(i)=y/w
      if(cna(i).lt.1d+100) goto 25
      n2=i
      n2p1=i+1
      n1=i+15
      goto 26
   25 continue
   26 continue
      rdna(n1)=0
      rdnb(n1)=0
      idnb(n1)=0
      x1=rbeta*rbeta+ibeta*ibeta
      x2=rbeta/x1
      x3=ibeta/x1
      sna(n1)=0
      sna(n1-1)=1
      do 30 kk=1,n1
      i=n1-kk
      x=rdnb(i+1)
      y=idnb(i+1)
      z=x+(i+1)*x2
      w=y-(i+1)*x3
      x4=z*z+w*w
      rdnb(i)=(i+1)*x2-z/x4
      idnb(i)=-(i+1)*x3+w/x4
      z=(i+1)/alpha
      x=rdna(i+1)
      rdna(i)=z-1/(x+z)
      sna(i-1)=(2*i+1)*sna(i)/alpha-sna(i+1)
      if (sna(i-1).le.1d+60) goto 40
      test=i-1
      x=sna(test)
            do 35 j=test,n2
   35 sna(j)=sna(j)/x
   40 continue
   30 continue
      q=-sna(0)/cna(-1)
      do 45 i1=1,n2p1
   45 sna(i1-1)=sna(i1-1)/q
      test=0
      un=1
      do 50 i=1,n2
      x1=sna(i)
      x2=cna(i)
      x3=rdnb(i)
      x4=idnb(i)
      x5=rdna(i)
      x6=rgna(i)
      x7=igna(i)
      y1=x3-rn*x5
      y2=x4-in*x5
      y3=x3-rn*x6+in*x7
```

```
      y4=x4-rn*x7-in*x6
      y5=rn*x3-in*x4-x5
      y6=in*x3+rn*x4
      y7=rn*x3-in*x4-x6
      y8=in*x3+rn*x4-x7
      x4=y2*y3-y1*y4
      x3=y1*y3+y2*y4
      x5=x1*x1+x2*x2
      x6=y3*y3+y4*y4
      x7=y5*y7+y6*y8
      x8=y6*y7-y5*y8
      x9=y7*y7+y8*y8
      q=(i+i+1.)/i/(i+1.)*un
      y1=x1*(x1*x3+x2*x4)/x5/x6
      y2=x1*(x1*x4-x2*x3)/x5/x6
      y3=x1*(x1*x7+x2*x8)/x5/x9
      y4=x1*(x1*x8-x2*x7)/x5/x9
      ra(i)=y2*q
      ib(i)=y3*q
      q=-q
      rb(i)=y4*q
      ia(i)=y1*q
      un=-un
   50 continue
      ra(0)=0
      ia(0)=0
      rb(0)=0
      ib(0)=0
      ra(n2p1)=0
      ia(n2p1)=0
      rb(n2p1)=0
      ib(n2p1)=0

      k1=0.0
      k2=0.0
      k3=0.0
      j=-1
      do 55 n=1,n2
      l1=n*n
      a2=(n+1.)*(n+1.)
      x=ra(n)
      y=ia(n)
      z=rb(n)
      t=ib(n)
      xp=ra(n+1)
      yp=ia(n+1)
      zp=rb(n+1)
      tp=ib(n+1)
      k1=k1+n*(n+1)*j*(y-t)
      k2=k2+l1*a2/(n+n+1.)*(x*x+y*y+z*z+t*t)
      y10=l1*(n+2.)*(n+2.)*(n+1.)/(2*n+1.)/(2*n+3.)
      k3=k3-y10*(x*xp+y*yp+z*zp+t*tp)
      k3=k3-n*(n+1.)/(2*n+1.)*(x*z+y*t)
      j=-j
   55 continue
      w6=2/alpha/alpha
c
c k1 = Qext
c k2 = Qscat
c k3 donne g
c
```

```
      k1=w6*k1
      k2=w6*k2
      k3=k3*4./alpha/alpha/k2
      call calcul
 9999 return
      end
c
c*******************************************************
c
      subroutine zero(it,n)
c
      parameter (ialfmx=10000,ialfmx2=2*ialfmx,nmumax=97)
      double precision it(n)
      do 1 i=1,n
    1 it(i)=0
      return
      end
c
c*******************************************************
c
      subroutine calcul
c
c calcul de i, q, u pour un parametre de Mie alpha :
c
      parameter (ialfmx=10000,ialfmx2=2*ialfmx,nmumax=97)
      implicit double precision (a-h,o-z)
c implicit integer*4 (i-n)
      double precision kma1,kma2,kma3,ia,ib,in,ims1,ims2
      double precision int,q,u
c real int,ay1,ay2,ay3,ay4,q,u
      dimension rmu(-nmumax:nmumax),chr(-nmumax:nmumax),
     &ra(0:ialfmx2),rb(0:ialfmx2),ib(0:ialfmx2), ia(0:ialfmx2),
     &int(-nmumax:nmumax),q(-nmumax:nmumax),u(-nmumax:nmumax)
      common/a/ra,ia,rb,ib,alpha,kma1,kma2,kma3,n2
      common /c/ int, q, u
      common /g/ nbmu,rmu,chr
      common /l/ rlam,rn,in
      common /cpi/p,cons
      ay1=alpha
      ay2=kma1
      ay3=kma2
      ay4=kma3
      coef=2./kma2/alpha**2
      do 1 j=-nbmu,nbmu
            x=-rmu(j)
            pim=0.
            pi=1.
            tau=x
            res1=0
            res2=0
            ims1=0
      ims2=0
      do 2 n=1,n2
            ai=ia(n)
            bi=ib(n)
            ar=ra(n)
            br=rb(n)
            res1=res1-ai*pi-bi*tau
            res2=res2+ai*tau+bi*pi
            ims1=ims1+ar*pi+br*tau
            ims2=ims2-ar*tau-br*pi
```

```
            pip=((2*n+1)*x*pi-(n+1)*pim)/n
            pim=pi
            pi=pip
            tau=(n+1)*x*pi-(n+2)*pim
    2 continue
      y1=res1**2+ims1**2
      y2=res2**2+ims2**2
      y3=2*res2*res1
      y4=2*ims2*ims1
      int(j)=coef*(y1+y2)
      q(j)=coef*(y2-y1)
      u(j)=coef*(y3+y4)
    1 continue
c write(1)ay1,ay2,ay3,ay4,int
c write(6,1234)alpha,kma1,kma2,kma3,int(-nbmu),int(nbmu)
  900 format(5d15.8)
 1234 format(1x,f7.2,5x,3e14.7,3x,2e13.6)
      return
      end
c
c*****************************************************************
c
      subroutine pp2
c
c integrations sur la granulometrie
c
c ---------------------------------------------------------------
c
      parameter (ialfmx=10000,ialfmx2=2*ialfmx,nmumax=97)
c
      implicit double precision (a-h,o-z)
      double precision in,ia,ib,kma1,kma2,kma3,i2,q2,u2,igna,idnb
      double precision kmat1,kmat2,kmat3,np,nr,it,i1
      dimension rmu(-nmumax:nmumax),chr(-nmumax:nmumax),
     &i2(-nmumax:nmumax),q2(-nmumax:nmumax),u2(-nmumax:nmumax)
      dimension ra(0:ialfmx2),rb(0:ialfmx2),ia(0:ialfmx2),
     &ib(0:ialfmx2),cna(-1:ialfmx2),rgna(-1:ialfmx2),
     &igna(-1:ialfmx2),rdna(0:ialfmx2), rdnb(0:ialfmx2),
     &idnb(0:ialfmx2),sna(-1:ialfmx2)
c
      dimension i1(-nmumax:nmumax),q1(-nmumax:nmumax),
     &pl(-1:2*nmumax+10),pol(0:2*nmumax+10),beta(0:2*nmumax+10),
     &gamma(0:2*nmumax+10),it(-nmumax:nmumax),
     &alp(0:2*nmumax+10),zeta(0:2*nmumax+10),delta(0:2*nmumax+10),
     &u1(-nmumax:nmumax),qt(-nmumax:nmumax),ut(-nmumax:nmumax)
c
      common/a/ra,ia,rb,ib,alpha,kma1,kma2,kma3,n2
      common /c/ i2, q2, u2
      common /g/ nbmu,rmu,chr
      common /l/ wa,rn,in
      common /cpi/pi,cons
      common /gr/ rn0,aa,bb,rmin,rmax,aaa,alri
      common /d/ pl,pol,beta,gamma,alp,zeta,delta,it,qt,ut
      common /r/ kmat1,kmat2,kmat3,i1,q1,u1,np
      common /p/ pas
c
      r=alpha*wa/2/pi
      nr=0.0
c write(6,1234)alpha,kma1,kma2,kma3,i2(-nbmu),i2(nbmu)
c
c la granulometrie est definie ici :
```

```
c log-normale distribution au coefficient devant l'exp. pres :
      if(r.lt.rmin) then
      nr=0.0
      goto 121
      endif

      if(r.gt.rmax) then
      nr=0.0
      goto 121
      endif

      nr=aaa*exp(-(log10(r)-alri)**2/2.0/bb**2)/r
  121 continue
c write(6,151)alpha,r,nr
c
      pr=wa*pas/2/pi
      x1=nr*pr*pi*r**2
      kmat1=kmat1+x1*kma1
      kmat2=kmat2+kma2*x1
      kmat3=kmat3+x1*kma2*kma3
      np=np+nr*pr
      nr=nr*pr*wa**2/4/pi
      x1=kma2*alpha*alpha*nr
      do 1 j=-nbmu,nbmu
      i1(j)=i1(j)+i2(j)*x1
      q1(j)=q1(j)+q2(j)*x1
      u1(j)=u1(j)+u2(j)*x1
    1 continue
c write(6,1234)alpha,kmat1,kmat2,kmat3,i1(-nbmu),i1(nbmu)
  151 format(e10.4,2x,e10.4,3x,i3,3x,e10.4)
 1234 format(1x,f7.2,5x,3e14.7,3x,2e13.6)
      return
      end
*--------------------------------------------------*
```

NMU192

The data are introduced to 'PRI' from 'nmu192'about the Gauss angles.
This is an example of 'nmu192' format.
The first column corresponds to the cosine of the angle.
The second column corresponds to the Gaussian weights.
These data are necessary for the precise calculation of the scattering phase function.

The first column corresponds to the variable **rmu(j)**.
The second column corresponds to the variable **chr(j)**.

```
-1.00000000000000E+00 0.00000000000000E-00
-0.99992196865919E+00 0.20025101477106E-03
-0.99958888033941E+00 0.46609448559436E-03
-0.99898972200822E+00 0.73220756663022E-03

             (Omitted data)

0.99898972200822E+00 0.73220756663022E-03
0.99958888033941E+00 0.46609448559436E-03
0.99992196865920E+00 0.20025101460134E-03
1.00000000000000E+00 0.00000000000000E-00
```

DONMIEPOLY

The characteristics of the log-normal aerosol size distribution are introduced to the polydisperse Mie scattering code from 'donMiePoly'. This is an example of a possible 'donMiePoly' input file.

N_0 is the number density (cm^{-3})
ri is mode radius (μm)
log10(σ_i) is the decimal logarithmic of the standard deviation
Rmin y **Rmax** are the minimal and maximal radius of the distribution (μm).
L is the wavelength (μm).
nr and **in** are the real and the imaginary part of the index of refraction.

N_0 ri log10(σ_i) Rmin Rmax (ici WMO DL)
1.0 0.0285 0.35005 0.0001 20.0

L nr in(<0)
0.5 1.530 -5.0E-03

REDL02550

The Mie polydisperse code creates an output text file containing the results. The name of the file is assigned by the code. This is an example of the output file from PRI.

In this file we can see the extinction and the scattering cross sections, the asymmetry factor and pizero, which is the single-scattering albedo (scattering over extinction).

This file also contains the development of the scattering phase function in terms of Legendre polynomial necessary to use in radiative transfer.

1. 0.5 0.47567 110.
nombre de particules : 0.10007E+01

Sections d`extinction et de diffusion ramenees a une particule :
----
extinction : 0.18891E+02 mic**2 **diffusion** : 0.15395E+02 mic**2

pizero : 0.814954 **facteur d`assymetrie** : 0.87635

3.921569 2550 1.00066751
18.8907199 15.3950663 0.814953923 0.876346984

```
   0.4109035E+03   0.3234592E+03   0.1879441E+03   0.1231003E+03
0.8750176E+02
   0.6575102E+02   0.5142553E+02   0.4144834E+02   0.3419030E+02
0.2872460E+02
   0.2448682E+02   0.2112105E+02   0.1839248E+02   0.1614244E+02
0.1425959E+02
   0.1266464E+02   0.1129929E+02   0.1012047E+02   0.9094596E+01
0.8196300E+01
   0.7405538E+01   0.6706228E+01   0.6085241E+01   0.5531643E+01
0.5036818E+01
   0.4593253E+01   0.4194709E+01   0.3835675E+01   0.3511632E+01
0.3218709E+01
   0.2953473E+01   0.2712954E+01   0.2494477E+01   0.2295893E+01
0.2115163E+01
   0.1950565E+01   0.1800424E+01   0.1663431E+01   0.1538315E+01
0.1423985E+01
   0.1319348E+01   0.1223539E+01   0.1135742E+01   0.1055225E+01
0.9812672E+00
```

(Omitted data)

```
   0.9698613E-01   0.9320693E-01   0.8965700E-01   0.8632009E-01
0.8318263E-01
   0.8023003E-01   0.7745277E-01   0.7484036E-01   0.7238273E-01
0.7007063E-01
   0.6789668E-01   0.6585493E-01   0.6488127E-01   0.6393818E-01
0.6214083E-01
   0.6045729E-01   0.5888360E-01   0.5741473E-01   0.5604636E-01
0.5477408E-01
   0.5359401E-01   0.5250235E-01   0.5149502E-01   0.5056826E-01
0.4971833E-01
   0.4894222E-01   0.4823672E-01   0.4759898E-01   0.4702659E-01
0.4651782E-01
   0.4607119E-01   0.4568541E-01   0.4535990E-01   0.4509453E-01
0.4488930E-01
   0.4474410E-01   0.4465923E-01   0.4463508E-01   0.4467176E-01
0.5194389E-01
   0.5257452E-01   0.5317633E-01   0.5373826E-01   0.5425058E-01
0.5470340E-01
   0.5508742E-01   0.5539473E-01   0.5562024E-01   0.5576203E-01
0.5581996E-01
   0.5579709E-01   0.5569995E-01   0.5553711E-01   0.5531922E-01
0.5505954E-01
   0.5477328E-01   0.5447608E-01   0.5418377E-01   0.5391319E-01
0.5368126E-01
   0.5350281E-01   0.5339132E-01   0.5335949E-01   0.5341788E-01
0.5357440E-01
   0.5383568E-01   0.5420729E-01   0.5469349E-01   0.5529772E-01
0.5602446E-01
   0.5688011E-01   0.5787237E-01   0.5901097E-01   0.6030923E-01
0.6178347E-01
   0.6345132E-01   0.6533153E-01   0.6744107E-01   0.6978628E-01
0.7234846E-01
   0.7506024E-01   0.7776510E-01   0.8016448E-01   0.8177707E-01
0.8195798E-01
   0.8004835E-01   0.7573272E-01   0.6957861E-01   0.6338309E-01
0.5966946E-01
   0.6037039E-01   0.6571750E-01   0.7383383E-01   0.8088551E-01
0.8290411E-01
```

Vita

María Santa María Iruzubieta was born on January 15, 1977 in Logroño, Spain. She studied in the catholic private school of Compañia de María in Logroño during 14 years. There she received not only an excellent academic formation but also a life philosophy that has guided her ever since. In Compañia de María, María was always among the top 1 percent of the class, and at the end of her formation, she was one of the two only students from her school to enter the Extraordinary High School award competition where she scored 13th on her state.

From an early age, María felt intrigued about other countries and cultures. This lead her to participate on several student exchange programs with Dax and Narbonne in France, Erkelenz in Germany, and Clondalkin in Ireland. She was also member of the theater school group and a member of the student board during several years.

In 1995, María began her studies of superior chemical engineering at the University of Zaragoza, in Spain. In 1998, María was awarded a Socrates-Erasmus scholarship, granted by the European community, to study one year in the University of Technology of Compiègne, France. In 1999, María was selected as the first student from Zaragoza to participate in a double diploma project between her Spanish school and Virginia Polytechnic Institute and State University. She worked simultaneously towards the completion of her chemical engineering studies in Spain and her Master of Science degree in mechanical engineering at Virginia Tech. In November 2001, María graduated in Spain, receiving an A-score for her final thesis. In December 2001, she graduated at Virginia Tech.

María Santa María Iruzubieta, December 2001